# Limits on Planetary Companions
# from Doppler Surveys of Nearby Stars

Andrew W. Howard & Benjamin J. Fulton

*Institute for Astronomy, University of Hawaii, 2680 Woodlawn Drive,
Honolulu, HI 96822, USA*

howard@ifa.hawaii.edu

November 3, 2014

# Contents

## Abstract

Most of our knowledge of planets orbiting nearby stars comes from Doppler surveys. Today we have detailed knowledge of hundreds of such planets, including their masses, orbits, and planetary system architectures. For spaced-based, high-contrast imaging missions, nearby stars with Doppler-discovered planets are attractive targets. The known orbits tell imaging missions where and when to observe, and the dynamically-determined masses provide important constraints for the interpretation of planetary spectra. Nearby stars with long histories of Doppler observations, but no detected planets, are also valuable. Quantifying the set of planet masses and orbits that could have been detected will enable more efficient planet discovery and characterization. For example, imaging missions only capable of detecting giant planets might exclude stars for which such planets have been ruled out by Doppler surveys. Alternatively, more capable missions might favor such stars because planetary systems without giant planets are dynamically quiescent and potentially more likely to host small planets. For this study we considered the historic Doppler measurements from Lick and Keck Observatories by the California Planet Survey. We focused on stars that are likely targets for three space-based planet imaging mission concepts currently being studied by NASA. The Doppler planet search targets are primarily main sequence stars with spectral type F8 and later, with observations spanning 1987–2014 and sensitivity to orbital periods comparable to Saturn's. We identified 76 stars with Doppler measurements that are included in the prospective target lists of the AFTA coronagraph, Exo-C coronagraph, and Exo-S starshade mission concepts. We developed an automated planet search and a methodology to estimate the completeness of Doppler measurements to planets using injection and recovery tests. We applied this computational machinery to the Lick and Keck data and computed planet detection limits for each star as a function of planet minimum mass and semi-major axis. We found that for typical stars in the survey, the Lick and Keck measurements are sensitive to approximately Saturn-mass planets inside of 1 AU, Jupiter-mass planets inside of ∼3 AU, and declining sensitivity out to ∼10 AU. For the best Doppler targets, we are sensitive to approximately Neptune-mass planets in 3 AU orbits. We used our automated planet detection software to calibrate a model of an idealized planet search with a specified number of observations, time baseline, and measurement precision. Using this model, we forecast the precision of future surveys of non-ideal Doppler targets that are likely targets of imaging missions. We conclude with recommendations for maximizing the efficiency and planet yield of space-based imaging missions by pre-observing target stars using Doppler techniques. Importantly, we note that absent a dedicated search, most imaging mission targets have not been probed by Doppler spectroscopy, but that such measurements could yield important constraints on giant planets in several AU orbits.

# 1. Introduction

NASA is studying three mission concepts capable of directly imaging extrasolar planets from space. The AFTA mission (formerly WFIRST) is envisioned as a wide-field, infrared imager on a 2.4-m telescope that could accomplish broad astrophysical goals (Spergel et al. 2013). This mission may include a coronagraph in the instrument suite for exoplanet detection and characterization (Traub et al. 2014; Goullioud et al. 2014). In addition, two Science and Technology Definition Teams (STDTs) have been studying probe-scale (cost less than $1B) mission concepts for the direct detection of extrasolar planets orbiting nearby stars. Exo-C is a mission concept based on a telescope with an internal coronagraph to generate the ultra-high contrast images needed for planet detection (Stapelfeldt et al. 2014). Exo-S would image extrasolar planets using a pair of spacecraft flying in formation — an external occulter (starshade) and a telescope (Seager et al. 2014).

Teams studying these possible missions are considering the scientific return of each, including the discovery of new exoplanets orbiting nearby stars, spectroscopy of exoplanet atmospheres, and imaging of debris and protoplanetary disks. Each mission needs a list of nearby stars to search for new planets and to characterize existing planetary systems. The characteristics of these stars (brightness, spectral type, distance, age, sky position, multiplicity, etc.) make some more favorable targets than others. Target selection will also be based on which stars have planets and debris disks already known. Most of our knowledge of exoplanets orbiting nearby stars comes from Doppler surveys that started in the late 1980s and have improved in sensitivity since then. These observational surveys have discovered hundreds of planets orbiting nearby stars, some of which are possible targets for Exo-C, Exo-S, and AFTA. Many of the Doppler target stars have clear non-detections of planets after hundreds of measurements spanning a decade or more. Knowing that certain stars lack planets with particular masses and semi-major axes constitutes useful information for the imaging missions. The priority of some stars may be reduced if the imaging search space in planet mass and semi-major axis has already been ruled out by Doppler observations. Conversely, other stars may be more attractive if Doppler surveys can rule out dynamically disruptive giant planets and the imaging missions are sensitive to smaller planets that are undetectable by the Doppler measurements.

This report is the product of a study titled 'Radial Velocity Data Review in Support of Direct Imaging Mission Concept Reports' that was carried out by the authors under contract from NASA Jet Propulsion Laboratory. We were charged with identifying the nearby stars that are likely targets of Exo-C, Exo-S, and AFTA and that have historical Doppler measurements at Lick Observatory and Keck Observatory taken by the California Planet Survey (Howard et al. 2010a). For stars with Doppler measurements, we were to

estimate the region of discovery space (planet masses and orbital semi-major axes) in which planets can be ruled out. These "completeness" estimates, and the lists of discovered planets orbiting those stars, provide a valuable input to the planning and eventual operation of space-based planet imaging missions.

This report is organized as follows. The next two sections describe target lists for the Exo-S, Exo-C, and AFTA imaging studies (Sec. 2) and the California Planet Search using Doppler spectroscopy (Sec. 3). We review Keplerian orbits in Sec. 4, describe our automated Doppler planet search in Sec. 5, and provide recommendations for future Doppler searches in Sec. 6. Machine-readable data files included with this report are described in Appendix A. The remaining appendices provide exhaustive data that is too large for the main text. Appendix B includes a complete list of the Exo-C, Exo-S, and AFTA stars that are not part of our Lick/Keck Doppler survey and the likely reasons for their exclusion. Appendix C contains plots summarizing the search results and completeness estimates for every star with Doppler measurements.

## 2.    Target Lists for the Exo-C, Exo-S, and AFTA Studies

The Exo-S, Exo-C, and AFTA study teams selected preliminary lists of nearby stars for their missions. These target lists contain real stars and allow for simulations of mission performance that depend on genuine stellar properties. Target lists were provided to us by representatives of the study teams (M. Turnbull and K. Stapelfeldt) and are current as of July 31, 2014. Stellar properties were taken from the "Properties of Nearby Stars" page on the NASA ExEP website[1]. This catalog was assembled by M. Turnbull and includes catalog numbers from Hipparcos, Henry Draper (HD), and Gliese catalogs, as well as sky coordinates, distances, $V$-band brightnesses, $B - V$ colors, spectral types, and luminosities. These Exo-S, Exo-C, and AFTA target stars are listed in two tables below. Table 2 includes stars for which we have Doppler measurements and provide completeness measurements. Stellar masses (to convert orbital periods into semi-major axes) are mostly derived from stellar synthesis fits using Spectroscopy Made Easy (Valenti & Fischer 2005). Table 4 lists Exo-S, Exo-C, and AFTA targets without Doppler measurements. We adopt HD numbers as the primary stellar names throughout this report because they are the standard star names used internally for our Keck program.

Figure 1 shows the Exo-S and Exo-C targets in a Hertzsprung-Russell diagram. Stars

---

[1]See http://nexsci.caltech.edu/missions/EXEP/EXEPstarlist.html

with Doppler measurements from Lick or Keck Observatories are highlighted in blue. These stars are nearly all main sequence stars with spectral type F8 and later ($B - V > 0.4$) with a handful of K-type subgiants and giants. Table 1 summarizes the number of stars in each of the three imaging missions for which we have Lick and/or Keck Doppler measurements. The table also attempts to reconstruct the reasons that stars in the imaging mission target lists were not observed by the Lick/Keck searches.
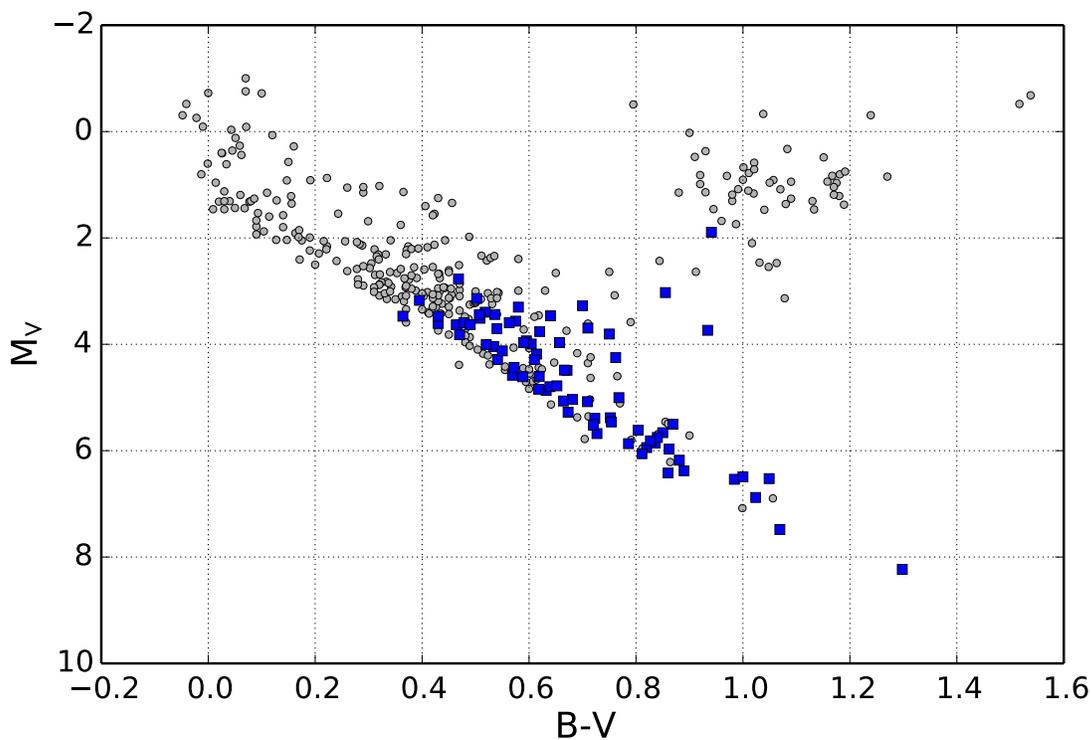


Fig. 1.— HR diagram of stars in the Exo-S, Exo-C, and AFTA target lists with (blue squares) and without (gray circles) Doppler observations from Lick and Keck Observatories. Doppler searches favor late-F through mid-M type dwarfs for planet detectability. Imaging searches for planets in reflected light typically prefer bright stars, which are dominated by early type stars. The region of overlap encompasses primarily F8–K0 dwarfs.

Table 1.   Summary of Reasons for Excluding Stars from Lick/Keck Programs[a]

| Mission | Total Stars | Have RVs[b] | No RVs | | | |
|---|---|---|---|---|---|---|
| | | | Hot[c] | Southern[d] | Evolved[e] | Binary[f] |
| Exo-S (S) | 127 | 57 | 19 | 24 | 3 | 22 |
| Exo-C (C) | 249 | 40 | 112 | 43 | 39 | 33 |
| AFTA (A) | 263 | 51 | 125 | 51 | 4 | 38 |
| Total (S+C+A) | 376 | 76 | 148 | 71 | 40 | 51 |

[a]Stars were not included in the Lick and Keck RV planet searches for a variety of reasons. Here we attempt to reconstruct the reasons that stars were not added to those programs, focussing on four non-exclusive and incomplete categories.

[b]All stars with RVs are listed in Table 2.

[c]The number of stars with $B - V < 0.44$, corresponding to spectral type F5 V.

[d]The number of stars with declination $< -30°$.

[e]The number of stars not listed as dwarf spectral types in Simbad.

[f]A rough estimate of the number of stellar multiples. We include targets noted as 'spectroscopic binary' or with multiple, distinct spectral types listed in Simbad, or a listing in the Washington Double Star Catalog.

Table 2.   Imaging Target Stars with Doppler Measurements

| Hipp. No. | HD No. | Gliese No. | Target[a] Lists | Dist. (pc) | $V$ (mag) | $B–V$ (mag) | $T_{\mathrm{eff}}$ (K) | $M_\star$ ($M_\odot$) | Sp. T. | Notes |
|---|---|---|---|---|---|---|---|---|---|---|
| 544 | 166 | 5 | S | 13.671 | 6.060 | 0.752 | 5577 | 0.987 | K0V | |
| 3093 | 3651 | 27 | S | 11.060 | 5.880 | 0.850 | 5221 | 0.920 | K0V | |
| 3821 | 4614 | 34A | S, C, A | 5.944 | 3.452 | 0.569 | 5941 | 0.986 | G3V | |
| 3765 | 4628 | 33 | S, C | 7.455 | 5.740 | 0.890 | 4944 | 0.728 | K1V | |
| 7513 | 9826 | 61 | C, A | 13.492 | 4.090 | 0.536 | 6213 | 1.310 | F8V | |
| 7981 | 10476 | 68 | S, C, A | 7.532 | 5.240 | 0.836 | 5181 | 0.863 | K1V | |
| 8102 | 10700 | 71 | S, C, A | 3.650 | 3.490 | 0.727 | 5283 | 0.762 | G8V | |
| 8362 | 10780 | 75 | S | 10.067 | 5.630 | 0.804 | 5327 | 0.879 | K0V | |
| 12114 | 16160 | 105A | S | 7.180 | 5.819 | 0.984 | 4866 | 0.750 | K3V | |
| 13402 | 17925 | 117 | S | 10.352 | 6.046 | 0.862 | 5236 | 0.800 | K1V | |
| 14632 | 19373 | 124 | S, C, A | 10.541 | 4.050 | 0.595 | 6032 | 1.204 | G0V | |
| 14954 | 19994 | 128A | A | 22.580 | 5.070 | 0.580 | 6188 | 1.300 | F8.5V | |
| 15457 | 20630 | 137 | S, C, A | 9.140 | 4.842 | 0.681 | 5742 | 0.900 | G5V | |

Table 2—Continued

| Hipp. No. | HD No. | Gliese No. | Target[a] Lists | Dist. (pc) | $V$ (mag) | $B–V$ (mag) | $T_{eff}$ (K) | $M_\star$ ($M_\odot$) | Sp. T. | Notes |
|---|---|---|---|---|---|---|---|---|---|---|
| 16537 | 22049 | 144 | C, A | 3.213 | 3.714 | 0.881 | 5146 | 0.815 | K2V | young |
| 16852 | 22484 | 147 | S, C, A | 13.963 | 4.290 | 0.575 | 6038 | 1.206 | F8V | |
| 17378 | 23249 | 150 | S, C | 9.041 | 3.518 | 0.934 | 5095 | 1.163 | K0IV | subgiant |
| 18859 | 25457 | 159 | A | 18.830 | 5.380 | 0.520 | 6308 | 1.179 | F7V | young |
| 19849 | 26965 | 166A | S, C, A | 4.984 | 4.430 | 0.820 | 5151 | 0.775 | K1V | |
| 22263 | 30495 | 177 | S | 13.277 | 5.486 | 0.632 | 5759 | 1.000 | G3V | |
| 22449 | 30652 | 178 | S, C, A | 8.068 | 3.167 | 0.464 | 6424 | 1.236 | F6V | |
| 23311 | 32147 | 183 | S | 8.708 | 6.225 | 1.049 | 4827 | 0.821 | K3V | |
| 23835 | 32923 | 188A | S, C, A | 15.434 | 4.910 | 0.657 | 5694 | 1.001 | G4V | |
| 24813 | 34411 | 197 | S, C, A | 12.631 | 4.691 | 0.614 | 5911 | 1.105 | G0V | |
| 26779 | 37394 | 211 | S | 12.277 | 6.198 | 0.840 | 5351 | 0.919 | K1V | young |
| 29650 | 43042 | 3390 | A | 20.810 | 5.200 | 0.430 | 6418 | 1.000 | F5.5IV-V | early type |
| 32480 | 48682 | 245 | A | 16.720 | 5.240 | 0.550 | 6064 | 1.177 | G0V | |
| 39780 | 67228 | $\cdots$ | A | 23.290 | 5.300 | 0.640 | 5862 | 1.220 | G2IV | |
| 40693 | 69830 | 302 | S | 12.494 | 5.943 | 0.754 | 5361 | 0.871 | K0V | |
| 40843 | 69897 | 303 | A | 18.270 | 5.130 | 0.470 | 6294 | 1.095 | F6V | early type |
| 42438 | 72905 | 311 | S | 14.355 | 5.630 | 0.618 | 5920 | 1.000 | G1.5Vb | young |
| 43587 | 75732 | 324A | S | 12.341 | 5.960 | 0.869 | 5235 | 0.966 | G8V | |
| 47592 | 84117 | 364 | S, C, A | 15.013 | 4.924 | 0.534 | 6152 | 1.159 | G0V | |
| 48113 | 84737 | 368 | A | 18.370 | 5.080 | 0.620 | 5960 | 1.164 | G0V | |
| 49081 | 86728 | 376 | S, A | 15.047 | 5.375 | 0.671 | 5700 | 1.095 | G1V | |
| 51459 | 90839 | 395 | S, C, A | 12.780 | 4.820 | 0.541 | 6126 | 1.200 | F8V | |
| 53721 | 95128 | 407 | A | 14.060 | 5.030 | 0.610 | 5882 | 1.083 | G1V | |
| 56452 | 100623 | 432A | S | 9.559 | 5.959 | 0.811 | 5189 | 0.747 | K0V | |
| 56997 | 101501 | 434 | S, C, A | 9.612 | 5.307 | 0.723 | 5488 | 0.913 | G8V | |
| 57443 | 102365 | 442A | S, C, A | 9.220 | 4.890 | 0.664 | 5630 | 0.863 | G5V | |
| 57757 | 102870 | 449 | S, C, A | 10.929 | 3.590 | 0.518 | 6161 | 1.100 | F9V | |
| 58576 | 104304 | 454 | S | 12.763 | 5.533 | 0.768 | 5565 | 1.018 | G8V | |
| 61317 | 109358 | 475 | S, C, A | 8.440 | 4.241 | 0.588 | 5930 | 0.929 | G0V | |
| 64394 | 114710 | 502 | S, C, A | 9.129 | 4.237 | 0.572 | 6075 | 1.150 | G0V | |
| 64408 | 114613 | 501.2 | A | 20.670 | 4.850 | 0.700 | 5782 | 1.266 | G3V | |
| 64792 | 115383 | 504 | A | 17.560 | 5.190 | 0.590 | 6234 | 2.310 | G0IV | young |
| 64924 | 115617 | 506 | S, C, A | 8.555 | 4.740 | 0.709 | 5571 | 0.954 | G5V | |
| 65721 | 117176 | 512.1 | A | 17.990 | 4.970 | 0.710 | 5545 | 1.109 | G5V | |
| 67275 | 120136 | 527A | S, C, A | 15.618 | 4.479 | 0.508 | 6387 | 1.341 | F7V | |
| 71284 | 128167 | 557 | S, C, A | 15.833 | 4.470 | 0.364 | 6566 | 1.500 | F3V | early type |

### 3.    Doppler Targets and Measurements

The historic Lick Planet Search (Fischer et al. 2014) with the the Hamilton spectrograph (Vogt 1987) began in 1987 with a spectrum of $\tau$ Ceti. The original target list included 120 stars from the Bright Star Catalog (Hoffleit & Jaschek 1982) and the Gliese–Jahreiss catalog (Gliese 1969; Gliese & Jahreiß 1979). In 1997 many fainter stars were moved to the new Keck Planet Search and 200 additional stars were added to the Lick Planet Search. An additional

Table 2—Continued

| Hipp. No. | HD No. | Gliese No. | Target[a] Lists | Dist. (pc) | $V$ (mag) | $B$–$V$ (mag) | $T_{\mathrm{eff}}$ (K) | $M_\star$ ($M_\odot$) | Sp. T. | Notes |
|---|---|---|---|---|---|---|---|---|---|---|
| 72659 | 131156 | 566A | S, C, A | 6.776 | 4.675 | 0.720 | 5380 | 0.920 | G7V | young |
| 73184 | 131977 | 570A | S, C | 5.861 | 5.720 | 1.024 | 4744 | 0.760 | K4V | |
| 73996 | 134083 | 578 | A | 19.550 | 4.930 | 0.430 | 6435 | 1.210 | F5V | early type |
| 75181 | 136352 | 582 | S | 14.810 | 5.650 | 0.639 | 5672 | 0.848 | G4V | |
| 77257 | 141004 | 598 | S, C, A | 12.124 | 4.413 | 0.604 | 5936 | 1.036 | G0Vvar | |
| 77760 | 142373 | 602 | S, C, A | 15.893 | 4.599 | 0.563 | 5861 | 1.100 | F9V | |
| 78072 | 142860 | 603 | S, C, A | 11.254 | 3.850 | 0.478 | 6262 | 1.300 | F6V | |
| 79672 | 146233 | 616 | S | 13.900 | 5.496 | 0.652 | 5791 | 1.038 | G5V | |
| 81300 | 149661 | 631 | S | 9.751 | 5.760 | 0.827 | 5277 | 0.883 | K1V | young |
| 84862 | 157214 | 672 | S, A | 14.327 | 5.383 | 0.619 | 5697 | 0.871 | G0V | |
| 86974 | 161797 | 695A | S, C, A | 8.310 | 3.405 | 0.750 | 5641 | 1.142 | G5IV | subgiant |
| 89962 | 168723 | 711 | C | 18.543 | 3.232 | 0.941 | 4975 | 1.721 | K0III-IV | subgiant |
| 91438 | 172051 | 722 | S | 13.084 | 5.860 | 0.673 | 5564 | 0.855 | G5V | |
| 92043 | 173667 | 725.2 | C, A | 19.209 | 4.189 | 0.468 | 6423 | 1.100 | F6V | |
| 95447 | 182572 | 759 | S, A | 15.177 | 5.157 | 0.762 | 5656 | 1.141 | G8IVvar | |
| 96100 | 185144 | 764 | S, C, A | 5.754 | 4.668 | 0.786 | 5246 | 0.801 | K0V | |
| 96441 | 185395 | 765A | C, A | 18.335 | 4.490 | 0.395 | 6594 | 1.380 | F4V | early type |
| 97675 | 187691 | 768.1A | A | 19.190 | 5.120 | 0.540 | 6139 | 1.370 | F8V | |
| 98036 | 188512 | 771A | S, C | 13.699 | 3.711 | 0.855 | 5163 | 1.257 | G8IVvar | |
| 99461 | 191408 | 783A | S, C, A | 6.015 | 5.317 | 0.860 | 4922 | 0.686 | K2.5V | |
| 104214 | 201091 | 820A | S, C, A | 3.496 | 5.200 | 1.069 | 4655 | 0.662 | K5V | |
| 104217 | 201092 | 820B | S | 3.496 | 5.950 | 1.298 | 4145 | 0.548 | K7V | |
| 109422 | 210302 | 849.1 | A | 18.280 | 4.940 | 0.490 | 6339 | 1.299 | F6V | early type |
| 112447 | 215648 | 872A | S, C, A | 16.297 | 4.200 | 0.502 | 6204 | 1.300 | F7V | |
| 113357 | 217014 | 882 | S | 15.608 | 5.452 | 0.666 | 5787 | 1.064 | G5V | |
| 114622 | 219134 | 892 | S, C | 6.543 | 5.570 | 1.000 | 4835 | 0.782 | K3V | |
| 116771 | 222368 | 904 | S, C, A | 13.714 | 4.130 | 0.507 | 6204 | 1.170 | F7V | |

[a]Target list code: S = starshade study mission target, C = coronagraph study mission target, A = AFTA study mission target.

67 metal-rich stars were added in 2001, bringing the total in the Lick Planet Search to 367 stars (Fischer et al. 2014). The Lick target list was dominated by hotter and brighter stars (typically $B - V = 0.4$–$0.7$). Earlier type stars were generally excluded because of increased Doppler noise ($> 5 \ \mathrm{m\,s^{-1}}$). Observations continued through 2011.

Doppler velocities were measured for the Lick and Keck Planet Searches with the aid of an iodine cell. These glass cells containing gaseous $I_2$ act a transmission filter, imprinting thousands of narrow iodine absorption lines on the stellar spectra in the wavelength region 5000–6200 Å. The dense set of molecular absorption lines provide a robust wavelength fiducial against which Doppler shifts are measured, and place strong constraints on the shape of the spectrometer instrumental profile at the time of each observation (Marcy & Butler 1992; Valenti et al. 1995). Relative radial velocities were measured using a forward-modeling technique that simultaneously solves for the spatially-varying instrumental profile, wavelength solution, and Doppler shift of each spectrum (Butler et al. 1996).

The Lick Planet Search was world-leading in the discovery and characterization of exoplanets. Major discoveries include the confirmation of 51 Peg b (Marcy et al. 1997), the discovery of the first planet in an eccentric orbit (Marcy & Butler 1996), the first multi-planet system (Butler et al. 1999), the first sub-Saturn-mass planets (Marcy et al. 2000), the discovery of 70 of the first 100 extrasolar planets (Marcy & Butler 2000), and the first planet search completeness limits for a large sample of stars (Cumming et al. 1999).

The Keck Planet Search has been in operation since 1996 July using the HIRES echelle spectrometer on the Keck I telescope (Vogt et al. 1994). Selection of the target stars is described in Wright et al. (2004) and Marcy et al. (2005b). By 2004, the Keck target list included $\sim$1000 stars with spectral types F5–M5. These stars generally lie close to the main sequence and are chromospherically quiet. Most have $B - V > 0.55$, declination $> -35°$, and have no stellar companion within $2''$ that would introduce a second, complicating spectrum into the Doppler analysis. Young, magnetically active stars are excluded from the primary planet search because of increased Doppler noise. The Keck Planet Search was expanded over the years with bright stars added from the original Lick program as it winded down, as well as large samples of subgiants (Johnson et al. 2007), metal-rich main sequence stars (Fischer et al. 2005; Robinson et al. 2007), young stars (Hillenbrand et al. 2014), and other stellar populations.

The Keck Planet Search was also highly successful at discovering and characterizing exoplanets. Highlights include discoveries of the the first Neptune-size planets (Maness et al. 2007) and numerous super-Earths (Howard et al. 2009, 2011a,b, 2014), demonstration of the planet-metallicity correlation (Fischer et al. 2005), statistical studies of planet occurrence

(Marcy et al. 2005a; Cumming et al. 2008; Howard et al. 2010b), and recently measurements of transiting planets discovered by NASA's Kepler Mission (Marcy et al. 2014).

Combining RVs and high-contrast imaging to discover planets, brown dwarfs, and other orbiting companions has a strong heritage at Keck Observatory. The TRENDS program has used the long RV time series to detect accelerations from wide companions. Followup imaging with Keck-NIRC2 and other instruments has revealed several brown dwarfs and more massive companions (Crepp et al. 2012a,b, 2013a,b, 2014). Similarly, statistical analyses of the long-period accelerations in the Keck RV time series have been used to estimate the fraction of stars with wide-orbit planets (Knutson et al. 2014; Montet et al. 2014)

For this Doppler planet search completeness study, we analyzed RVs from four instruments with independent RV zero points at Lick and Keck. Instrument codes p and l refer to data from the Hamilton spectrograph on the Shane Telescope at Lick Observatory before and after a major detector upgrade (Fischer et al. 2014). Similarly, codes k and j refer to data taken with HIRES on the Keck I telescope before and after an upgrade in 2004 (Vogt et al. 1994). The detector and/or optics in the Hamilton spectrograph were upgraded several times during its 25 years of operation. The commissioning of the Lick Planet Search in 1987 used a TI 800×800 pixel CCD that was upgraded to a 2048×2048 pixel detector in 1990 (dewar 16). During this era, nightly velocity corrections were made at the level of 10 m s$^{-1}$ to account for uncontrolled changes in the instrumental setup (Fischer et al. 2014). In November 1994 the Schmidt camera optics were replaced and a field flattener and new CCD were installed. We treat data prior to November of 1994 as a single instrument with instrument code "p". After the 1994 camera and optics upgrade the CCD was changed another two times in February of 1998, and 2001. We treat these CCDs as a single instrument in our analysis with telescope code "l". RV zero-point offsets between the three dewars on the telescope from 1998 to 2011 have been solved for and removed as best as possible by (Fischer et al. 2014). The final CCD (dewar 8) was in operation until 2011 when the iodine cell failed and the Lick Planet Search ceased. Lick RVs were taken from Fischer et al. (2014) with no additional processing (with the exception of binning measurements in 2 hour intervals, as needed). The CCD on HIRES was upgraded and a new field flattener was installed on 19 August 2004, introducing an RV zero-point uncertainty. Data taken on or before the HIRES upgrade are assigned the instrument code "k", and post-upgrade data use the code "j". Keck RVs reported here run through 26 August 2014.

Table 3 summarizes the observational histories of each star, including the time baseline, UT date of the first RV measurement, and the number and scatter (RMS) of the RVs for each instrument code. When multiple measurements were gathered in short succession for the same star, we binned the data in 2 hr intervals.

Table 3.   Properties of Doppler Measurements

| Hipp. no. | HD no. | $t_{\rm span}$ (yr) | Start Date | Number of RVs | | | | RMS of RVs $(\rm m\,s^{-1})$ [a] | | | |
| | | | | Lick Dewars | | Keck Dewars | | Lick Dewars | | Keck Dewars | |
| | | | | p | l | k | j | p | l | k | j |
| 544 | 166 | 27.1 | 1987-06-13 | 22 | 22 | $\cdots$ | 17 | 18.8 | 20.7 | $\cdots$ | 17.5 |
| 3093 | 3651 | 26.3 | 1987-09-09 | 16 | 139 | 29 | 54 | 11.1 | 7.2 | 3.7 | 3.3 |
| 3821 | 4614 | 18.9 | 1995-09-09 | $\cdots$ | 21 | $\cdots$ | 48 | $\cdots$ | 10.4 | $\cdots$ | 10.2 |
| 3765 | 4628 | 26.9 | 1987-09-08 | 15 | 37 | $\cdots$ | 89 | 10.4 | 6.1 | $\cdots$ | 2.7 |
| 7513 | 9826 | 26.9 | 1987-09-08 | 17 | 312 | $\cdots$ | 8 | 30.7 | 13.0 | $\cdots$ | 2.9 |
| 7981 | 10476 | 26.8 | 1987-09-09 | 15 | 49 | 65 | 69 | 8.9 | 8.1 | 5.1 | 2.7 |
| 8102 | 10700 | 27.0 | 1987-09-08 | 95 | 535 | 87 | 191 | 8.9 | 6.0 | 3.9 | 2.5 |
| 8362 | 10780 | 15.6 | 1998-12-05 | $\cdots$ | 16 | $\cdots$ | 16 | $\cdots$ | 6.2 | $\cdots$ | 4.1 |
| 12114 | 16160 | 25.9 | 1987-09-10 | 14 | 48 | $\cdots$ | 61 | 12.4 | 5.8 | $\cdots$ | 2.5 |
| 13402 | 17925 | 10.9 | 1995-02-20 | $\cdots$ | 15 | $\cdots$ | $\cdots$ | $\cdots$ | 32.1 | $\cdots$ | $\cdots$ |
| 14632 | 19373 | 27.0 | 1987-09-08 | 71 | 158 | 8 | 74 | 9.0 | 8.8 | 4.7 | 2.9 |
| 15457 | 20630 | 24.1 | 1987-09-08 | 25 | 19 | $\cdots$ | $\cdots$ | 21.9 | 25.6 | $\cdots$ | $\cdots$ |
| 16537 | 22049 | 27.0 | 1987-09-08 | 49 | 127 | $\cdots$ | 61 | 17.8 | 9.6 | $\cdots$ | 8.3 |
| 16852 | 22484 | 18.8 | 1995-02-18 | $\cdots$ | 34 | $\cdots$ | 5 | $\cdots$ | 10.0 | $\cdots$ | 5.3 |
| 17378 | 23249 | 16.8 | 1997-01-14 | $\cdots$ | $\cdots$ | 20 | 20 | $\cdots$ | $\cdots$ | 4.1 | 3.5 |
| 19849 | 26965 | 19.5 | 1995-02-21 | $\cdots$ | 77 | 7 | 92 | $\cdots$ | 7.8 | 2.0 | 3.3 |
| 22263 | 30495 | 11.0 | 2000-10-19 | $\cdots$ | 42 | $\cdots$ | $\cdots$ | $\cdots$ | 16.4 | $\cdots$ | $\cdots$ |
| 22449 | 30652 | 11.1 | 2000-09-09 | $\cdots$ | 48 | $\cdots$ | $\cdots$ | $\cdots$ | 31.0 | $\cdots$ | $\cdots$ |
| 23311 | 32147 | 26.3 | 1987-09-08 | 7 | 23 | $\cdots$ | 96 | 7.8 | 3.6 | $\cdots$ | 2.8 |
| 23835 | 32923 | 14.7 | 1998-12-05 | $\cdots$ | 24 | $\cdots$ | 55 | $\cdots$ | 8.5 | $\cdots$ | 5.7 |
| 24813 | 34411 | 26.0 | 1987-09-10 | 17 | 259 | 8 | 60 | 8.6 | 6.7 | 8.6 | 2.9 |
| 26779 | 37394 | 16.8 | 1995-11-11 | $\cdots$ | 8 | $\cdots$ | 12 | $\cdots$ | 10.7 | $\cdots$ | 15.4 |
| 40693 | 69830 | 13.3 | 2000-11-12 | $\cdots$ | 31 | $\cdots$ | 106 | $\cdots$ | 7.4 | $\cdots$ | 3.2 |
| 42438 | 72905 | 11.0 | 2002-10-25 | $\cdots$ | $\cdots$ | 4 | 12 | $\cdots$ | $\cdots$ | 45.0 | 40.9 |
| 43587 | 75732 | 25.3 | 1989-02-21 | 14 | 274 | 24 | 193 | 19.7 | 6.8 | 4.4 | 3.0 |
| 47592 | 84117 | 9.2 | 2004-11-29 | $\cdots$ | $\cdots$ | $\cdots$ | 44 | $\cdots$ | $\cdots$ | $\cdots$ | 4.1 |
| 49081 | 86728 | 26.5 | 1987-06-13 | 15 | 59 | $\cdots$ | 44 | 9.2 | 8.0 | $\cdots$ | 3.2 |
| 51459 | 90839 | 17.0 | 1987-12-20 | 16 | 12 | $\cdots$ | $\cdots$ | 18.5 | 9.3 | $\cdots$ | $\cdots$ |
| 56452 | 100623 | 17.1 | 1996-12-01 | $\cdots$ | $\cdots$ | 16 | 3 | $\cdots$ | $\cdots$ | 19.0 | 6.1 |
| 56997 | 101501 | 24.8 | 1987-06-12 | 20 | 69 | $\cdots$ | 4 | 17.8 | 10.6 | $\cdots$ | 15.9 |
| 57443 | 102365 | 6.6 | 2007-05-26 | $\cdots$ | $\cdots$ | $\cdots$ | 16 | $\cdots$ | $\cdots$ | $\cdots$ | 2.5 |
| 57757 | 102870 | 21.4 | 1987-06-13 | 28 | 70 | $\cdots$ | $\cdots$ | 20.2 | 12.6 | $\cdots$ | $\cdots$ |
| 58576 | 104304 | 13.2 | 2001-05-11 | $\cdots$ | 23 | $\cdots$ | 36 | $\cdots$ | 8.6 | $\cdots$ | 2.5 |

Table 3—Continued

| Hipp. no. | HD no. | $t_{\mathrm{span}}$ (yr) | Start Date | Number of RVs | | | | RMS of RVs $(\mathrm{m\,s^{-1}})$ [a] | | | |
|---|---|---|---|---|---|---|---|---|---|---|---|
| | | | | Lick Dewars | | Keck Dewars | | Lick Dewars | | Keck Dewars | |
| | | | | p | l | k | j | p | l | k | j |
| 61317 | 109358 | 14.4 | 2000-02-09 | $\cdots$ | $\cdots$ | 10 | 69 | $\cdots$ | $\cdots$ | 3.9 | 3.2 |
| 64394 | 114710 | 21.7 | 1987-06-13 | 35 | 66 | $\cdots$ | $\cdots$ | 25.8 | 11.7 | $\cdots$ | $\cdots$ |
| 64924 | 115617 | 23.2 | 1991-04-28 | 14 | 95 | $\cdots$ | 103 | 10.8 | 9.1 | $\cdots$ | 3.0 |
| 67275 | 120136 | 23.7 | 1987-06-12 | 24 | 99 | $\cdots$ | $\cdots$ | 92.7 | 24.9 | $\cdots$ | $\cdots$ |
| 71284 | 128167 | 20.2 | 1988-03-04 | 18 | 36 | $\cdots$ | $\cdots$ | 53.4 | 51.1 | $\cdots$ | $\cdots$ |
| 72659 | 131156 | 19.4 | 1995-02-21 | $\cdots$ | 15 | $\cdots$ | 5 | $\cdots$ | 56.8 | $\cdots$ | 41.9 |
| 73184 | 131977 | 14.8 | 1993-08-01 | 5 | 77 | $\cdots$ | $\cdots$ | 18.7 | 8.2 | $\cdots$ | $\cdots$ |
| 75181 | 136352 | 7.2 | 2007-05-26 | $\cdots$ | $\cdots$ | $\cdots$ | 23 | $\cdots$ | $\cdots$ | $\cdots$ | 4.4 |
| 77257 | 141004 | 26.9 | 1987-09-09 | 16 | 149 | 8 | 81 | 16.1 | 10.2 | 2.7 | 6.2 |
| 77760 | 142373 | 20.8 | 1987-09-10 | 34 | 61 | $\cdots$ | $\cdots$ | 16.8 | 8.8 | $\cdots$ | $\cdots$ |
| 78072 | 142860 | 21.1 | 1987-06-11 | 27 | 30 | $\cdots$ | $\cdots$ | 56.7 | 19.2 | $\cdots$ | $\cdots$ |
| 79672 | 146233 | 18.0 | 1996-07-19 | $\cdots$ | $\cdots$ | 27 | 79 | $\cdots$ | $\cdots$ | 3.7 | 6.2 |
| 81300 | 149661 | 19.0 | 1991-04-28 | 14 | 67 | 31 | 3 | 14.7 | 10.4 | 7.6 | 9.6 |
| 84862 | 157214 | 26.9 | 1987-09-08 | 25 | 71 | 8 | 42 | 10.5 | 7.8 | 1.6 | 3.4 |
| 86974 | 161797 | 26.9 | 1987-09-10 | 29 | 132 | 13 | 40 | 13.1 | 8.5 | 3.7 | 4.4 |
| 89962 | 168723 | 24.1 | 1987-09-10 | 17 | 81 | 47 | 27 | 10.6 | 7.8 | 14.5 | 5.9 |
| 91438 | 172051 | 18.0 | 1996-07-19 | $\cdots$ | $\cdots$ | 32 | 36 | $\cdots$ | $\cdots$ | 4.0 | 3.0 |
| 92043 | 173667 | 24.4 | 1987-06-11 | 31 | 56 | $\cdots$ | $\cdots$ | 89.3 | 76.0 | $\cdots$ | $\cdots$ |
| 95447 | 182572 | 17.8 | 1996-10-10 | $\cdots$ | $\cdots$ | 49 | 33 | $\cdots$ | $\cdots$ | 4.4 | 3.6 |
| 96100 | 185144 | 23.2 | 1991-04-30 | 5 | 18 | 21 | 229 | 4.5 | 4.1 | 2.4 | 2.1 |
| 96441 | 185395 | 10.2 | 2001-07-21 | $\cdots$ | 223 | $\cdots$ | $\cdots$ | $\cdots$ | 57.1 | $\cdots$ | $\cdots$ |
| 98036 | 188512 | 27.2 | 1987-06-13 | 28 | 155 | 7 | 20 | 8.0 | 7.4 | 3.9 | 3.9 |
| 99461 | 191408 | 10.0 | 2004-08-20 | $\cdots$ | $\cdots$ | $\cdots$ | 45 | $\cdots$ | $\cdots$ | $\cdots$ | 2.3 |
| 104214 | 201091 | 27.1 | 1987-06-11 | 44 | 24 | $\cdots$ | 77 | 13.3 | 10.9 | $\cdots$ | 5.4 |
| 104217 | 201092 | 27.1 | 1987-06-12 | 30 | 26 | $\cdots$ | 74 | 17.0 | 11.7 | $\cdots$ | 7.0 |
| 112447 | 215648 | 23.3 | 1988-06-19 | 23 | 77 | $\cdots$ | $\cdots$ | 17.3 | 11.9 | $\cdots$ | $\cdots$ |
| 113357 | 217014 | 18.8 | 1995-10-12 | $\cdots$ | 202 | $\cdots$ | 41 | $\cdots$ | 6.2 | $\cdots$ | 2.4 |
| 114622 | 219134 | 21.9 | 1992-10-11 | 11 | 35 | 1 | 113 | 11.8 | 6.4 | $\cdots$ | 7.8 |
| 116771 | 222368 | 24.1 | 1987-09-08 | 30 | 23 | $\cdots$ | $\cdots$ | 52.7 | 134.5 | $\cdots$ | $\cdots$ |
| 14954 | 19994 | 24.1 | 1987-09-09 | 16 | 82 | $\cdots$ | $\cdots$ | 33.2 | 13.4 | $\cdots$ | $\cdots$ |
| 18859 | 25457 | 11.1 | 2002-08-29 | $\cdots$ | $\cdots$ | 7 | 14 | $\cdots$ | $\cdots$ | 27.5 | 16.9 |
| 29650 | 43042 | 10.9 | 2000-11-19 | $\cdots$ | 29 | $\cdots$ | $\cdots$ | $\cdots$ | 13.7 | $\cdots$ | $\cdots$ |
| 32480 | 48682 | 27.0 | 1987-09-10 | 16 | 74 | $\cdots$ | 48 | 13.0 | 10.2 | $\cdots$ | 4.4 |

This study is limited to Lick and Keck RVs gathered by the California Planet Search and its predecessor the California/Carnegie Planet Search. For a complete planet census and search completeness estimate, we urge other groups to undertake analyses for the historic Doppler measurements from the CFHT planet search (Walker et al. 1995), the Anglo-Australian Planet Search (Tinney et al. 2001), the ELODIE, CORALIE, and HARPS planet searches (Mayor et al. 2011), the McDonald planet search (Wittenmyer et al. 2006), the Lick giant star planet search (Quirrenbach et al. 2011), and others.


## 4. Doppler Planet Detection


A planetary orbit is defined by an orbital period $P$ (or semi-major axis $a$), eccentricity $e$, inclination to the line of sight $i$, argument of periastron $\omega$, and longitude of the ascending node $\Omega$ (see e.g., Murray & Dermott 1999). Imaging measurements of planetary (and stellar companions) consist of measuring the projected separation and position angle of the secondary relative to the primary source of light. Given a sufficient number, precision, and timing of such two-dimensional measurements, all five Keplerian orbital elements and the primary-secondary mass ratio can be inferred.

Doppler planet searches measure the line-of-sight velocity (radial velocity, RV) of the

Table 3—Continued

| Hipp. no. | HD no. | $t_{\rm span}$ (yr) | Start Date | Number of RVs | | | | RMS of RVs $(\mathrm{m\,s^{-1}})$ [a] | | | |
|---|---|---|---|---|---|---|---|---|---|---|---|
| | | | | Lick Dewars | | Keck Dewars | | Lick Dewars | | Keck Dewars | |
| | | | | p | l | k | j | p | l | k | j |
| 39780 | 67228 | 12.8 | 1998-12-26 | $\cdots$ | 39 | 16 | 21 | $\cdots$ | 11.8 | 16.5 | 8.9 |
| 40843 | 69897 | 21.4 | 1987-09-10 | 23 | 46 | $\cdots$ | $\cdots$ | 22.2 | 9.6 | $\cdots$ | $\cdots$ |
| 48113 | 84737 | 26.5 | 1987-06-13 | 22 | 66 | $\cdots$ | 44 | 14.2 | 7.8 | $\cdots$ | 3.4 |
| 53721 | 95128 | 27.1 | 1987-06-13 | 19 | 215 | $\cdots$ | 48 | 15.5 | 8.2 | $\cdots$ | 2.9 |
| 64408 | 114613 | 5.7 | 2007-05-26 | $\cdots$ | $\cdots$ | $\cdots$ | 24 | $\cdots$ | $\cdots$ | $\cdots$ | 5.9 |
| 64792 | 115383 | 21.7 | 1987-06-12 | 21 | 16 | $\cdots$ | $\cdots$ | 28.8 | 23.6 | $\cdots$ | $\cdots$ |
| 65721 | 117176 | 26.6 | 1988-02-03 | 21 | 98 | $\cdots$ | 54 | 9.5 | 9.1 | $\cdots$ | 3.5 |
| 73996 | 134083 | 21.0 | 1987-06-11 | 22 | 23 | $\cdots$ | $\cdots$ | 218.2 | 204.8 | $\cdots$ | $\cdots$ |
| 97675 | 187691 | 11.1 | 2000-09-09 | $\cdots$ | 15 | $\cdots$ | $\cdots$ | $\cdots$ | 15.2 | $\cdots$ | $\cdots$ |
| 109422 | 210302 | 15.1 | 1999-06-12 | $\cdots$ | $\cdots$ | 11 | 30 | $\cdots$ | $\cdots$ | 22.7 | 9.3 |

[a]The RMS of the RVs is computed as the standard deviation of the velocities after subtracting the signals discussed in Sec. 5.2.

bright primary star and over time fit the measurements with a Keplerian model. Doppler measurements are sensitive to $P$, $e$, and $\omega$, but not $i$ or $\Omega$. They also are sensitive to the Doppler amplitude $K$ and an orbital reference time (typically a time of periastron passage, $t_{\mathrm{p}}$, or a time of transit, $t_{\mathrm{c}}$). For a planetary system with $n$ planets, the stellar reflex velocity is the sum of Keplerian contributions from each planet,

$$v(t) = \sum_{j=1}^{n} \Big( K_j(\cos(\omega_j + f_j(t)) + e_j \cos\omega_j) \Big) + \gamma + \dot{\gamma} \cdot (t - t_0), \tag{1}$$

where the term in big parentheses refers to the Keplerian signal from planet $j$, $f_j(t)$ is the true anomaly of planet $j$ at time $t$, $\gamma$ is the time-independent velocity offset (often degenerate with instrument-specific velocity zero points), $\dot{\gamma}$ describes a linear velocity term ("slope," "trend," or constant acceleration, often from a massive, secondary companion whose orbit is only partially sampled), and $t_0$ is a conveniently chosen epoch of the observations. The assumption in Eq. 1 that the total Doppler signal is the superposition of each planet's contribution implies that the planets are not dynamically interacting with one another. This is a good assumption because detectable planet-planet interactions require planets to be near or in mean-motion resonances, which have only been detected for a handful of Doppler systems (e.g., Rivera et al. 2010; Tan et al. 2013), and those systems can be *discovered* using their Keplerian approximations (Eq. 1).

The true anomaly in Eq. 1 is defined implicitly in terms of the other three Keplerian parameters $P_j$, $t_{\mathrm{p},j}$, and $e_j$ through the relations

$$\tan\frac{f_j(t)}{2} = \sqrt{\frac{1 + e_j}{1 - e_j}} \tan\frac{E_j(t)}{2}, \tag{2}$$

$$E_j(t) - e_j \sin E_j(t) = \frac{2\pi(t - t_{\mathrm{p},j})}{P_j} = M_j(t). \tag{3}$$

Here $E_j$ is called the eccentric anomaly of planet $j$, $M_j$ is the mean anomaly, and Eq. 3 is Kepler's Equation. The Keplerian function $v(t)$ is sinusoidal for a single planet and $e = 0$, but the function becomes significantly cusp-like as $e \to 1$ and the planet's orbital speed varies dramatically over one orbit (Fig. 2). The RV semi-amplitude of the star, $K$, can be expressed in units of $\mathrm{m\,s^{-1}}$ with the planet mass in units of Jupiter masses ($M_{\mathrm{J}}$),

$$K = \frac{28.4\,\mathrm{m\,s^{-1}}}{\sqrt{1 - e^2}} \frac{M_p \sin i}{M_{\mathrm{J}}} \left(\frac{M_\star + M_p}{M_\odot}\right)^{-2/3} \left(\frac{P}{\mathrm{yr}}\right)^{-1/3}, \tag{4}$$

using Kepler's Third Law, $K \propto a^{-1/2}$. Thus, Doppler signals from giant planets in few AU orbits are of order $\sim 10\,\mathrm{m\,s^{-1}}$, while Neptune-mass planets and super-Earths produce

10–100× smaller signals. The timescales to discover a planet using Doppler velocities are daunting for $a$ larger than a couple AU; recall that Jupiter has $a = 5.2$ AU and $P = 11.9$ yr and Saturn has $a = 9.6$ AU and $P = 29.5$ yr.

Also note that $K \propto M_{\mathrm{p}} \sin i$, the planet's "minimum mass," where $\sin i$ is in the range 0–1 and accounts for the unknown orbital inclination $i$. For example, $i = 45°$ corresponds to
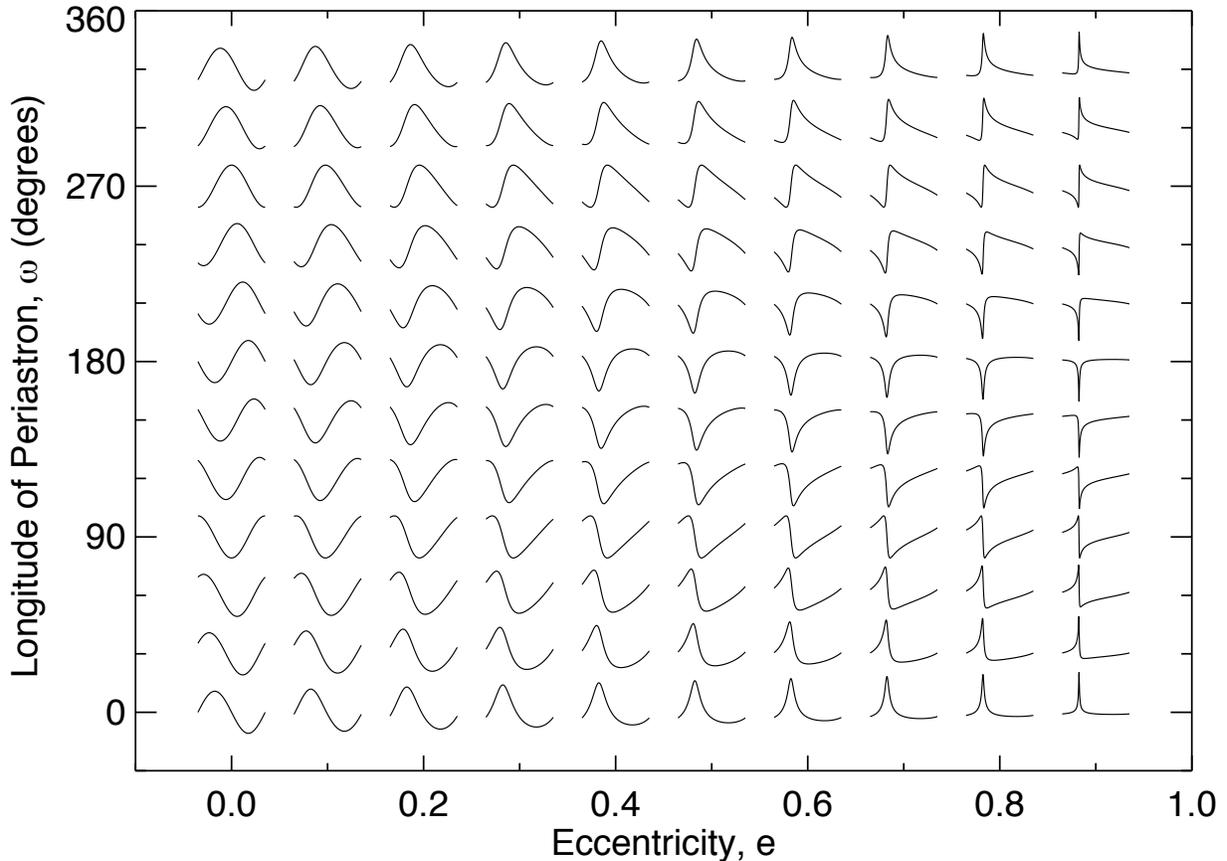


Fig. 2.— Keplerian function shape versus orbital eccentricity, $e$ (0-0.9 in 0.1 steps), and longitude of periastron, $\omega$ (0–330° in 30° steps). This function represents the Doppler shift of a planet host star. It is sinusoidal for $e = 0$, but becomes closer to a $\delta$-function as $e \to 1$. Orbits with $e \lesssim 0.4$ are reasonably well fit by sinusoids, but more eccentric orbits are increasingly less likely to be detected by orbit fitting techniques that assume circular orbits. Each curve represents a Keplerian function with unit amplitude ($K$), unit orbital period ($P$), and a time of periastron passage ($t_p = t_c + P/4$ is shown, where $t_c$ is a time of transit), evaluated on the grid of $e$ and $\omega$.

$\sin i = 1/\sqrt{2}$ and the true mass $M_{\mathrm{p}}$ being 41% larger than $M_{\mathrm{p}} \sin i$. Large $\sin i$ corrections are rare because orbital orientations are randomly distributed on the celestial sphere. (The distribution of $\cos i$ is uniform.) The statistical probability that the orbit inclination is within a range $i_1 < i < i_2$ is $P_{\mathrm{incl}} = |\cos(i_2) - \cos(i_1)|$. This means that 87% of orbits have $30° < i < 90°$, and $M_{\mathrm{p}}$ within a factor of two of $M_{\mathrm{p}} \sin i$. Randomly finding $i < 30°$ is equivalent to randomly selecting a location in the Northern Hemisphere with latitude $> 60°$, i.e. nearly in the Arctic Circle (latitude $= 66.5°$).

## 5. Radial Velocity Analysis

### 5.1. Automated Planet Search

We search for planets in the RV data using an iterative multi-planet detection algorithm based on the two-dimensional Keplerian Lomb-Scargle (2DKLS) periodogram (O'Toole et al. 2009). We create the periodogram by fitting a Keplerian RV model to the dataset at many starting points on a two-dimensional grid of $P$ and $e$. The primary advantages of the 2DKLS periodogram over the Lomb-Scargle periodogram (Lomb 1976; Scargle 1982) are that it is more sensitive to eccentric planets, and both measurement errors and zero point offsets between instruments ($\gamma_i$) can be incorporated directly into the periodogram.

We fit models to the data using the Levenberg-Marquardt (L-M) $\chi^2$-minimization in the RV fitting package (RVLIN, Wright & Howard 2009). Each RV model is a sum of single planet models ($P$, $t_{\mathrm{p}}$, $e$, $\omega$, and $K$), but with $\gamma_i$ (and $\dot{\gamma}$, if needed) shared by all planets (Eq. 1). We define a grid of search periods following the prescription of Horne & Baliunas (1986) for optimal frequency sampling. At each period we start an L-M fit at five eccentricities between 0.05 and 0.7. All parameters are free to vary in each fit, but $P$ and $e$ are constrained to intervals that allow them to vary only half the distance to adjacent search $P$ and $e$ ranges in parameter space. All parameters for any previously detected planets are simultaneously re-fit so that slightly incorrect fits (sometimes caused by the presence of other planets) do not lead to the false detection of additional planets. The periodogram power is

$$Z(P, e) = \frac{\chi^2 - \chi_B^2}{\chi_B^2},\qquad(5)$$

where $\chi^2$ is the sum of the squared, error-normalized residuals to the current $N$-planet Keplerian fit, and $\chi_B^2$ is for the best $N$-1-planet fit. In the first iteration of the planet search (comparing 1-planet models to a 0-planet fit), $\chi_B^2$ is simply the sum of the squared, error-normalized residuals to the mean or a linear fit.

We start the iterative planet search by fitting for any known planets in the system using the orbital parameters cataloged in the Exoplanet Orbit Database (Wright et al. 2011) and well-established planet candidates (Howard et al. 2014 in prep.) as initial guesses for RVLIN. We then look for a significant linear trend by fitting a line to the RVs and checking if the total change in RV due to the fitted line is greater than 10 times the median of the individual measurement errors. If a significant trend is detected we allow $\dot{\gamma}$ to vary at each point in the 2DKLS periodogram, or if no trend is detected we fix $\dot{\gamma} = 0$. For systems with known planets, we start by creating a periodogram to test if a $N+1$ planet model is a better fit than the model of $N$ known planets; otherwise we start by searching for a single planet and compare to the null hypothesis (the $N = 0$ planet model).

Since RV measurement errors are often underestimated due to the presence of systematic and/or poorly-understood astrophysical noise, periodogram power can not be directly converted into a significance estimate using traditional $\chi^2$ statistics. Instead we derive an empirical false alarm probability (FAP) by fitting a histogram of the periodogram amplitudes higher than the median power value to a linear function in $\log n$ vs. $\log Z$. This provides an estimate of the number of peaks that should fall above a given value, and when multiplied by the number of independent test periods, the approximate probability that we would find a peak of a given value within the particular periodogram. We use this to define a threshold of $\mathrm{FAP} = 1\%$ above which spikes in the periodogram are marked as a planet candidates and we continue searching for the next potential planet in the system. If no significant signals are detected, we stop the search.

If a periodogram peak is found to have an empirical FAP less than the 1% threshold some sanity checks are applied before it is considered a viable candidate. If greater than 20 peaks are found above the threshold we do not consider any of them viable unless the highest peak has an empirical $\mathrm{FAP} \leq 10^{-4}$. If the period corresponding to the highest peak is within 10% of the periods of any previously found planets we mask this period and continue searching for additional periods until none are above the FAP threshold or a viable candidate is identified at a different period. Finally, if the L-M fit seeded at the period corresponding to the highest peak outputs a period that is $\geq 50\%$ away from the input period we consider the period very poorly constrained and not a viable candidate.

Note that our empirical approach of estimating a FAP threshold differs from the bootstrapping strategy of scrambling RVs and searching for periodic signals in many realizations of the data, each with the RVs scrambled differently (e.g., Howard et al. 2010a). One advantage of our FAP calculation here is that time-correlated RV noise is reflected in the distribution of periodogram peak heights, while the scrambling technique does not preserve that information.
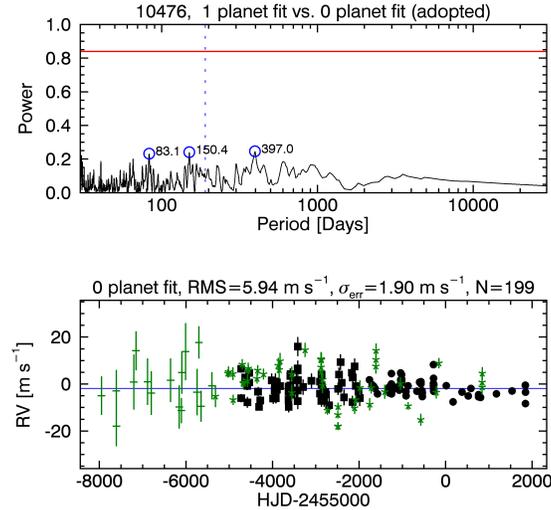
Fig. 3.— Two panel plot showing the results from an automated search for periodic signals in Lick and Keck RVs for the star HD 10476. Appendix C includes plots like this one for all stars without detected signals or Fig. 4 for stars with significant signals. *Top panel:* 2DKLS periodogram of the RVs from Lick and Keck. Periodogram power is calculated using Eq. 5 by comparing $\chi^2$ for prospective single planet fits having the range of periods on the horizontal axis to $\chi^2$ of the best-fit model without any planets (but with floating, telescope-specific RV zero points). The three most significant periodogram periods are labeled and circled in blue. In this case none of the peaks exceeds the 1% empirical FAP (solid red line) required for a solution to be adopted. The dashed vertical line marks the one year alias with the most significant peak (397 days). No planets were found significant in this fit, as indicated by "0 planet fit (adopted)" in the title of the top plot. *Bottom panel:* RVs as a function of time with $\gamma$ offsets between datasets minimized are plotted (the best-fit "0 planet fit"). The plot symbols are: green crosses (Lick "p"), green stars (Lick "l"), black squares (Keck "k"), black circles (Keck "j"). Annotations above the bottom panel indicate the RMS of the RVs, the median estimated Doppler uncertainty ($\sigma_{\rm err}$), and the number of RVs plotted ($N_{\rm obs}$).
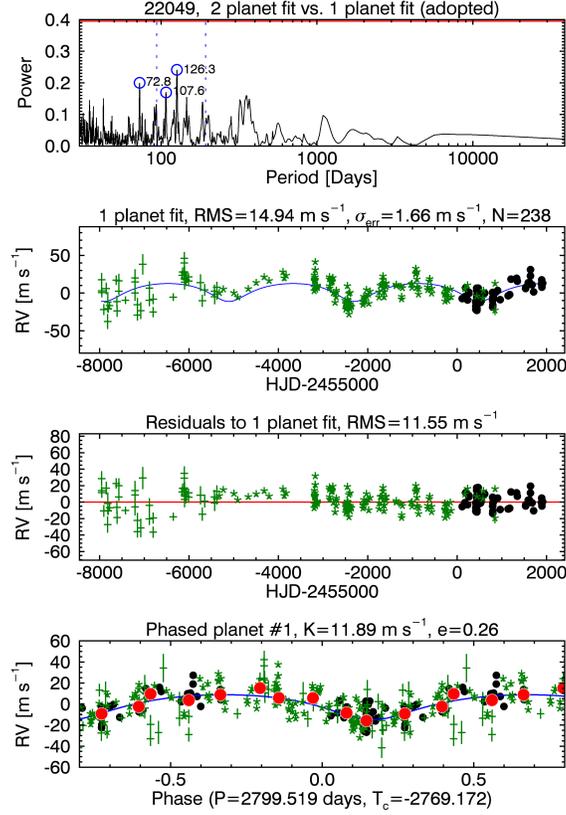
Fig. 4.— Four panel plot showing the results from an automated search for periodic signals in Lick and Keck RVs for the star HD 22049 ($\epsilon$ Eridani; see Sec. 5.2 for a discussion). Appendix C includes plots of this type for all stars with detected planets. *Top panel:* 2DKLS periodogram of the RVs from Lick and Keck, as in Fig. 3. Periodogram power is calculated using Eq. 5 by comparing $\chi^2$ for prospective two-planet fits having the range of periods on the horizontal axis to $\chi^2$ of the best-fit single planet model. The three most significant periodogram periods are labeled and circled in blue. In this case none of the peaks exceeds the 1% empirical FAP (solid red line) required for a solution to be adopted. The dashed vertical lines mark the one year aliases with the most significant peak (126.3 days). The single planet fit is adopted, as indicated by "1 planet fit (adopted)" in the title of the top plot. *Second panel:* RVs as a function of time with the best-fit single planet model overplotted (blue line). Plot symbols are the same as in Fig. 3. Annotations above the bottom panel indicate the RMS of the RVs, the median estimated Doppler uncertainty ($\sigma_{\rm err}$), and the number of RVs plotted ($N_{\rm obs}$). *Third panel:* RV time series showing residuals to the best-fit single planet model in the second panel. The RMS of these residuals is indicated in the panel title. *Bottom panel:* RVs phased at the period of the adopted single planet model (2799 days). The panel title lists $K$ and $e$ for this planet.

See Figure 3 for an example of the automated planet search algorithm on the star HD 10476. The example shows data from all four instrument codes and the search did not detect any credible planetary signals. Figure 4 provides a second example, in this case a search for a second planet orbiting HD 22049 ($\epsilon$ Eridani), which is known to host a single giant planet (Hatzes et al. 2000). A complete set of automated planet search plots for all stars in Table 2 is included in Appendix C.

## 5.2.  Known Signals in Doppler Data

The automated planet searches for each star describe the completeness of our Doppler data in a search for planets in addition to the already known planets. That is, the completeness limits are for an $N + 1$ planet model, compared to an $N$ planet model. We adopt the Exoplanet Orbit Database at exoplanets.org as the definitive source of "known planets" (Wright et al. 2011). In addition, we list below the other "known signals" (wide stellar binaries, activity correlations, etc.) that were seeded into our automated planet searches and that our completeness estimates are with respect to. We also list stars with interesting histories relevant to our RV planet searches. Not all stars with Doppler observations are listed below, only those with known signals/planets and a few for which we make comments.
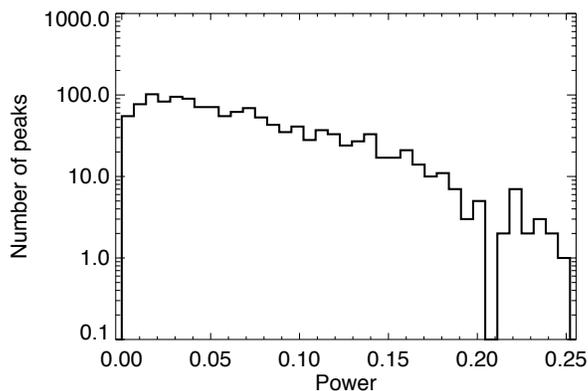


Fig. 5.— Distribution of 2KDLS periodogram peak heights for the HD 10476. (The periodogram is showing the top panel of Fig. 3.) We fit a linear profile to this distribution and define the FAP = 1% threshold as the periodogram power where the linear extrapolation intersects N = 0.01. As shown by the red line in the top panel of Fig. 3, this FAP threshold is at a power of $Z = 0.4$, well separated from the forrest of peaks that have a maximum value of $Z = 0.25$.

*HD 3651 (HIP 3093; program: S)*—Fischer et al. (2003) discovered an eccentric ($e = 0.63$) sub-Saturn mass planet with $P = 62$ day orbiting 54 Piscium. A T dwarf in a wide orbit was later discovered, making this the first known planetary system with an imaged brown dwarf (Mugrauer et al. 2006; Luhman et al. 2007; Liu et al. 2007). See Fig. 15.

*HD 4614 (HIP 3821; programs: S, C, A)*—$\eta$ Cassiopeiae shows a significant linear trend with no detectable curvature, presumably due to its K7V stellar companion, HD 4614B ($\eta$ Cassiopeiae B). See Fig. 16.

*HD 9826 (HIP 7513; programs: C, A)*—$\upsilon$ Andromedae hosts three known planets with masses of 0.67, 1.9, and 4.1 $M_J$ with orbital periods of 4.6, 241, and 1278 days (Butler et al. 1997, 1999; Wright et al. 2009). We detect an additional periodicity at $\sim$4000 days and interpret this as the signature of a stellar magnetic activity cycle. See Fig. 18.

*HD 10700 (HIP 8102; programs: S, C, A)*—$\tau$ Ceti is an extremely quiet RV standard star. Five low-mass planets were reported to orbit $\tau$ Ceti (Tuomi et al. 2013). However, we detect no periodic signals. The automated pipeline does detect a long-period signal but it appears to be caused by a poorly constrained offset between datasets. $\tau$ Ceti has long been an attractive planet search target because of its proximity (3.7 pc) and brightness ($V = 3.5$). Frank Drake (1961) started modern SETI by searching for radio signals from $\tau$ Ceti and $\epsilon$ Eridani. See Fig. 20.

*HD 16160 (HIP 12114; program: S)*—The RV time-series for this star shows significant curvature, likely from a late M-type companion (Golimowski et al. 1995a,b; Tanner et al. 2010). The RV curvature makes it difficult to detect small, long-period planets ($P \gtrsim t_{\text{span}}$) in this system. See Fig. 22.

*HD 17925 (HIP 13402; program: S)*—The automated pipeline detects a marginally significant linear trend in the RV time series. See Fig. 23.

*HD 19994 (HIP 14954; program: A)*—The star 94 Ceti hosts a giant planet in a 1.4 AU orbit Mayor et al. (2004). See Fig. 25.

*HD 22049 (HIP 16537; programs: C, A)*—$\epsilon$ Eridani is a young K2 dwarf that exhibits an RV period of $\sim$2500 days, interpretable as a Jovian-mass planet (Hatzes et al. 2000). This star is one of the best prospects for directly imaging planets (Marengo et al. 2009) due to the star's proximity (3.2 pc) and youth, and the detection of a debris disk (Greaves et al. 1998; Moran et al. 2004; Backman et al. 2009). The planet has remained controversial because of stellar magnetic activity (Metcalfe et al. 2013; Jeffers et al. 2014). However, our measurements of the activity-sensitive Ca II H & K lines (Isaacson & Fischer 2010) have a period of $\sim$3 yr

and do not correlate with RVs spanning 5 yr in our Keck spectra. See Fig. 27.

*HD 25457 (HIP 18859; program: A)*—This young, F6 dwarf is a T Tauri star and a member of the AB Dor moving group (López-Santiago et al. 2006). Ground-based direct imaging searches for planets having yielded non-detections to date, with planet mass limits of $\sim$7 $M_J$ at 1 AU (Maire et al. 2014). Our pipeline formally identifies a planet candidate based on 21 Keck RVs. Given the high jitter and small number of observations, we deem this candidate not credible with the current data. See Fig. 30.

*HD 30652 (HIP 22449; programs: S, C, A)*—$\pi^3$ Orionis hosts no known planets. We detect a marginally significant periodic signal with a period of 338 days. However, the poor observing history and the proximity of the period to one year, we conclude that this signal is not caused by a real planetary companion. The nature of the signal is most likely non-astrophysical in nature. Wittenmyer et al. (2006) did not detect companions in their McDonald Observatory Doppler search. See Fig. 33.

*HD 34411 (HIP 24813; programs: S, C, A)*—The automated pipeline picks up a long-period, high-eccentricity signal that is likely due to poorly constrained offsets between instruments for $\lambda$ Aurigae. See Fig. 36.

*HD 37394 (HIP 26779; program: S)*—This young star is in the Pleiades association (López-Santiago et al. 2006) and shows a small, marginally significant linear trend. See Fig. 37.

*HD 48682 (HIP 32480; program: A)*—56 Aurigae has a formally adopted signal that appears to be due to uncorrected zero-point offsets in the Lick RVs and not due a planet. See Fig. 39.

*HD 69830 (HIP 40693; program: S)*—This star hosts three Neptune-mass planets (Lovis et al. 2006). However, the automated pipeline can only pick out the planets at 8.7 and 197 days. While we do not detect the 31.6 day period in the Lick or Keck data, we have not performed an analysis to show that our non-detection is dispositive. See Fig. 41.

*HD 75732 (HIP 43587; program: S)*—55 Cancri hosts five known planets (Fischer et al. 2009) with at least one that transits (Winn et al. 2011). The orbital periods are $P = 0.74$, 14.6, 44, 260, and 5200 days. The middle three planets (b, c, and f) are approximately Saturn-mass while the innermost, transiting planet (e) is a super-Earth and the outermost planet (d) is a super-Jupiter. See Fig. 44.

*HD 84737 (HIP 48113; program: A)*—This star has a formally adopted signal that appears to be due to uncorrected zero-point offsets in the Lick RVs and not due a planet. See Fig.

46.

*HD 95128 (HIP 53721; program: A)*—47 Ursae Majoris has hosts two well-known giant planets with semi-major axes of 2 and 3.6 AU (Fischer et al. 2002), and possibly a third planet at ∼11 AU (Gregory & Fischer 2010). Our automated search prefers a model with three planets, although the outer most planet has a poorly constrained orbit. See Fig. 49.

*HD 100623 (HIP 56452; program: S)*—This star shows a significant linear trend with no detectable curvature. The Keck RVs (code = j) are very sparse and only 19 observations were collected in total for this star. See Fig. 50.

*HD 104304 (HIP 58576; program: S)*—This system shows a strong long-term linear trend with curvature, likely due to a detected low-mass, stellar companion (Tanner et al. 2010; Schnupp et al. 2010). Our automated search prefers a model with a linear velocity trend (constant acceleration) in addition to the orbit segment from the companion (three bodies total), with considerable model degeneracy between the slope and the mass of the companion causing the RV curvature. See Fig. 54.

*HD 115617 (HIP 64924; programs: S, C, A)*—Vogt et al. (2010) reported three small planets orbiting 61 Virginis with $P$ = 4.2, 38, and 124 days. We see evidence for only the first two planets in our Keck RVs. The inner planet b is a small super-Earth with a mass of 5.3 $M_\oplus$ and planet c is approximately Neptune-mass (19 $M_\oplus$). See Fig. 59.

*HD 117176 (HIP 65721; program: A)*—70 Virginis hosts a ∼7 $M_J$ planet in a 0.5 AU orbit (Marcy & Butler 1996). See Fig. 60.

*HD 120136 (HIP 67275; programs: S, C, A)*—$\tau$ Bootis b was one of the first exoplanets discovered (Butler et al. 1997). It is an extreme hot Jupiter with a mass 6 $M_J$ and an orbital period of 3.3 days. We also detect a significant linear trend in the RV data and a periodicity at ∼5000 days. However, due to the possibilities of offsets within the Lick data, it is difficult to trust a long-period signal in the Lick data alone (Fischer et al. 2014). The trend is likely real, but the 5000 day periodicity could be due to instrumental effects or a stellar magnetic activity cycle. See Fig. 61.

*HD 131156 (HIP 72659; program: S, C, A)*—$\xi$ Bootis A is a young (200 Myr), late G star in a binary stellar system with the late K star, $\xi$ Bootis B (Mamajek & Hillenbrand 2008) . The significant linear trend with no detectable curvature in the RV time series of $\xi$ Bootis A is likely due to the stellar companion. See Fig. 63.

*HD 131977 (HIP 73184; programs: S, C)*—This star has a significant linear RV trend, likely

due to a binary companion (Gl 570B). See Fig. 64.

*HD 161797 (HIP 86974; programs: S, C, A)*—The RV time-series for $\mu$ Herculis shows a strong linear trend and significant curvature (or a possibly closed orbit). $\mu$ Herculis is a hierarchical triple stellar system. The data can be well-fit by a Keplerian orbit with a period of 9800 days, but this is very poorly constrained and the period is likely to be much longer. See Fig. 73.

*HD 168723 (HIP 89962; program: C)*—The Lick data for $\eta$ Serpentis show a marginal linear trend while the long-baseline pre-upgrade Keck data does not show the trend. See Fig. 74.

*HD 185395 (HIP 96441; program: C, A)*—This early-type star (F4 V) has high jitter and a claimed, controversial planet with $P \approx 150$ days (Desort et al. 2009). We see evidence in our Lick data for RV variation at this period and other periods related by the yearly alias, however these signals are not statistically significant. See Fig. 79.

*HD 191408 (HIP 99461; programs: S, C, A)*—This star shows a slight linear trend with no detectable curvature, presumably due to its common proper motion companion LHS 487 (K4V). See Fig. 82.

*HD 201091 (HIP 104214; programs: S, C, A)*—61 Cygni A shows a strong linear trend caused by 61 Cygni B. Under the direction of Peter van de Kamp, Strand (1943, 1957) suggested that 61 Cygni A was orbited by one or two giant planets. These claims were later rejected by high precision RVs (Walker et al. 1995; Cumming et al. 2008). See Fig. 83.

*HD 201092 (HIP 104217; program: S)*—61 Cygni B shows a strong linear trend caused by 61 Cygni A. See Fig. 84.

*HD 217014 (HIP 113357; program: S)*—51 Pegasi is the host to the first known exoplanet; a hot Jupiter with a mass of 0.5 $M_J$ and an orbital period of 4.2 days (Mayor & Queloz 1995). We also detect a long-period signal but this is likely caused by instrumental offsets within the Lick dataset. See Fig. 87.

*HD 219134 (HIP 114622; programs: S, C)*—This star has candidate planets including a giant planet in a 3 AU orbit that we will continue to examine as more RVs are gathered.

## 5.3.   Injection-Recovery Completeness

To determine our sensitivity to planets as a function of $M_\mathrm{p}\sin i$ and $P$ we injected synthetic planetary RV signals into the real RV data for each star, preserving the actual times of observation and measurement uncertainties. We then used the iterative automated planet search algorithm (Sec. 5.1) to attempt to recover the injected signals. We injected planets on circular orbits uniformly distributed in $\log(K)$ and $\log(P)$ centered around the sensitivity threshold line determined from the method of Howard et al. (2010b). We did not study sensitivity as a function of eccentricity because $>80\%$ of known Doppler-discovered planets have $e < 0.4$ (Wright et al. 2011), for which a circular orbit approximation is adequate (Fig. 2).

We injected 5000 synthetic planets into the RV time-series for each star in the sample. The synthetic planets are injected in addition to any known planets in the system and the search algorithm starts by searching for one additional planet while simultaneously fitting for all known planets in the system. An injected planet is considered recovered if the highest peak in the periodogram is above the 1% FAP detection threshold, the period of that peak is within 25% of the injected period, and the phase of the recovered orbit is within $\pi/6$ of the injected phase. In some cases multiple planets are recovered when only a single planet is injected. We still consider these cases good recoveries if any of the detected periods are within 25% of the injected period.

Completeness contours are derived from the injection-recovery tests by computing a two-dimensional moving average of the recovery rate over a $100\times100$ grid in semi-major axis ($a$) and $M_\mathrm{p}\sin i$ with an averaging window of width 0.5 dex. Figure 6 shows an example completeness plot. The full set of completeness contours for all stars in the sample are in Appendix C.

In some cases anomalies are visible in the shape of the completeness contours derived from the injection-recovery tests. A feature of enhanced sensitivity is sometimes seen at long periods. This is caused by stellar magnetic activity masquerading as the injected planet. Although we require that the period of the recovered planet is within 25% of the period of the injected planet and the recovered phase is within $\pi/6$ of the injected phase, some of the injected planet signals will happen to look very similar to the magnetic activity signal. Planets that are well below the local completeness threshold will still be "recovered" when the algorithm finds the magnetic activity cycle as the most significant periodic signal and finds that it has the correct period and phase to match the injected signal. This situation can occur in $\lesssim 10\%$ of cases and can corrupt the 16% and 84% completeness contours. In other cases narrow spikes of decreased sensitivity are seen well above the local completeness
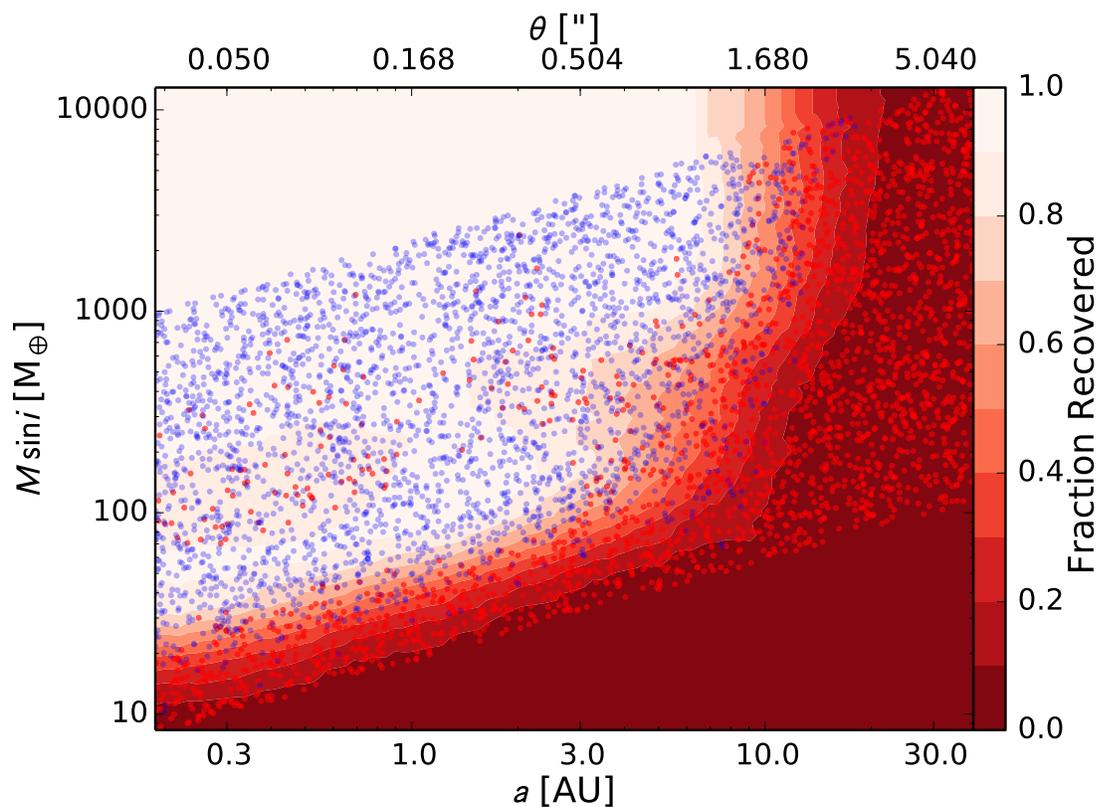
Fig. 6.— Example completeness plot for HD 4614 showing the results of our injection/recovery tests. Blue dots indicate the $M_{\rm p}\sin i$ and $a$ combinations of injected planets that were successfully recovered by our automated planet search, while red dots indicate injections that were not recovered. The contours are computed from a two-dimensional moving average over a $100{\times}100$ grid with window widths of 0.5 dex in $M_{\rm p}\sin i$ and $a$. Completeness in regions of the grid outside the limits of the injection-recovery tests are extrapolated vertically along columns from the nearest point in the grid that contains at least 20 injections within the averaging window. Appendix C includes a completeness plot for every star with Doppler measurements.

threshold. This occurs in systems with known planets. For example, see Fig. 44. When a planet is injected at nearly the same period as a known planet, it can be absorbed by the fit for the known planets. Fortunately for the estimate, it is unlikely that two planets with very similar orbital periods could remain dynamically stable. Kepler-36bc has the smallest period ratio detected to date with $P_c/P_b \simeq 7/6$ (Carter et al. 2012).

The one-dimensional contours provided in machine-readable tables as a supplement to this report were derived by scanning the 2D completeness grid column-by-column starting at low then progressively higher $M_\mathrm{p} \sin i$ values until recovery rates of 16%, 50%, and 84% are first reached. We report $M_\mathrm{p} \sin i$ as a function of $P$, $a$, and projected on-sky separation ($\theta$) for each of the three 1D completeness lines which corresponds to the minimum $M_\mathrm{p} \sin i$ that is detectable in the given fraction of injections. In separate machine-readable files, we include the two-dimensional completeness for each star using the grid of semi-major axes and $M_\mathrm{p} \sin i$ values in the completeness plots. See Appendix A.

Appendix C includes completeness estimates for every star with RVs.

## 5.4.  Summary Results

Figures 7 and 8 summarize the results of our completeness estimates. Figure 7 shows the 50% detection thresholds for every star in the sample, with the median completeness contour shown in red. Note that the completeness contours span more than order of magnitude in $M_\mathrm{p} \sin i$, while having similar shapes. This variation is mostly due to the differing jitter values for stars observed in the Lick and Keck surveys. Figure 8 summarizes the full set of contours, slicing in both $M_\mathrm{p} \sin i$ and semi-major axis.

## 5.5.  Idealized Completeness

An idealized Doppler planet search can be characterized by the number of observations ($N_\mathrm{obs}$), their time span ($t_\mathrm{span}$), and the precision of a single measurement ($\sigma_\mathrm{RV}$). Precision stems from astrophysical noise sources ("jitter") that produce apparent Doppler shifts and measurements uncertainties stemming from the signal-to-noise ratio and the Doppler information content (number of lines, $v \sin i$, etc.) of each spectrum. In practice, $\sigma_\mathrm{RV}$ for a particular star can be empirically estimated as the standard deviation of the RVs measured over a long time span (assuming no orbital companions are present). That is, single measurement errors are approximately the measurement scatter. To improve sensitivity, several
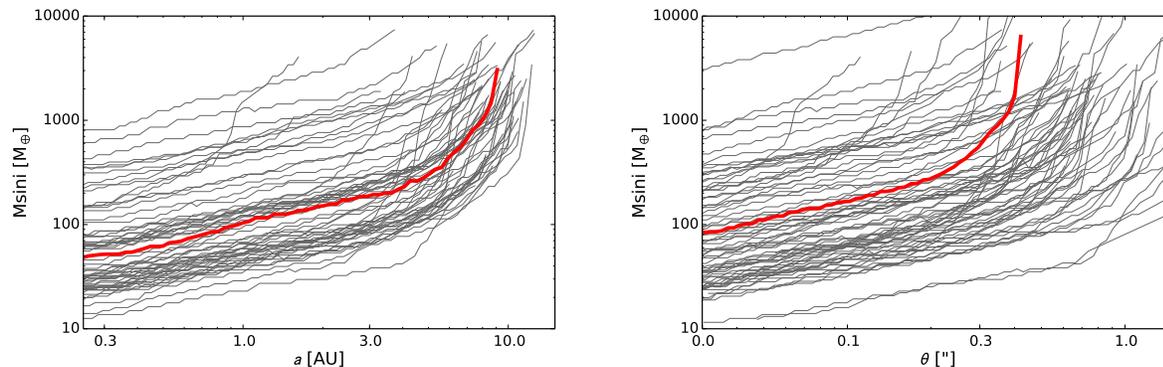
Fig. 7.— Contours showing 50% completeness for every star with Doppler measurements (gray lines) and the median of those contours (red line). The panels show the same completeness curves as a function of semi-major axis (left) and projected separation (right).
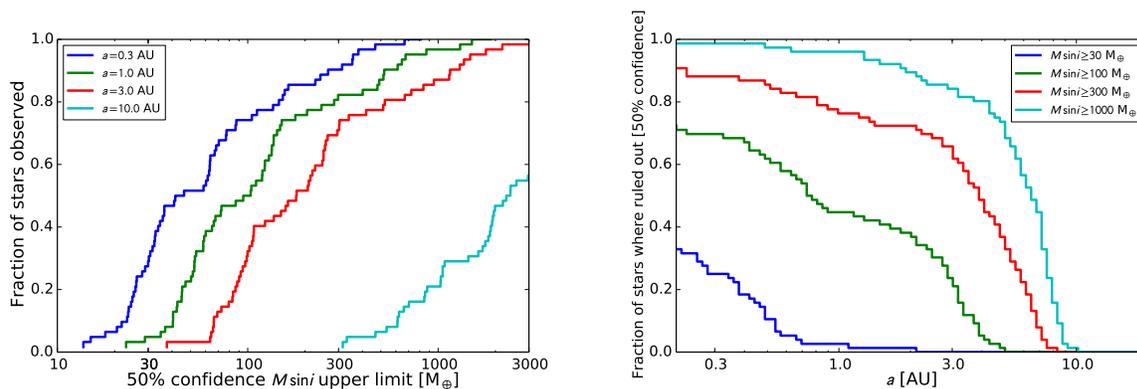


Fig. 8.— Fraction of stars observed by Lick/Keck Planet Searches whose RV observations can exclude planets of particular masses and semi-major axes. The left panel depicts the mass upper limits ($M_{\mathrm{p}} \sin i$ at 50% confidence) at four semi-major axes while the right panel shows the fractions of stars with ruled out companions for four $M_{\mathrm{p}} \sin i$ values, as a function of semi-major axis.

RVs of the same star are often gathered on a given night to average over stellar noise and to improve signal-to-noise. In such cases, $\sigma_{\mathrm{RV}}$ represents the scatter in the nightly averages (or the appropriate binning timescale).

In the limit of large $N_{\mathrm{obs}}$, uniform orbital phase coverage (random times of observation), and an orbital period $P < t_{\mathrm{span}}$, 50% completeness can be characterized by a Doppler amplitude $K_{50}$ that is related to the survey parameters by

$$K_{50} = \alpha \frac{\sigma_{\mathrm{RV}}}{\sqrt{N_{\mathrm{obs}}}}, \tag{6}$$

where $\alpha$ is a dimensionless parameter that represents the signal-to-noise ratio of a detectable plant, accounting for $\sqrt{N_{\mathrm{obs}}}$ measurements. Naively, we expect $\alpha$ to be greater than one and of order a few. We estimated $\alpha$ using three techniques described below.

First, we estimated $\alpha$ using the completeness plots in Appendix C using $N_{\mathrm{obs}}$ and $t_{\mathrm{span}}$ from our measurements and taking $\sigma_{\mathrm{RV}}$ to be the RMS of the RVs after subtracting all significant signals. Using this technique we found $\alpha$ in the range $\sim$5–20. This range accounts for the ways that real observations violate our assumptions of the idealized survey: telescope/instrument combinations have heterogenous Doppler precision (choosing the "typical" $\sigma_{\mathrm{RV}}$ difficult to estimate), RV zero point offsets between datasets must be fitted for, and non-random observing cadences. Nevertheless, this factor of four range in $\alpha$ suggests that we might simulate completeness with similar mass precision simply by estimating survey and stellar parameters.

Our second method to estimate $\alpha$ was calculating completeness for an ideal observing campaign. Note in Eq. 6 that $K_{50}$ and $\sigma_{\mathrm{RV}}$ have the same units and scale linearly with one another. Searching for a $K = 10$ m s$^{-1}$ signal with $\sigma_{\mathrm{RV}} = 1$ m s$^{-1}$ precision is equivalent to searching for a $K = 100$ m s$^{-1}$ signal with $\sigma_{\mathrm{RV}} = 10$ m s$^{-1}$. Making the problem dimensionless, we define a survey sensitivity,

$$\kappa_{50} = \frac{K_{50}}{\sigma_{\mathrm{RV}}} = \frac{\alpha}{\sqrt{N_{\mathrm{obs}}}}, \tag{7}$$

that is valid for dimensionless orbital periods $\tau = P/t_{\mathrm{span}} \lesssim 1$.

We tested and calibrated this idealized completeness model with injection-recovery simulations. Fig. 9 shows the simulation results and their parameters, with the plots demonstrating that $\kappa \propto K/(\sigma_{\mathrm{RV}} \cdot \sqrt{N_{\mathrm{obs}}})$. $\kappa_{50}(\tau)$ is flat in these three simulations for short period orbits. Based on these simulations, we estimate $\alpha \approx 6$. For $\tau \gtrsim 1.5$, the $\kappa_{50}$ contour rises rapidly; we estimate a slope of $\sim$10 and $\kappa_{50}(\tau) = \alpha \cdot 10^{\tau-1.5}/\sqrt{N_{\mathrm{obs}}}$. We can combine these two functions smoothly using quadrature addition,

$$\kappa_{50}(\tau) = \frac{\alpha}{\sqrt{N_{\mathrm{obs}}}} \cdot \sqrt{1 + (10^{\tau-1.5})^2}, \tag{8}$$
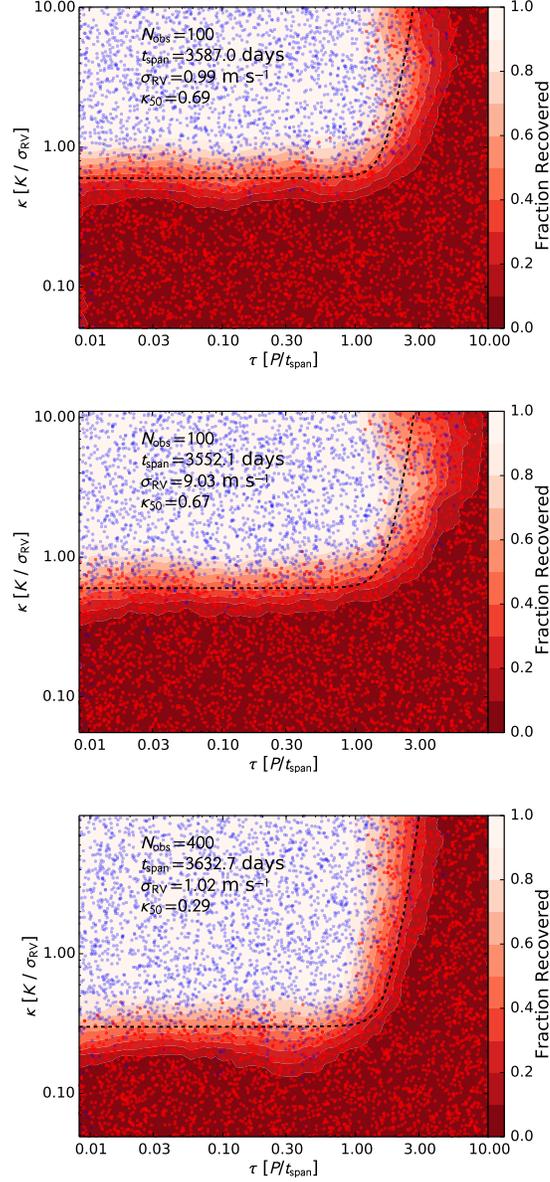
Fig. 9.— Planet search completeness in dimensionless Doppler amplitude $\kappa = K/\sigma_{\rm RV}$ versus dimensionless orbital period $\tau = P/t_{\rm span}$ for three idealized observational surveys. The survey parameters are: $N_{\rm obs} = 100$, $\sigma_{\rm RV} = 1 \ {\rm m\,s}^{-1}$, $t_{\rm span} = 10$ yr (top); $N_{\rm obs} = 100$, $\sigma_{\rm RV} = 10 \ {\rm m\,s}^{-1}$, $t_{\rm span} = 10$ yr (middle); $N_{\rm obs} = 400$, $\sigma_{\rm RV} = 1 \ {\rm m\,s}^{-1}$, $t_{\rm span} = 10$ yr (bottom). The three surveys give consistent $\alpha = \kappa_{50} \cdot \sqrt{N_{\rm obs}} \approx 6$ for $\tau < 1$, showing that idealized completeness is scale invariant (see caveats in Sec. 5.5). Dashed black lines show $\kappa_{50}(\tau)$ estimated from Eq. 8.

giving

$$K_{50}(\tau) = \frac{\sigma_{\mathrm{RV}}\,\alpha}{\sqrt{N_{\mathrm{obs}}}} \cdot \sqrt{1 + (10^{\tau - 1.5})^2}. \tag{9}$$

Eq. 9 nicely encapsulates the 50% percentile search completeness as a function of a three observational parameters: $\sigma_{\mathrm{RV}}$, $N_{\mathrm{obs}}$, and $t_{\mathrm{span}}$. However, the simplistic form is only a fit to an idealized observational campaign and is likely accurate to a factor of a few (perhaps good enough for planning observations). Real life observing is more complicated. One should consider the following caveats when applying this idealized completeness model:

1. Measurement errors are rarely Gaussian distributed. Velocity errors from stellar jitter and instrument systematics are often time correlated. Periodic astrophysical noise sources (i.e., magnetic activity cycles) can masquerade as planets and/or the hinder detectability of small planets. Thus, $\sigma_{\mathrm{RV}}$ doesn't fully encapsulate the Doppler noise sources.

2. Times of observation are non-random, depending on daily, monthly, and yearly cycles, not to mention scientific interests and the vicissitudes of telescope time allocation committees. Our assumption of uniform phase coverage (from random times of observation and large $N_{\mathrm{obs}}$) is rarely achieved for real surveys. Non-randomly timed clusters of observation times inject period aliases into the periodograms, which can suppress or enhance the detectability at particular periods (Dawson & Fabrycky 2010). Furthermore, combining RVs from multiple telescopes can reduce sensitivity to long-period signals since such signals can be absorbed into the fitted zero-point offsets.

3. Completeness estimates using quantified detection criteria often fail to account for human evaluation of data. Many observers are cautious about announcing planet discoveries, having seen instrumental systematics and correlated astrophysical noise exceed their prior expectations.

Our third method of estimating $\alpha$ involves examining the parameters of known planets on exoplanets.org (Wright et al. 2011). Fig. 10 shows estimates of $\kappa$ and $\alpha$ for planets with Doppler-measured masses with 100 pc. Only a handful of planets having been discovered with $\kappa < 1$, i.e. a signal smaller than the noise. Such planets include $\alpha$ Cen Bb (Dumusque et al. 2012) and HD 156668b (Howard et al. 2011a). Our estimate of $\alpha \gtrsim 6$ for successful detection based on injection-recovery simulations appears to be slightly optimistic compared to the distribution of discovered planets that have a discovery threshold of $\alpha \gtrsim 10$ more commonly. Note that Fig. 10 plots $\kappa$ and $\alpha$ that are defined slightly differently than in Eq. 7 and 9. The figure shows the Doppler amplitude $K$, not the 50% completeness value
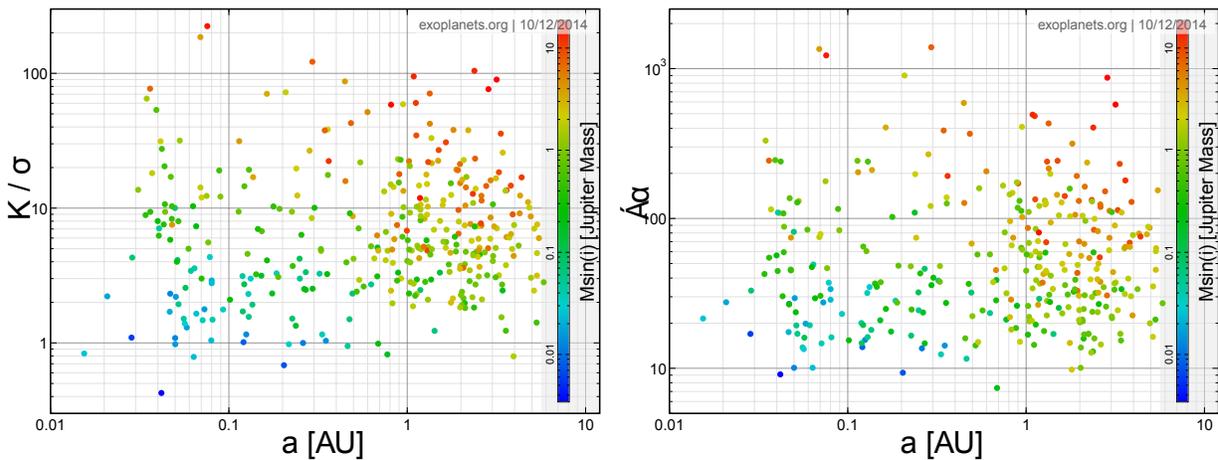
Fig. 10.— Distributions of $\kappa = K/\sigma_{RV}$ (left) and $\alpha = \sqrt{N_{obs}}\,K/\sigma_{RV}$ (right) vs. semi-major axis $a$ for real planets within 100 pc with Doppler-measured masses on exoplanets.org (Wright et al. 2011). Point color indicates $M_p \sin i$.

$K_{50}$. And $N_{obs}$ is the number of measurements in the "orbit reference" paper (ORBREF on exoplanets.org), not the number of measurements when the planet was first detectable. Still, the discovery of some exoplanets with $\alpha \approx 10$ suggests that our estimate of $\alpha \approx 6$ is not wildly off.

## 5.6. Prospective Completeness for Unobserved Stars

For stars without Doppler observations, it is often helpful to estimate the sensitivity of a prospective Doppler campaign. With the above caveats in mind, we can use the idealized completeness formalism of Sec. 5.5 to estimate completeness. The campaign is characterized by $N_{obs}$ and $t_{span}$, while the the RV observations are characterized by $\sigma_{RV}$. The general procedure to estimate the 50% completeness in mass as a function of semi-major axis, $M_p \sin i_{50}(a)$, is:

1. Choose $N_{obs}$ and $t_{span}$ for the survey. Choose a star with a particular $M_\star$ and estimate $\sigma_{RV}$ from the expected jitter and measurement uncertainties.

2. Compute $K_{50}(P)$ from Eq. 9 using $\alpha = 6$ (idealized simulations) or $\alpha = 10$ (the threshold of detection for historical discoveries).

3. Convert $K_{50}(P)$ into a 50% mass contour $M_p \sin i_{50}(P)$ using the inverted form of Eq. 4

for circular orbits,

$$\frac{M_p \sin i_{50}(P)}{M_{\mathrm{J}}} = \frac{K_{50}(P)}{28.4\,\mathrm{m\,s^{-1}}} \left(\frac{M_\star + M_p}{M_\odot}\right)^{2/3} \left(\frac{P}{\mathrm{yr}}\right)^{1/3}. \tag{10}$$

For planetary mass companions ($M_\star \gg M_p$), the first term in parentheses simplifies to $(M_\star/M_p)^{2/3}$.

4. Convert $P$ to $a$ using Kepler's Third Law, $a = (GM_\star P^2/4\pi^2)^{1/3}$, again assuming $M_\star \gg M_p$.

Computing idealized completeness for all unobserved stars (Table 4) requires good estimates of $M_\star$ and $\sigma_{\mathrm{RV}}$ for every star. $M_\star$ could be reasonably estimated from photometry and other sources, but the expected RV scatter, $\sigma_{\mathrm{RV}}$, is difficult to estimate accurately without a detailed study of each star. In lieu of detailed completeness estimates for every star in Table 4, we provide the above recipe for estimating completeness with due caution that the $M_p \sin i_{50}(P)$ limits scale linearly with $\sigma_{\mathrm{RV}}$. Underestimated astrophysical and/or measurement errors will give false hope for planet detectability.

Stars were not included in our historical Lick/Keck Doppler search for several reasons enumerated in Table 4. These include: the star is too far South for Keck/Lick; the star has evolved into a subgiant or giant; the star is earlier spectral type than $\sim$F8V; the star is young and chromospherically active; and the star is a spectroscopic binary. We discuss the expected Doppler precision $\sigma_{\mathrm{RV}}$ for each class below.

**Southern Hemisphere**—Many excellent main sequence G and K dwarfs are simply too far South to be easily observed at Keck and/or Lick Observatory (the cutoff is $-30°$ to $-40°$ declination). Observations of these stars could yield completeness curves comparable to our best cases in Fig. 7. Other teams are likely observing many of these stars (e.g., Mayor et al. 2011).

**Early Spectral Type**—Spectral types earlier than $\sim$F8V have a decreasing density of spectral lines and an increasing average $v \sin i$, both of which degrade Doppler precision to $\gtrsim 5$ m s$^{-1}$ for the sample identified for Lick and transferred to Keck. Galland et al. (2005) developed a Doppler planet search for A–F stars. They measured the RV scatter for a sample of stars observed with ELODIE and HARPS finding an RV scatter of $\sigma_{\mathrm{RV}} \approx 0.16 \times v \sin i^{1.54}$ (for ELODIE observations with S/N = 200). This relationship provided an accurate precision forecast at the factor of two level. The $v \sin i$ scaling to the $\sim$1.5 power is consistent with a study by Bouchy et al. (2001) on the fundamental photon noise limit to radial velocity measurements, in the case of early F type main sequence stars. In the examples below,

we adopt the Galland et al. (2005) prescription for $\sigma_{\mathrm{RV}}$. Note however that this relation fails for late A and early F type stars ($B - V$ between 0.2 and 0.4) that are often highly RV variable. This $B - V$ range corresponds to the intersection of the instability strip and the main sequence, where pulsators including $\delta$ Scuti and $\gamma$ Doradus stars are found. The most massive stars in the Exo-C/Exo-S/AFTA target lists are B stars ($B - V < 0$; Fig. 1). Doppler measurements have achieved $\sigma_{\mathrm{RV}} = 0.8$ to 2.0 km s$^{-1}$ for such targets, depending on $v \sin i$ (J. Johnson, personal communication).

**Evolved Stars**—Surface gravity is reduced as stars evolve off the main sequence. The resulting surface oscillations produce RV variations that can be used to measure precise stellar properties (asteroseismology), and that serve as a noise source for Doppler planet searches. Kjeldsen & Bedding (1995) estimated the Doppler oscillation amplitude, finding a dependence on the light-to-mass ratio, $v_{\mathrm{osc}} = 0.234(L_\star/M_\star)$ m s$^{-1}$. We adopt this estimate of $v_{\mathrm{osc}}$ for $\sigma_{\mathrm{RV}}$ for giant stars. As a check, this formula predicts $v_{\mathrm{osc}} = 6$ m s$^{-1}$ for Pollux and Reffert et al. (2006) observed an RV scatter of 9 m s$^{-1}$, which is the level of agreement we expect for estimates like these.

**Young Stars**—Line shape distortions due to rotationally modulated stellar surface features (e.g., spots and plage) make young stars difficult targets for planets searches (Crockett et al. 2012). Hillenbrand et al. (2014) measured the RV scatter for a set of young stars observed by HIRES, finding $\sim$100 m s$^{-1}$ scatter for young stars ($\sim$30 Myr) with the activity measure $\log R'_{\mathrm{HK}} = -4.0$, and RV scatter decreasing approximately linearly with $\log R'_{\mathrm{HK}}$ to $\sim$3 m s$^{-1}$ for old, quiet stars with $\log R'_{\mathrm{HK}} = -5.0$.

**Spectroscopic Binaries**—Spectroscopic binaries are routinely excluded from Doppler surveys because their spectra cannot be modeled by standard cross-correlation or forward-modeling techniques. However, techniques developed by Konacki et al. (2009) show promise for detecting $\sim M_{\mathrm{J}}$ planets for close-in orbits and several $M_{\mathrm{J}}$ planets for $\sim$AU orbits. We decline to provide specific advice for the expected Doppler precision and completeness for these stars since such estimates would be highly uncertain.

Using the above estimates for $\sigma_{\mathrm{RV}}$, we computed prospective completeness curves for eight stars that are representative of the imaging targets that lack Doppler measurements. These idealized completeness curves are based on a hypothetic survey with $n_{\mathrm{obs}} = 100$ and $t_{\mathrm{span}} = 10$ yr and $\sigma_{\mathrm{RV}}$ dependent on stellar characteristics. See Fig. 11, which includes four early type stars ($\beta$ Leo, A3V; $\rho$ Gem, F0V; HD 195689, A0V; RR Lyr, F0V, pulsator), a quiet dwarf in the Southern Hemisphere (p Eri A, K0V), and and the three brightest giant stars in Table 4 (Arcturus, K0III; Aldebaran, K5III; Pollux, K0III). These simulations suggest that giant planets orbiting giant stars in $\sim$AU orbits can be detected by dedicated Doppler

campaigns, as indeed they have been (e.g., Quirrenbach et al. 2011; Trifonov et al. 2014). Estimating completeness for all stars in Table 4 can be obtained by applying the formulas for $\sigma_{\rm RV}$ (above) or measuring it directly (preferred), estimating $M_\star$ for each star, and carefully identifying pulsating and young stars that will be particular unpredictable.

## 6.   Recommendations for Future Doppler Surveys

### 6.1.   Limits to Doppler Precision

The Doppler uncertainty of a single measurement is often expressed as the quadrature sum of three terms: stellar jitter, Poisson uncertainty stemming from the signal-to-noise ratio of the spectrum and the information content in spectrum (Bottom et al. 2013), and instrumental uncertainty.

Next-generation Doppler instruments are pushing for $\leq 0.5$ m s$^{-1}$ precision (e.g., Pepe et al. 2014) with the ultimate goal of reaching $<0.1$ m s$^{-1}$ precision (Pepe & Lovis 2008; Pasquini et al. 2010). These are engineering challenges that will only bear fruit if the stars
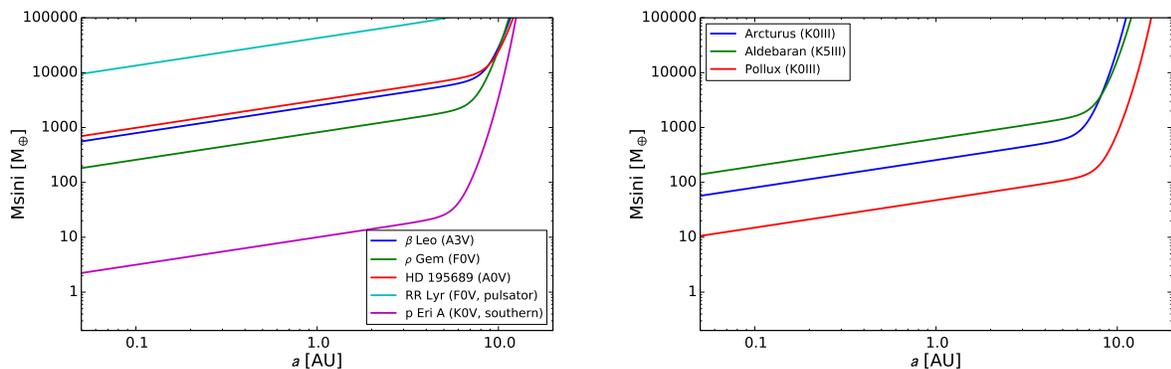


Fig. 11.— Simulated planet sensitivity thresholds, $M_p \sin i_{50}(P)$, for a representative sample of early-type and Southern Sun-like stars that were not observed by the Lick and Keck planet searches (left) and evolved stars (right). See Sec. 5.6 for details on the selected stars and the method to compute the sensitivity thresholds. We adopt $\alpha = 6$ for these plots. These predictions depend critically on the estimated RV scatter, $\sigma_{\rm RV}$, which is uncertain at the factor of two or more level for most stars. The excellent sensitivity for p Eri A ($\sim 10$ $M_\oplus$ at 1 AU) is driven by our adopted $\sigma_{\rm RV} = 1$ m s$^{-1}$, a factor of 2–2.5 better than we routinely achieve with HIRES. See also the caveats to the idealized completeness method in Sec. 5.5.

themselves are quiet enough for planet detection at those levels.

Stellar jitter represents a major challenge for Doppler planet detection. All stars except for old G and K dwarfs have jitter that precludes the the detection of small planets in few AU orbits (Fig. 11). There are many sources of jitter. Acoustic oscillations including p-modes cause the stellar surface to oscillate with a characteristic timescale of a few minutes and a characteristic amplitude of $\sim 1$ m s$^{-1}$ for Solar-type stars. The convective overturning of granules on the stellar surface (granulation) changes the flux balance between sinking cool regions and rising hot cells, producing a jitter of a similar scale. These effects can be mitigated by observational strategies that average over the relevant timescales with multiple RV measurements taken per night (Dumusque et al. 2011a,b). Jitter from rotationally modulated stellar surface features (spots, plate, faculae) cause apparent Doppler shifts due to distorted line profiles at the $\sim 1$ m s$^{-1}$ level even for quiet stars. These signals can be mitigated by measuring stellar activity proxies and de-correlating the RVs (Dumusque et al. 2011c). In some sense, these short-term jitter signals are less troublesome for searches for long-period planets. Short-timescale jitter sets an error floor for single measurements, but multiple measurements on the appropriate timescales can average over these noise sources.

Long-term magnetic cycles analogous to our Sun's activity cycle pose perhaps the greatest challenge in the search for long-period planets (Isaacson & Fischer 2010; Lovis et al. 2011). Coherent, nearly sinusoidal Doppler shifts of a few m s$^{-1}$ amplitude with 5–20 yr periods are common even for "inactive" G and K dwarfs and have led to a small number of apparent false planet claims. For example, one of the best Jupiter analog exoplanets is HD 154345 b (Wright et al. 2008), whose existence has been questioned because of a strong correlation between the RVs and the $S_{HK}$ measure of stellar activity. Current Doppler planet searches routinely monitor activity diagnostics, including the Ca II H & K lines (from which the $S_{HK}$ values are derived) and the width and bisectors of the spectrum's cross correlation function. Figure 12 shows two example stars form our Keck-HIRES planet search. Both are "inactive stars." The top star (HD 14412) has a $K \approx 3$ m s$^{-1}$ signal with $P \approx 6$ yr, the signature of an apparent Saturn-mass planet. This signal is mirrored in the $S_{HK}$ time series, which has the same period and phase as the RVs. The bottom star (HD 23439) is even less active and has no detectable variation in $S_{HK}$, and a reduced overall jitter.

Doppler planet searches are pushing the sensitivity limits by modeling and subtracting jitter, de-correlating it, selecting spectral lines and regions less sensitive to jitter, and selecting low-jitter stars for searches. For imaging search to take advantage of Doppler searches with $K \lesssim 0.5$ m s$^{-1}$ sensitivity, these developing techniques must be incorporated.
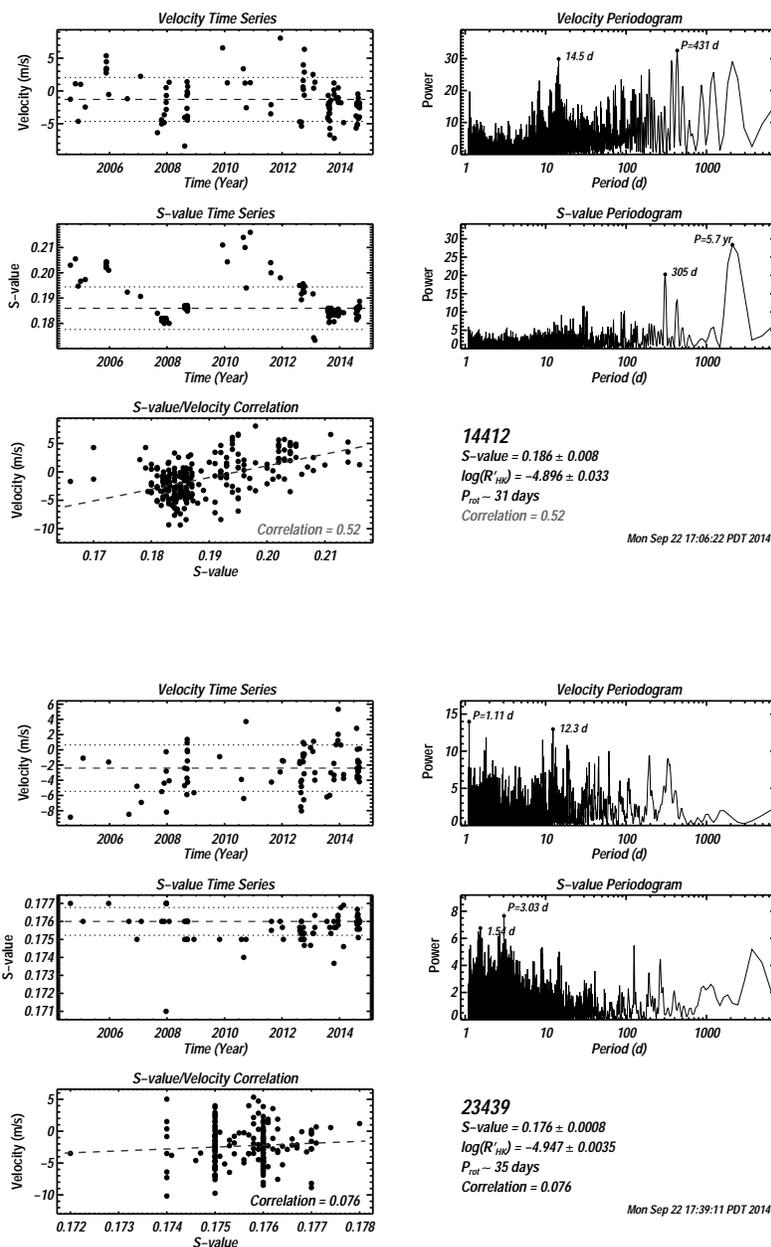
Fig. 12.— Automated reports on the correlations between RVs and $S_{\mathrm{HK}}$ activity measurements for two stars observed by the California Planet Survey using Keck-HIRES. Each six-panel plot (HD 14412 – top; HD 23439 – bottom) shows the RV time series (top left) and its periodogram (top right), the $S_{\mathrm{HK}}$ time series (middle left) and its periodogram (middle right), a linear correlation between them (lower left), and annotations (lower right). Both stars are considered "inactive," yet HD 14412 displays a clear RV–$S_{\mathrm{HK}}$ correlation resulting in ∼3 m s$^{-1}$ jitter with a timescale of 5.7 yr (presumably the stellar rotation period). HD 23429 is less active (log $R'_{\mathrm{HK}}$= −4.95 vs. −4.90) and has no detectable RV–$S_{\mathrm{HK}}$ correlation.

## 6.2.   Ten Year Forecast

We estimated the improvement in completeness that could be produced by continuing our Doppler observations for the next ten years. Fig. 13 shows our current completeness estimates (top row) for two stars observed at Keck (but not Lick). HD 102365 (left column in Fig. 13) is one of the most poorly observed stars in our sample with only $N_{\rm obs} = 16$ measurements spanning the last 6.6 yr with an RMS of 2.5 m s$^{-1}$. (It has been poorly observed because it is relatively far South, $\delta \simeq -40°$.) HD 182572 (right column in Fig. 13) has $N_{\rm obs} = 82$ measurements spanning 17.8 yr with an RMS of 4.0 m s$^{-1}$ (3.6 m s$^{-1}$ for HIRES instrument code j).

The Fig. 13 plots also show the results of two simulations. In the middle row, we simulated adding $N_{\rm obs} = 30$ measurements over 10 yr to the existing RVs with $\sigma_{\rm RV}$ of the new measurements equal to the RMS of the most recent HIRES RVs (code = j). This simulation represents the improvement in completeness from continuing observations with the current precision and a cadence of $N_{\rm obs} = 3$ RVs per year.

The bottom row of Fig. 13 shows the gain in completeness resulting from improved Doppler precision. Here we adopted $\sigma_{\rm RV} = 0.5$ m s$^{-1}$ with $N_{\rm obs} = 100$ over 10 yr. This level of precision is possible, but on the cutting edge. It requires the most Doppler quiet stars— old, choromospherically inactive late-G and early-K dwarfs—and observational strategies that average over stellar noise. To date, the lowest noise RV planet detections have been with HARPS. For example, HD 88512 b was detected with RVs whose per-night measurement uncertainties are $< 0.3$ m s$^{-1}$ and the data set has an RMS of 0.75 m s$^{-1}$ after subtracting the single planet model with $K = 0.77$ m s$^{-1}$ (Pepe et al. 2011). Achieving this level of precision would enable 50% completeness to $\sim$10 $M_{\oplus}$ planets (typical for super-Earths) at 3 AU, a factor of $\sim$6 improvement in mass sensitivity compared adding $N_{\rm obs} = 30$ RVs over 10 yr with the current HIRES precision.

## 6.3.   Maximizing Planet Yield and Completeness

The RVs used in this report were gathered as part of the Lick and Keck Planet Searches. These blind planet searches were supported over decades by telescope time allocation committees (TACs) because of the historic value of planet discoveries. With thousands of planets now known, times have changed. The Lick Planet Search was completed in 2011 and the Keck Telescope time is being used for a wider variety of RV projects, especially follow-up of transiting planet missions like Kepler. This leaves fewer Doppler resources to monitor the
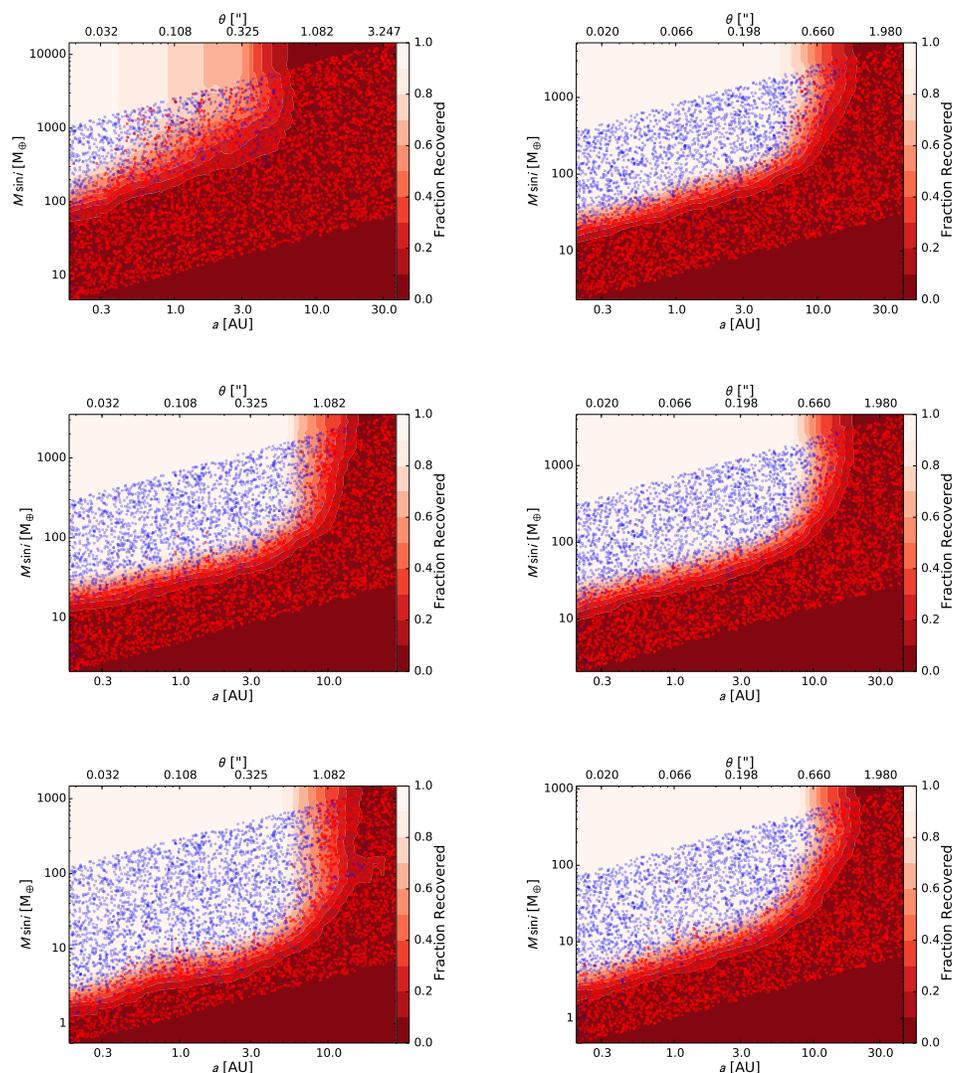
Fig. 13.— Completeness for two stars, HD 102365 (left) and HD 182572 (right). The top row shows the completeness with the observations to date (through 2014). The middle row shows the expected completeness of the same stars after adding ten years of measurements with 3 RVs per year having the same precision as the recent Keck-HIRES observations. The bottom row shows the expected completeness after adding 10 years of 10 RVs per year with $\sigma_{\rm RV} = 0.5$ m s$^{-1}$. Such a high-precision planet search would be sensitive to $\lesssim 10$ $M_\oplus$ super-Earth planets in 3 AU orbits.

likely targets of a space-based imaging mission. *We therefore recommend that the Exo-C, Exo-S, and AFTA teams write into their mission requirements all needs for Doppler measurements before, during, and after the missions.* In the absence of such a requirement, it is likely that only a small fraction of the stars in Table 3 will have substantially more RVs suitable for updated completeness estimates when those analyses are needed for target selection.

The Doppler precision and completeness (Fig. 11) achievable for stars in the Exo-S, Exo-C, and AFTA target lists varies considerably as a function of stellar type. For main sequence G and K dwarfs in the Southern hemisphere, a 10-year survey could be complete to super-Earths ($M_\mathrm{p} \sin i = 10\ M_\oplus$) in few AU orbits. *We recommend that all target G and K dwarfs (in the North and South) be observed at least 10 times per year with as high a precision as possible ($\leq 2\ \mathrm{m\,s^{-1}}$) to detect or place limits on super-Earths and Neptune-mass planets in few AU orbits.* Higher precision ($\leq 0.5\ \mathrm{m\,s^{-1}}$) is desired and the above simulation demonstrates that it significantly improves mass sensitivity. But it must be sustained over multiyear timescales to significantly impact completeness.

After G and K dwarfs, evolved giants stars with modest jitter are the most promising targets for Doppler planet discoveries that are helpful for imaging searches. Detecting giant planets in few AU orbits is feasible and provides valuable targeting information. *We recommend that all giant stars that are plausible imaging targets have their jitter measured by current Doppler instruments. For the large fraction with jitter small enough to permit the detection of giant planets in few AU orbits, we recommend 10 observations per year per star for at least 10 years at a precision no worse than the jitter.* High precision, high cadence photometric observations can also be used to estimate Doppler jitter using photometric "Flicker" (Bastien et al. 2014). TESS (Ricker et al. 2014) will provide such photometry for nearly the entire sky, however the bright limit is expected to be $I \gtrsim 4$ mag, which would exclude many Exo-C, Exo-S, and AFTA targets. We recommend that the TESS team explore observing all Exo-C, Exo-S, and AFTA targets by expanding photometric apertures for targets not positioned near the detector edges, where charge leakage would limit photometric precision.

Stars with spectral types earlier than F6V are less desirable because of their rapidly increasing jitter. However, *we recommend dedicated Doppler campaigns to measure the jitter of every early-type Exo-C and Exo-S target. For stars showing low enough jitter to enable completeness encompassing giant planets in few AU orbits, we recommend 10 RV epochs per year, with a short-term observing cadence designed to average over photospheric jitter.*

Close binary star systems (sky separation $\lesssim 2''$) are likely to remain poor Doppler targets for the foreseeable future. Young active stars are best observed by infrared Doppler

planet searches where the spot contrast and associated jitter is reduced.

Finally, *we recommend a NASA investment in ground-based Doppler facilities specifically to search for low-mass planets orbiting nearby stars and to prepare for direct imaging missions.* Sensitivity to low-mass planets requires high Doppler precision and a large number of independent measurements. Such a facility could also serve other NASA goals by measuring the masses of transiting planets discovered by the NASA missions TESS and Kepler.

## REFERENCES

Backman, D., et al. 2009, Epsilon Eridani's Planetary Debris Disk: Structure and Dynamics Based on Spitzer and Caltech Submillimeter Observatory Observations, ApJ, 690, 1522

Bastien, F. A., et al. 2014, Radial Velocity Variations of Photometrically Quiet, Chromospherically Inactive Kepler Stars: A Link between RV Jitter and Photometric Flicker, AJ, 147, 29

Bottom, M., Muirhead, P. S., Johnson, J. A., & Blake, C. H. 2013, Optimizing Doppler Surveys for Planet Yield, PASP, 125, 240

Bouchy, F., Pepe, F., & Queloz, D. 2001, Fundamental photon noise limit to radial velocity measurements, A&A, 374, 733

Butler, R. P., Marcy, G. W., Fischer, D. A., Brown, T. M., Contos, A. R., Korzennik, S. G., Nisenson, P., & Noyes, R. W. 1999, Evidence for Multiple Companions to Upsilon Andromedae, ApJ, 526, 916

Butler, R. P., Marcy, G. W., Williams, E., Hauser, H., & Shirts, P. 1997, Three New "51 Pegasi-Type" Planets, ApJ, 474, L115

Butler, R. P., Marcy, G. W., Williams, E., McCarthy, C., Dosanjh, P., & Vogt, S. S. 1996, Attaining Doppler Precision of 3 M s-1, PASP, 108, 500

Carter, J. A., et al. 2012, Kepler-36: A Pair of Planets with Neighboring Orbits and Dissimilar Densities, Science, 337, 556

Crepp, J. R., Johnson, J. A., Howard, A. W., Marcy, G. W., Brewer, J., Fischer, D. A., Wright, J. T., & Isaacson, H. 2014, The TRENDS High-contrast Imaging Survey. V. Discovery of an Old and Cold Benchmark T-dwarf Orbiting the Nearby G-star HD 19467, ApJ, 781, 29

Crepp, J. R., Johnson, J. A., Howard, A. W., Marcy, G. W., Gianninas, A., Kilic, M., & Wright, J. T. 2013a, The TRENDS High-contrast Imaging Survey. III. A Faint White Dwarf Companion Orbiting HD 114174, ApJ, 774, 1

Crepp, J. R., et al. 2012a, The Dynamical Mass and Three-dimensional Orbit of HR7672B: A Benchmark Brown Dwarf with High Eccentricity, ApJ, 751, 97

—. 2012b, The TRENDS High-contrast Imaging Survey. I. Three Benchmark M Dwarfs Orbiting Solar-type Stars, ApJ, 761, 39

—. 2013b, The TRENDS High-contrast Imaging Survey. II. Direct Detection of the HD 8375 Tertiary, ApJ, 771, 46

Crockett, C. J., Mahmud, N. I., Prato, L., Johns-Krull, C. M., Jaffe, D. T., Hartigan, P. M., & Beichman, C. A. 2012, A Search for Giant Planet Companions to T Tauri Stars, ApJ, 761, 164

Cumming, A., Butler, R. P., Marcy, G. W., Vogt, S. S., Wright, J. T., & Fischer, D. A. 2008, The Keck Planet Search: Detectability and the Minimum Mass and Orbital Period Distribution of Extrasolar Planets, PASP, 120, 531

Cumming, A., Marcy, G. W., & Butler, R. P. 1999, The Lick Planet Search: Detectability and Mass Thresholds, ApJ, 526, 890

Dawson, R. I., & Fabrycky, D. C. 2010, Radial Velocity Planets De-aliased: A New, Short Period for Super-Earth 55 Cnc e, ApJ, 722, 937

Desort, M., et al. 2009, Extrasolar planets and brown dwarfs around A-F type stars. VII. $\theta$ Cygni radial velocity variations: planets or stellar phenomenon?, A&A, 506, 1469

Drake, F. D. 1961, Project Ozma, Physics Today, 14, 40

Dumusque, X., Santos, N. C., Udry, S., Lovis, C., & Bonfils, X. 2011a, Planetary detection limits taking into account stellar noise. II. Effect of stellar spot groups on radial-velocities, A&A, 527, A82

Dumusque, X., Udry, S., Lovis, C., Santos, N. C., & Monteiro, M. J. P. F. G. 2011b, Planetary detection limits taking into account stellar noise. I. Observational strategies to reduce stellar oscillation and granulation effects, A&A, 525, A140

Dumusque, X., et al. 2011c, The HARPS search for southern extra-solar planets. XXX. Planetary systems around stars with solar-like magnetic cycles and short-term activity variation, A&A, 535, A55

—. 2012, An Earth-mass planet orbiting $\alpha$ Centauri B, Nature, 491, 207

Fischer, D., et al. 2009, Five Planets and an Independent Confirmation of HD 196885Ab from Lick Observatory, ApJ, 703, 1545

Fischer, D. A., Butler, R. P., Marcy, G. W., Vogt, S. S., & Henry, G. W. 2003, A Sub-Saturn Mass Planet Orbiting HD 3651, ApJ, 590, 1081

Fischer, D. A., Marcy, G. W., Butler, R. P., Laughlin, G., & Vogt, S. S. 2002, A Second Planet Orbiting 47 Ursae Majoris, ApJ, 564, 1028

Fischer, D. A., Marcy, G. W., & Spronck, J. F. P. 2014, The Twenty-five Year Lick Planet Search, ApJS, 210, 5

Fischer, D. A., et al. 2005, The N2K Consortium. I. A Hot Saturn Planet Orbiting HD 88133, ApJ, 620, 481

Galland, F., Lagrange, A.-M., Udry, S., Chelli, A., Pepe, F., Queloz, D., Beuzit, J.-L., & Mayor, M. 2005, Extrasolar planets and brown dwarfs around A-F type stars. I. Performances of radial velocity measurements, first analyses of variations, A&A, 443, 337

Gliese, W. 1969, Catalogue of Nearby Stars. Edition 1969, Veroeffentlichungen des Astronomischen Rechen-Instituts Heidelberg, 22, 1

Gliese, W., & Jahreiß, H. 1979, Nearby Star Data Published 1969-1978, A&AS, 38, 423

Golimowski, D. A., Fastie, W. G., Schroeder, D. J., & Uomoto, A. 1995a, Hubble Space Telescope Observations of the Very Low Mass Companion to Gliese 105A, ApJ, 452, L125

Golimowski, D. A., Nakajima, T., Kulkarni, S. R., & Oppenheimer, B. R. 1995b, Detection of a very low mass companion to the astrometric binary Gliese 105A, ApJ, 444, L101

Goullioud, R., Zhao, F., Tang, H., & Wu, J. 2014, The WFIRST-AFTA coronagraph design update, Society of Photo-Optical Instrumentation Engineers (SPIE) Conference Series, Vol. 9143, Society of Photo-Optical Instrumentation Engineers (SPIE) Conference Series

Greaves, J. S., et al. 1998, A Dust Ring around $\epsilon$ Eridani: Analog to the Young Solar System, ApJ, 506, L133

Gregory, P. C., & Fischer, D. A. 2010, A Bayesian periodogram finds evidence for three planets in 47UrsaeMajoris, MNRAS, 403, 731

Hatzes, A. P., et al. 2000, Evidence for a Long-Period Planet Orbiting $\epsilon$ Eridani, ApJ, 544, L145

Hillenbrand, L., Isaacson, H., Marcy, G., Barenfeld, S., Fischer, D., & Howard, A. 2014, Empirical Limits on Radial Velocity Planet Detection for Young Stars, arXiv:1408.3475

Hoffleit, D., & Jaschek, C. 1982, The Bright Star Catalogue (Yale Univ. Obs.)

Horne, J. H., & Baliunas, S. L. 1986, A prescription for period analysis of unevenly sampled time series, ApJ, 302, 757

Howard, A. W., et al. 2009, The NASA-UC Eta-Earth Program. I. A Super-Earth Orbiting HD 7924, ApJ, 696, 75

—. 2010a, The California Planet Survey. I. Four New Giant Exoplanets, ApJ, 721, 1467

—. 2010b, The Occurrence and Mass Distribution of Close-in Super-Earths, Neptunes, and Jupiters, Science, 330, 653

—. 2011a, The NASA-UC Eta-Earth Program. II. A Planet Orbiting HD 156668 with a Minimum Mass of Four Earth Masses, ApJ, 726, 73

—. 2011b, The NASA-UC Eta-Earth Program. III. A Super-Earth Orbiting HD 97658 and a Neptune-mass Planet Orbiting Gl 785, ApJ, 730, 10

—. 2014, The NASA-UC Eta-Earth Program: IV. A Close-in Super-Earth Orbiting an M Dwarf 3.6 PC from Earth, ApJ, 794, 51

Isaacson, H., & Fischer, D. 2010, Chromospheric Activity and Jitter Measurements for 2630 Stars on the California Planet Search, ApJ, 725, 875

Jeffers, S. V., Petit, P., Marsden, S. C., Morin, J., Donati, J.-F., & Folsom, C. P. 2014, $\epsilon$ Eridani: an active K dwarf and a planet hosting star?. The variability of its large-scale magnetic field topology, A&A, 569, A79

Johnson, J. A., et al. 2007, Retired A Stars and Their Companions: Exoplanets Orbiting Three Intermediate-Mass Subgiants, ApJ, 665, 785

Kjeldsen, H., & Bedding, T. R. 1995, Amplitudes of stellar oscillations: the implications for asteroseismology., A&A, 293, 87

Knutson, H. A., et al. 2014, Friends of Hot Jupiters. I. A Radial Velocity Search for Massive, Long-period Companions to Close-in Gas Giant Planets, ApJ, 785, 126

Konacki, M., Muterspaugh, M. W., Kulkarni, S. R., & Hełminiak, K. G. 2009, The Radial Velocity Tatooine Search for Circumbinary Planets: Planet Detection Limits for a Sample of Double-Lined Binary Stars—Initial Results from Keck I/Hires, Shane/CAT/Hamspec, and TNG/Sarg Observations, ApJ, 704, 513

Liu, M. C., Leggett, S. K., & Chiu, K. 2007, The Late-T Dwarf Companion to the Exoplanet Host Star HD 3651: A New Benchmark for Gravity and Metallicity Effects in Ultracool Spectra, ApJ, 660, 1507

Lomb, N. R. 1976, Least-squares frequency analysis of unequally spaced data, Ap&SS, 39, 447

López-Santiago, J., Montes, D., Crespo-Chacón, I., & Fernández-Figueroa, M. J. 2006, The Nearest Young Moving Groups, ApJ, 643, 1160

Lovis, C., et al. 2006, An extrasolar planetary system with three Neptune-mass planets, Nature, 441, 305

—. 2011, The HARPS search for southern extra-solar planets. XXXI. Magnetic activity cycles in solar-type stars: statistics and impact on precise radial velocities, arXiv:1107.5325

Luhman, K. L., et al. 2007, Discovery of Two T Dwarf Companions with the Spitzer Space Telescope, ApJ, 654, 570

Maire, A.-L., et al. 2014, Search for cool giant exoplanets around young and nearby stars. VLT/NaCo near-infrared phase-coronagraphic and differential imaging, A&A, 566, A126

Mamajek, E. E., & Hillenbrand, L. A. 2008, Improved Age Estimation for Solar-Type Dwarfs Using Activity-Rotation Diagnostics, ApJ, 687, 1264

Maness, H. L., Marcy, G. W., Ford, E. B., Hauschildt, P. H., Shreve, A. T., Basri, G. B., Butler, R. P., & Vogt, S. S. 2007, The M Dwarf GJ 436 and its Neptune-Mass Planet, PASP, 119, 90

Marcy, G., Butler, R. P., Fischer, D., Vogt, S., Wright, J. T., Tinney, C. G., & Jones, H. R. A. 2005a, Observed Properties of Exoplanets: Masses, Orbits, and Metallicities, Progress of Theoretical Physics Supplement, 158, 24

Marcy, G. W., & Butler, R. P. 1992, Precision radial velocities with an iodine absorption cell, PASP, 104, 270

—. 1996, A Planetary Companion to 70 Virginis, ApJ, 464, L147

—. 2000, Planets Orbiting Other Suns, PASP, 112, 137

Marcy, G. W., Butler, R. P., & Vogt, S. S. 2000, Sub-Saturn Planetary Candidates of HD 16141 and HD 46375, ApJ, 536, L43

Marcy, G. W., Butler, R. P., Vogt, S. S., Fischer, D. A., Henry, G. W., Laughlin, G., Wright, J. T., & Johnson, J. A. 2005b, Five New Extrasolar Planets, ApJ, 619, 570

Marcy, G. W., Butler, R. P., Williams, E., Bildsten, L., Graham, J. R., Ghez, A. M., & Jernigan, J. G. 1997, The Planet around 51 Pegasi, ApJ, 481, 926

Marcy, G. W., et al. 2014, Masses, Radii, and Orbits of Small Kepler Planets: The Transition from Gaseous to Rocky Planets, ApJS, 210, 20

Marengo, M., Stapelfeldt, K., Werner, M. W., Hora, J. L., Fazio, G. G., Schuster, M. T., Carson, J. C., & Megeath, S. T. 2009, Spitzer/Infrared Array Camera Limits to Planetary Companions of Fomalhaut and epsilon Eridani, ApJ, 700, 1647

Mayor, M., & Queloz, D. 1995, A Jupiter-mass companion to a solar-type star, Nature, 378, 355

Mayor, M., Udry, S., Naef, D., Pepe, F., Queloz, D., Santos, N. C., & Burnet, M. 2004, The CORALIE survey for southern extra-solar planets. XII. Orbital solutions for 16 extra-solar planets discovered with CORALIE, A&A, 415, 391

Mayor, M., et al. 2011, The HARPS search for southern extra-solar planets XXXIV. Occurrence, mass distribution and orbital properties of super-Earths and Neptune-mass planets, arXiv:1109.2497

Metcalfe, T. S., et al. 2013, Magnetic Activity Cycles in the Exoplanet Host Star epsilon Eridani, ApJ, 763, L26

Montet, B. T., Crepp, J. R., Johnson, J. A., Howard, A. W., & Marcy, G. W. 2014, The TRENDS High-contrast Imaging Survey. IV. The Occurrence Rate of Giant Planets around M Dwarfs, ApJ, 781, 28

Moran, S. M., Kuchner, M. J., & Holman, M. J. 2004, The Dynamical Influence of a Planet at Semimajor Axis 3.4 AU on the Dust around $\epsilon$ Eridani, ApJ, 612, 1163

Mugrauer, M., Seifahrt, A., Neuhäuser, R., & Mazeh, T. 2006, HD3651B: the first directly imaged brown dwarf companion of an exoplanet host star, MNRAS, 373, L31

Murray, C., & Dermott, S. 1999, Solar System Dynamics (Cambridge University Press)

O'Toole, S. J., Tinney, C. G., Jones, H. R. A., Butler, R. P., Marcy, G. W., Carter, B., & Bailey, J. 2009, Selection functions in doppler planet searches, MNRAS, 392, 641

Pasquini, L., Cristiani, S., Garcia-Lopez, R., Haehnelt, M., & Mayor, M. 2010, CODEX: An Ultra-stable High Resolution Spectrograph for the E-ELT, The Messenger, 140, 20

Pepe, F., et al. 2011, The HARPS search for Earth-like planets in the habitable zone. I. Very low-mass planets around HD 20794, HD 85512, and HD 192310, A&A, 534, A58

—. 2014, ESPRESSO: The next European exoplanet hunter, Astronomische Nachrichten, 335, 8

Pepe, F. A., & Lovis, C. 2008, From HARPS to CODEX: exploring the limits of Doppler measurements, Physica Scripta Volume T, 130, 014007

Quirrenbach, A., Reffert, S., & Bergmann, C. 2011, Planets around Giant Stars, American Institute of Physics Conference Series, Vol. 1331, American Institute of Physics Conference Series, ed. S. Schuh, H. Drechsel, & U. Heber, 102–109

Reffert, S., Quirrenbach, A., Mitchell, D. S., Albrecht, S., Hekker, S., Fischer, D. A., Marcy, G. W., & Butler, R. P. 2006, Precise Radial Velocities of Giant Stars. II. Pollux and Its Planetary Companion, ApJ, 652, 661

Ricker, G. R., et al. 2014, Transiting Exoplanet Survey Satellite (TESS), Society of Photo-Optical Instrumentation Engineers (SPIE) Conference Series, Vol. 9143, Society of Photo-Optical Instrumentation Engineers (SPIE) Conference Series

Rivera, E. J., Laughlin, G., Butler, R. P., Vogt, S. S., Haghighipour, N., & Meschiari, S. 2010, The Lick-Carnegie Exoplanet Survey: a Uranus-Mass Fourth Planet for GJ 876 in an Extrasolar Laplace Configuration, ApJ, 719, 890

Robinson, S. E., Ammons, S. M., Kretke, K. A., Strader, J., Wertheimer, J. G., Fischer, D. A., & Laughlin, G. 2007, The N2K Consortium. VII. Atmospheric Parameters of 1907 Metal-rich Stars: Finding Planet-Search Targets, ApJS, 169, 430

Scargle, J. D. 1982, Studies in astronomical time series analysis. II - Statistical aspects of spectral analysis of unevenly spaced data, ApJ, 263, 835

Schnupp, C., et al. 2010, Discovery of a stellar companion to the nearby solar-analogue HD 104304, A&A, 516, A21

Seager, S., et al. 2014, Exo-S: A Probe-scale Space Mission to Directly Image and Spectroscopically Characterize Exoplanetary Systems Using a Starshade and Telescope System, American Astronomical Society Meeting Abstracts, Vol. 224, American Astronomical Society Meeting Abstracts #224, #311.06

Spergel, D., et al. 2013, WFIRST-2.4: What Every Astronomer Should Know, ArXiv e-prints

Stapelfeldt, K. R., et al. 2014, Exo-C: a probe-scale space mission to directly image and spectroscopically characterize exoplanetary systems using an internal coronagraph, Society of Photo-Optical Instrumentation Engineers (SPIE) Conference Series, Vol. 9143, Society of Photo-Optical Instrumentation Engineers (SPIE) Conference Series

Strand, K. A. 1943, 61 Cygni as a Triple System, PASP, 55, 29

—. 1957, The orbital motion of 61 Cygni., AJ, 62, 35

Tan, X., Payne, M. J., Lee, M. H., Ford, E. B., Howard, A. W., Johnson, J. A., Marcy, G. W., & Wright, J. T. 2013, Characterizing the Orbital and Dynamical State of the HD 82943 Planetary System with Keck Radial Velocity Data, ApJ, 777, 101

Tanner, A. M., Gelino, C. R., & Law, N. M. 2010, A High-Contrast Imaging Survey of SIM Lite Planet Search Targets, PASP, 122, 1195

Tinney, C. G., Butler, R. P., Marcy, G. W., Jones, H. R. A., Penny, A. J., Vogt, S. S., Apps, K., & Henry, G. W. 2001, First Results from the Anglo-Australian Planet Search: A Brown Dwarf Candidate and a 51 Peg-like Planet, ApJ, 551, 507

Traub, W. A., et al. 2014, Science yield estimation for AFTA coronagraphs, Society of Photo-Optical Instrumentation Engineers (SPIE) Conference Series, Vol. 9143, Society of Photo-Optical Instrumentation Engineers (SPIE) Conference Series

Trifonov, T., Reffert, S., Tan, X., Lee, M. H., & Quirrenbach, A. 2014, Precise radial velocities of giant stars. VI. A possible 2:1 resonant planet pair around the K giant star $\eta$ Ceti, A&A, 568, A64

Tuomi, M., et al. 2013, Signals embedded in the radial velocity noise. Periodic variations in the $\tau$ Ceti velocities, A&A, 551, A79

Valenti, J. A., Butler, R. P., & Marcy, G. W. 1995, Determining Spectrometer Instrumental Profiles Using FTS Reference Spectra, PASP, 107, 966

Valenti, J. A., & Fischer, D. A. 2005, Spectroscopic Properties of Cool Stars (SPOCS). I. 1040 F, G, and K Dwarfs from Keck, Lick, and AAT Planet Search Programs, ApJS, 159, 141

Vogt, S. S. 1987, The Lick Observatory Hamilton Echelle Spectrometer, PASP, 99, 1214

Vogt, S. S., et al. 1994, HIRES: the high-resolution echelle spectrometer on the Keck 10-m Telescope, Proc. SPIE Instrumentation in Astronomy VIII, David L. Crawford; Eric R. Craine; Eds., Vol. 2198, p. 362

Vogt, S. S., et al. 2010, A Super-Earth and Two Neptunes Orbiting the Nearby Sun-like Star 61 Virginis, ApJ, 708, 1366

Walker, G. A. H., Walker, A. R., Irwin, A. W., Larson, A. M., Yang, S. L. S., & Richardson, D. C. 1995, A search for Jupiter-mass companions to nearby stars., Icarus, 116, 359

Winn, J. N., et al. 2011, A Super-Earth Transiting a Naked-eye Star, ApJ, 737, L18

Wittenmyer, R. A., Endl, M., Cochran, W. D., Hatzes, A. P., Walker, G. A. H., Yang, S. L. S., & Paulson, D. B. 2006, Detection Limits from the McDonald Observatory Planet Search Program, AJ, 132, 177

Wright, J. T., & Howard, A. W. 2009, Efficient Fitting of Multiplanet Keplerian Models to Radial Velocity and Astrometry Data, ApJS, 182, 205

Wright, J. T., Marcy, G. W., Butler, R. P., & Vogt, S. S. 2004, Chromospheric Ca II Emission in Nearby F, G, K, and M Stars, ApJS, 152, 261

Wright, J. T., Marcy, G. W., Butler, R. P., Vogt, S. S., Henry, G. W., Isaacson, H., & Howard, A. W. 2008, The Jupiter Twin HD 154345b, ApJ, 683, L63

Wright, J. T., Upadhyay, S., Marcy, G. W., Fischer, D. A., Ford, E. B., & Johnson, J. A. 2009, Ten New and Updated Multiplanet Systems and a Survey of Exoplanetary Systems, ApJ, 693, 1084

Wright, J. T., et al. 2011, The Exoplanet Orbit Database, PASP, 123, 412

## A.    Machine-readable Data

The set of RV time series for every star with measurements is supplied as a supplement to this report. Each star has a separate ASCII file for RV data that is named *starname*_rv.csv (e.g., 10700_rv.csv). The file header lists the star name and instrument codes. Each column is briefly labeled in the first row. The four data columns are Heliocentric Julian Date (HJD) less 2,440,000, relative radial velocity ($\mathrm{m\,s^{-1}}$), uncertainty in the radial velocity ($\mathrm{m\,s^{-1}}$), and instrument code. Statistical uncertainties in determining the Doppler shifts are accounted for, but astrophysical jitter is not.

We summarize the completeness contours for each star (Appendix C) with two sets of machine-readable files using a format similar to the RV files. The first set of ASCII files are named *starname*_contours.csv (e.g., 10700_contours.csv). The header lists the star name as well as the stellar mass and distance used to convert between orbital period, semi-major axis, and projected sky separation. Each column is briefly labeled in the first row. The six data columns are orbital period (days), semi-major axis (AU), sky-projected angular distance (arcsec), and the $M \sin i$ ($M_\oplus$) values that corresponds to completeness levels of 16%, 50%, and 84%, respectively.

A second set of ASCII files provide complete, two-dimensional sampling of the completeness measurements. In files named *starname*_2D_recovery.txt (e.g., 10700_2D_recovery.txt), we list the completeness values (the red shading) at every cell in the completeness plots. These files have headers listing the star masses, distances and column names. The columns are sky-projected angular distance (arcsec), and the $M \sin i$ ($M_\oplus$), and fractional completeness (0–1).

## B.   Properties of Stars without Doppler Measurements

Table 4 contains the complete list of 244 stars that are on the Exo-S and Exo-C target lists and were not observed at Lick or Keck Observatories.  The Notes column lists the reason(s) that the stars were *likely* not included in our Keck/Lick Planet Searches.  This table is the complement to Table 2, which includes stars with observations.  Because of the quantity of this data, we relegated Table 4 to this appendix.

Table 4.   Imaging Target Stars Without Doppler Measurements

| Hipp. No. | HD No. | Gliese No. | Target[a] List | Dist. (pc) | $V$ (mag) | $B–V$ (mag) | $T_{\text{eff}}$ (K) | Sp. T. | Notes[b] |
|---|---|---|---|---|---|---|---|---|---|
| 171 | 224930 | 914A | S | 12.170 | 5.800 | 0.690 | 5502 | G3V | B |
| 677 | 358 | $\cdots$ | C, A | 29.740 | 2.060 | −0.048 | 13098 | B9p | H |
| 746 | 432 | 8 | C, A | 16.780 | 2.260 | 0.365 | 6915 | F2III-IV | H |
| 910 | 693 | 10 | C, A | 18.750 | 4.890 | 0.487 | 6255 | F5V | H |
| 950 | 739 | 3013 | A | 21.280 | 5.240 | 0.430 | 6548 | F5V | H, S |
| 1599 | 1581 | 17 | S, C, A | 8.590 | 4.230 | 0.576 | 5948 | G0V | S |
| 2021 | 2151 | 19 | S, C, A | 7.460 | 2.820 | 0.618 | 5873 | G1IV | S |
| 2072 | 2262 | 20 | C, A | 23.810 | 3.930 | 0.175 | 7922 | A6VN | S |
| 2081 | 2261 | $\cdots$ | C | 25.970 | 2.400 | 1.083 | 4436 | K0IIIB | E |
| 2762 | 3196 | 23A | A | 21.250 | 5.200 | 0.570 | 6067 | F8V | B |
| 2941 | 3443 | 25A | S | 15.400 | 5.570 | 0.715 | 5480 | K1V+G | B |
| 3419 | 4128 | 31 | C | 29.530 | 2.020 | 1.038 | 4944 | K0III | E |
| 3505 | 4247 | 31.3 | A | 26.740 | 5.220 | 0.320 | 6903 | F3V | H |
| 3810 | 4676 | 34.1 | A | 23.450 | 5.070 | 0.500 | 6254 | F8V | H |
| 3909 | 4813 | 37 | S, A | 15.753 | 5.164 | 0.514 | 6250 | F7V | H, $N_{\text{obs}} = 2$ |
| 4151 | 5015 | 41 | C, A | 18.740 | 4.800 | 0.540 | 6196 | F8V | B |
| 5336 | 6582 | 53A | S, C, A | 7.550 | 5.170 | 0.704 | 5526 | G5Vp | B |
| 5799 | 7439 | 54.2A | A | 23.380 | 5.140 | 0.450 | 6465 | F5V | H |
| 5862 | 7570 | 55 | S, C, A | 15.110 | 4.960 | 0.571 | 6116 | G0V | S |
| 5896 | 7788 | 55.3A | A | 20.950 | 4.250 | 0.450 | 6505 | F5V | H, S |
| 6537 | 8512 | $\cdots$ | C | 34.900 | 3.800 | 1.070 | $\cdots$ | K0III | E |
| 6686 | 8538 | $\cdots$ | C | 30.500 | 2.700 | 0.160 | $\cdots$ | A5Vv | B, H |
| 6706 | 8723 | $\cdots$ | A | 25.210 | 5.350 | 0.370 | 6690 | F2V | H |
| 6813 | 8799 | $\cdots$ | A | 28.620 | 4.830 | 0.420 | 6555 | F4V | H |
| 7751 | 10360 | 66AB | S | 7.820 | 5.680 | 0.864 | 5016 | K0/4 | S |
| 7918 | 10307 | 67 | S, C, A | 12.740 | 4.960 | 0.618 | 5874 | G2V | B |

Table 4—Continued

| Hipp. No. | HD No. | Gliese No. | Target[a] List | Dist. (pc) | $V$ (mag) | $B$–$V$ (mag) | $T_{\rm eff}$ (K) | Sp. T. | Notes[b] |
|---|---|---|---|---|---|---|---|---|---|
| 8209 | 10830 | $\cdots$ | A | 28.110 | 5.290 | 0.400 | 6740 | F2V | H |
| 8497 | 11171 | $\cdots$ | C, A | 23.190 | 4.650 | 0.333 | 7087 | F0V | H |
| 8796 | 11443 | 78.1 | C, A | 19.420 | 3.420 | 0.488 | 6273 | F6IV | B |
| 8903 | 11636 | 80 | C, A | 17.990 | 2.630 | 0.156 | 8300 | A5V | H |
| 9007 | 11937 | 81A | C | 17.850 | 3.690 | 0.844 | 5182 | G8III | S, E |
| 9236 | 12311 | 83 | C, A | 22.010 | 2.860 | 0.290 | 7201 | F0V | S, H |
| 9884 | 12929 | 84.3 | C | 20.180 | 2.010 | 1.151 | 4504 | K2III | E |
| 10138 | 13445 | 86 | S | 10.780 | 6.120 | 0.812 | 5151 | K1V | S |
| 10306 | 13555 | $\cdots$ | A | 28.870 | 5.230 | 0.440 | 6496 | F5V | H |
| 10644 | 13974 | 92 | S, C, A | 10.780 | 4.860 | 0.607 | 5667 | G0V | B |
| 10670 | 14055 | $\cdots$ | C | 34.400 | 4.000 | 0.020 | $\cdots$ | A1Vnn | H |
| 11072 | 14802 | 97 | A | 21.950 | 5.190 | 0.610 | 5854 | G1V | B |
| 11783 | 15798 | $\cdots$ | A | 26.690 | 4.740 | 0.450 | 6502 | F5V | H |
| 12390 | 16620 | 105.4A | A | 26.960 | 4.830 | 0.430 | 6516 | F4V | H |
| 12623 | 16739 | 105.6 | A | 24.190 | 4.910 | 0.580 | 5973 | F9V | H |
| 12706 | 16970 | 106.1A | C, A | 24.410 | 3.470 | 0.093 | 8673 | A2Va | H |
| 12777 | 16895 | 107A | S, C, A | 11.127 | 4.098 | 0.489 | 6344 | F7V | H, $N_{\rm obs} = 2$ |
| 12828 | 17094 | $\cdots$ | C, A | 25.770 | 4.270 | 0.311 | 7225 | F1III-IV | H |
| 12843 | 17206 | 111 | S, C, A | 14.220 | 4.470 | 0.481 | 6378 | F5/6V | H |
| 14146 | 18978 | 121 | C, A | 27.170 | 4.080 | 0.163 | 8045 | A4V | H |
| 14576 | 19356 | $\cdots$ | C, A | 27.570 | 2.110 | −0.010 | 9634 | B8V | H |
| 14668 | 19476 | $\cdots$ | C | 34.600 | 4.000 | 0.980 | $\cdots$ | K0III | E |
| 14879 | 20010 | 127A | S, C, A | 14.240 | 3.800 | 0.543 | 6258 | F8V | B |
| 15330 | 20766 | 136 | S | 12.010 | 5.530 | 0.641 | 5699 | G3/5V | S |
| 15371 | 20807 | 138 | S, C, A | 12.030 | 5.240 | 0.600 | 5845 | G2V | S |
| 15510 | 20794 | 139 | S, C, A | 6.040 | 4.260 | 0.711 | 5401 | G8.0V | S |
| 16245 | 22001 | 143.2A | C, A | 21.680 | 4.700 | 0.410 | 6629 | F3IV/V | S, H |
| 17440 | $\cdots$ | $\cdots$ | C | 29.860 | 3.840 | 1.133 | 4514 | K0IV | B, S |
| 17651 | 23754 | 155 | C, A | 17.630 | 4.220 | 0.434 | 6631 | F3/5V | H |
| 18907 | 25490 | $\cdots$ | C | 35.900 | 3.900 | 0.030 | $\cdots$ | A1V | H |
| 19205 | 25867 | $\cdots$ | A | 27.600 | 5.210 | 0.340 | 6979 | F1V | H |
| 19747 | 26967 | $\cdots$ | C | 35.300 | 4.000 | 1.090 | $\cdots$ | K1III | E |
| 19893 | 27290 | 167.1 | C, A | 20.460 | 4.250 | 0.312 | 7060 | F0V | S, H |
| 19921 | 27442 | 167.3 | C | 18.240 | 4.440 | 1.078 | 4846 | K1/2III | S, E |
| 19990 | 27045 | $\cdots$ | A | 28.940 | 4.930 | 0.260 | 7384 | A3M | H |
| 21421 | 29139 | 171.1A | C | 20.430 | 0.870 | 1.538 | 3889 | K5III | E |

Table 4—Continued

| Hipp. No. | HD No. | Gliese No. | Target[a] List | Dist. (pc) | $V$ (mag) | $B$–$V$ (mag) | $T_{\mathrm{eff}}$ (K) | Sp. T. | Notes[b] |
|---|---|---|---|---|---|---|---|---|---|
| 21547 | 29391 | $\cdots$ | A | 29.430 | 5.220 | 0.280 | 7257 | F0V | H |
| 21770 | 29875 | 174.1A | C, A | 20.170 | 4.440 | 0.342 | 6991 | F1V | H |
| 21861 | 29992 | 176.1 | A | 28.660 | 5.040 | 0.390 | 6666 | F3IV | H, S |
| 23482 | 32743 | 187 | A | 26.070 | 5.370 | 0.420 | 6624 | F5V | H, S |
| 23693 | 33262 | 189 | S, C, A | 11.650 | 4.710 | 0.526 | 6246 | F6/7V | S, H |
| 23783 | 32537 | 187.2A | A | 26.290 | 4.980 | 0.320 | 7018 | F2V | H |
| 23875 | 33111 | $\cdots$ | C, A | 27.400 | 2.760 | 0.150 | 8377 | A3IVn | H |
| 23941 | 33256 | 189.2 | A | 25.460 | 5.110 | 0.430 | 6411 | F5.5V | H |
| 24608 | 34029 | 194A | C | 13.120 | 0.080 | 0.795 | 5356 | M1 | B |
| 25110 | 33564 | 196 | A | 20.890 | 5.080 | 0.480 | 6394 | F7V | H |
| 25278 | 35296 | 202 | S, C, A | 14.390 | 5.000 | 0.523 | 6202 | F8V | Y, B |
| 27072 | 38393 | 216A | S, C, A | 8.927 | 3.590 | 0.481 | 6372 | F7V | Y, $N_{\mathrm{obs}} = 8$ |
| 27288 | 38678 | 217.1 | C, A | 21.610 | 3.550 | 0.104 | 8337 | A2 | H |
| 27321 | 39060 | 219 | C, A | 19.440 | 3.850 | 0.171 | 8052 | A5V | S, H |
| 27628 | 39425 | $\cdots$ | C | 26.730 | 3.100 | 1.175 | 4545 | K1.5III | E |
| 27654 | 39364 | $\cdots$ | C | 34.900 | 3.900 | 0.980 | $\cdots$ | G8III/IV | E |
| 27890 | 40409 | 224.1 | C | 26.250 | 4.640 | 1.048 | 4661 | K1III/IV | S, E |
| 27913 | 39587 | 222AB | S, C, A | 8.663 | 4.395 | 0.594 | 5882 | G0V | B |
| 28103 | 40136 | 225 | S, C, A | 14.880 | 3.710 | 0.337 | 7069 | F1V | H |
| 28360 | 40183 | $\cdots$ | C, A | 24.870 | 1.890 | 0.071 | 9024 | A2V | H |
| 29271 | 43834 | 231 | S, C, A | 10.200 | 5.080 | 0.714 | 5587 | G6V | S |
| 29800 | 43386 | 9207 | A | 19.250 | 5.040 | 0.430 | 6602 | F5V | H |
| 31592 | 47205 | 239.1 | C | 19.750 | 3.950 | 1.063 | 4799 | K1III | E, B |
| 32349 | 48915 | 244A | S, C, A | 2.630 | $-1.440$ | 0.009 | 9580 | A1.0V | H |
| 32362 | 48737 | 242 | C, A | 18.000 | 3.320 | 0.443 | 6455 | F5IV | H |
| 32607 | $\cdots$ | $\cdots$ | C, A | 29.600 | 3.230 | 0.222 | 7536 | A7IV | S, H |
| 32765 | 50223 | 249.1 | A | 25.260 | 5.140 | 0.450 | 6482 | F5.5V | H, S |
| 33202 | 50635 | $\cdots$ | C, A | 25.630 | 4.730 | 0.321 | 7064 | F0Vp | H |
| 33302 | 51199 | $\cdots$ | A | 29.580 | 4.660 | 0.370 | 6790 | F3V | H |
| 34065 | 53705 | 264.1A | S | 16.520 | 5.560 | 0.624 | 5827 | G3V | B, S |
| 34834 | 55892 | 268.1 | C, A | 21.430 | 4.490 | 0.324 | 6907 | F0IV | H |
| 35350 | 56537 | $\cdots$ | C | 30.900 | 3.600 | 0.110 | $\cdots$ | A3V | H |
| 35550 | 56986 | 271A | C, A | 18.540 | 3.500 | 0.374 | 6906 | F0IV | H |
| 36046 | 58207 | $\cdots$ | C | 36.900 | 4.000 | 1.020 | $\cdots$ | G9III | E |
| 36366 | 58946 | 274A | C, A | 18.050 | 4.160 | 0.320 | 7035 | F0V | H |
| 36439 | 58855 | $\cdots$ | A | 20.240 | 5.350 | 0.450 | 6457 | F6V | H |

Table 4—Continued

| Hipp. No. | HD No. | Gliese No. | Target[a] List | Dist. (pc) | $V$ (mag) | $B$–$V$ (mag) | $T_{\text{eff}}$ (K) | Sp. T. | Notes[b] |
|---|---|---|---|---|---|---|---|---|---|
| 36795 | 60532 | 279 | C, A | 25.300 | 4.440 | 0.521 | 6262 | F6V | H |
| 36850 | 60179 | 278A | S, C, A | 15.600 | 1.580 | 0.034 | 8932 | A2Vm | H |
| 37279 | 61421 | 280A | S, C, A | 3.510 | 0.400 | 0.432 | 6543 | F5IV-V | H |
| 37606 | 62644 | 284 | A | 24.670 | 5.040 | 0.760 | 5343 | G8IV-V | S |
| 37826 | 62509 | 286 | C | 10.360 | 1.160 | 0.991 | 4850 | K0IIIvar | E |
| 37853 | 63077 | 288A | S, A | 15.210 | 5.360 | 0.589 | 6002 | G0V | B |
| 38382 | 64096 | 291A | S, A | 16.500 | 5.160 | 0.600 | 5826 | G2V | B |
| 38423 | 64379 | 292A | A | 17.940 | 5.010 | 0.430 | 6554 | F5V | H, S, B |
| 38908 | 65907 | 294A | S | 16.200 | 5.580 | 0.573 | 5949 | G0V | S |
| 39757 | 67523 | $\cdots$ | C, A | 19.480 | 2.790 | 0.456 | 6449 | F2 | H |
| 39903 | 68456 | 297.1 | C, A | 19.980 | 4.740 | 0.437 | 6467 | F5V | S, H |
| 40167 | 68255 | $\cdots$ | C, A | 25.080 | 5.240 | 0.531 | 5741 | G0V | B |
| 40702 | 71243 | 305 | C, A | 19.560 | 4.050 | 0.404 | 6625 | F5V | S, H |
| 40706 | 70060 | 1109 | C, A | 28.630 | 4.440 | 0.222 | 7790 | A4 | H |
| 41312 | 71878 | $\cdots$ | C | 33.000 | 3.900 | 1.130 | $\cdots$ | K2IIIvar | S, E |
| 42430 | 73752 | 314A | A | 19.400 | 5.050 | 0.710 | 5499 | G5IV | E |
| 42913 | 74956 | 321.3A | C, A | 24.700 | 1.930 | 0.043 | 9021 | A0V | S, H |
| 44127 | 76644 | 331A | S, C, A | 14.510 | 3.100 | 0.207 | 7769 | A7IV | H |
| 44143 | 77370 | 333.1 | A | 26.420 | 5.170 | 0.420 | 6690 | F4V | H, S |
| 44248 | 76943 | 332A | S, C, A | 16.070 | 3.970 | 0.443 | 6538 | F5V | H |
| 44901 | 78209 | $\cdots$ | C, A | 28.820 | 4.440 | 0.288 | 7231 | Am | H |
| 45038 | 78154 | 335A | C, A | 20.380 | 4.800 | 0.489 | 6180 | F7IV-V | B |
| 45238 | 80007 | $\cdots$ | C | 34.700 | 1.700 | 0.070 | $\cdots$ | A2IV | S, H |
| 45333 | 79028 | 337.1 | A | 19.570 | 5.180 | 0.590 | 5871 | G0V | B |
| 46509 | 81997 | 348A | C, A | 17.330 | 4.590 | 0.411 | 6488 | F5V | H |
| 46651 | 82434 | 351A | C, A | 18.810 | 3.600 | 0.371 | 6837 | F2IV | H |
| 46733 | 81937 | $\cdots$ | C, A | 23.820 | 3.640 | 0.360 | 6875 | F0IV | H |
| 46853 | 82328 | 354A | S, C, A | 13.480 | 3.160 | 0.469 | 6334 | F6IV | H |
| 47080 | 82885 | 356A | S, C, A | 11.370 | 5.390 | 0.770 | 5370 | G8IV-V | B |
| 48319 | 84999 | $\cdots$ | C | 35.600 | 3.800 | 0.290 | $\cdots$ | F0IV | H |
| 48833 | 86146 | $\cdots$ | A | 28.130 | 5.110 | 0.470 | 6393 | F6V | H |
| 49593 | 87696 | 378.3 | C, A | 28.240 | 4.490 | 0.190 | 7839 | A7V | H |
| 49669 | 87901 | $\cdots$ | C, A | 24.310 | 1.410 | $-0.041$ | 11962 | B7V | H |
| 49809 | 88215 | $\cdots$ | A | 27.730 | 5.300 | 0.370 | 6776 | F3V | H |
| 50191 | 88955 | $\cdots$ | C | 31.100 | 3.900 | 0.050 | $\cdots$ | A2V | H |
| 50564 | 89449 | 388.1 | C, A | 21.370 | 4.780 | 0.452 | 6476 | F6IV | E |

Table 4—Continued

| Hipp. No. | HD No. | Gliese No. | Target[a] List | Dist. (pc) | V (mag) | B–V (mag) | $T_{\text{eff}}$ (K) | Sp. T. | Notes[b] |
|---|---|---|---|---|---|---|---|---|---|
| 50954 | 90589 | 391 | S, C, A | 16.220 | 3.980 | 0.369 | 6885 | F2/3IV/V | S, H |
| 51502 | 90089 | 392.1 | A | 21.480 | 5.250 | 0.370 | 6762 | F4V | H |
| 51523 | 91324 | 397.2 | A | 21.810 | 4.890 | 0.500 | 6287 | F9V | S |
| 51814 | 91480 | $\cdots$ | A | 26.520 | 5.160 | 0.330 | 6972 | F2V | H |
| 51986 | 92139 | $\cdots$ | C, A | 26.840 | 3.830 | 0.299 | 7274 | A3 | H |
| 52727 | 93497 | $\cdots$ | C | 35.900 | 2.800 | 0.900 | $\cdots$ | G5III | B |
| 53229 | 94264 | $\cdots$ | C | 29.090 | 3.790 | 1.040 | 4833 | K0III-IV | E |
| 53253 | 94510 | 404.1 | C | 29.130 | 3.780 | 0.945 | 5014 | K1III | S |
| 53910 | 95418 | $\cdots$ | C, A | 24.450 | 2.350 | 0.026 | 9342 | A1V | H |
| 54182 | 96097 | $\cdots$ | C, A | 28.990 | 4.620 | 0.332 | 7010 | F2III-IVvar | H |
| 54872 | 97603 | 419 | C, A | 17.910 | 2.560 | 0.128 | 8037 | A4V | H |
| 55642 | 99028 | 426.1A | C, A | 23.670 | 4.000 | 0.423 | 6600 | F2IV | B, H |
| 55705 | 99211 | $\cdots$ | C, A | 25.240 | 4.070 | 0.216 | 7805 | A9V | H |
| 55779 | 99453 | 3663 | A | 27.220 | 5.180 | 0.500 | 6361 | F7V | H, S |
| 57632 | 102647 | 448 | S, C, A | 11.000 | 2.140 | 0.090 | 8378 | A3Vvar | H |
| 58001 | 103287 | $\cdots$ | C, A | 25.500 | 2.390 | 0.045 | 9272 | A0V | B, H |
| 58803 | 104731 | 3701 | A | 25.320 | 5.150 | 0.420 | 6638 | F5V | H, S |
| 59072 | 105211 | 455.2 | C, A | 19.760 | 4.140 | 0.353 | 6950 | F0IV | S, H |
| 59199 | 105452 | 455.3 | S, C, A | 14.940 | 4.020 | 0.334 | 7081 | F0IV/V | H |
| 59774 | 106591 | 459 | C, A | 24.690 | 3.280 | 0.077 | 8613 | A3Vvar | H |
| 60965 | 108767A | $\cdots$ | C, A | 26.630 | 2.930 | −0.013 | 10207 | B9.5V | H |
| 61084 | 108903 | 470 | C | 27.150 | 1.650 | 1.517 | 3385 | M4III | S |
| 61174 | 109085 | 471.2 | C, A | 18.280 | 4.300 | 0.388 | 6784 | F2V | H |
| 61941 | 110379 | 482A | S, C, A | 11.680 | 3.440 | 0.362 | 5674 | F1V | H |
| 62956 | 112185 | $\cdots$ | C, A | 25.310 | 1.760 | −0.022 | 9020 | A0p | H |
| 63076 | 112429 | $\cdots$ | A | 29.290 | 5.230 | 0.290 | 7129 | F0V | H |
| 63125 | 112413 | $\cdots$ | C | 35.200 | 2.800 | 0.120 | $\cdots$ | A0spe | H |
| 63503 | 113139 | $\cdots$ | A | 25.440 | 4.930 | 0.370 | 6829 | F2V | H |
| 63608 | 113226 | $\cdots$ | C | 33.600 | 3.000 | 0.930 | $\cdots$ | G8IIIvar | E |
| 63613 | 112985 | $\cdots$ | C | 27.870 | 3.600 | 1.189 | 4390 | K2III | S, E |
| 64241 | $\cdots$ | $\cdots$ | C, A | 17.830 | 4.320 | 0.455 | 6399 | F5V | H |
| 64583 | 114837 | 503 | C, A | 18.200 | 4.910 | 0.469 | 6390 | F5V | S, H |
| 65109 | 115892 | 508.1 | C, A | 18.020 | 2.720 | 0.068 | 10207 | A2V | H |
| 65378 | 116656 | $\cdots$ | C, A | 26.310 | 2.220 | 0.051 | 9330 | A2V | H |
| 65477 | 116842 | $\cdots$ | C, A | 25.060 | 3.980 | 0.169 | 7955 | A5V | B, H |
| 66249 | 118098 | $\cdots$ | C, A | 22.710 | 3.380 | 0.114 | 8633 | A0/1IV | H |

Table 4—Continued

| Hipp. No. | HD No. | Gliese No. | Target[a] List | Dist. (pc) | $V$ (mag) | $B$–$V$ (mag) | $T_{\rm eff}$ (K) | Sp. T. | Notes[b] |
|---|---|---|---|---|---|---|---|---|---|
| 67153 | 119756 | 525.1 | C, A | 19.400 | 4.230 | 0.375 | 6781 | F3V | H |
| 67301 | 120315 | $\cdots$ | C | 31.900 | 1.800 | 0.100 | $\cdots$ | B3V | B, H |
| 67927 | 121370 | 534 | S, C, A | 11.400 | 2.680 | 0.580 | 6116 | G0IV | B |
| 68895 | 123123 | $\cdots$ | C | 31.000 | 3.400 | 1.090 | $\cdots$ | K2III | E |
| 68933 | 123139 | 539 | C | 18.030 | 2.060 | 1.011 | 4823 | K0IIIB | E |
| 69673 | 124897 | 541 | C | 11.260 | -0.050 | 1.239 | 4336 | K2IIIp | E |
| 69701 | 124850 | $\cdots$ | C, A | 22.240 | 4.070 | 0.511 | 6234 | F6III | H |
| 69713 | 125161 | $\cdots$ | A | 29.070 | 4.750 | 0.240 | 7700 | A7IV | H |
| 69732 | 125162 | $\cdots$ | C | 30.400 | 4.200 | 0.090 | $\cdots$ | A0sh | H |
| 70497 | 126660 | 549A | S, C, A | 14.530 | 4.040 | 0.497 | 6192 | F7V | B |
| 71075 | 127762 | $\cdots$ | C, A | 26.610 | 3.040 | 0.191 | 8047 | A7IIIvar | H |
| 71681 | 128621 | 559B | S, C, A | 1.340 | 1.350 | 0.900 | 5178 | K0V | S |
| 71683 | 128620 | 559A | S, C, A | 1.340 | -0.010 | 0.710 | 5801 | G2.0V | S |
| 71908 | 128898 | 560A | S, C, A | 16.570 | 3.160 | 0.256 | 7631 | $\cdots$ | S, H |
| 71957 | 129502 | $\cdots$ | C, A | 18.270 | 3.860 | 0.385 | 6751 | F2V | H |
| 72603 | 130819 | 563.4 | A | 22.980 | 5.150 | 0.400 | 6745 | F4V | H |
| 72622 | 130841 | 564.1 | C, A | 23.240 | 2.750 | 0.147 | 8128 | A3III/V | H |
| 72848 | 131511 | 567 | S | 11.510 | 5.996 | 0.841 | 5335 | K2V | B? |
| 73165 | 132052 | $\cdots$ | C, A | 26.900 | 4.460 | 0.318 | 7079 | F2V | H |
| 73695 | 133640 | 575A | S, C, A | 12.510 | 4.830 | 0.647 | 5533 | G2V+G2V | B |
| 74395 | 134505 | $\cdots$ | C | 36.000 | 3.600 | 0.920 | $\cdots$ | G8III | S |
| 74605 | 136064 | 580.2 | A | 25.340 | 5.150 | 0.540 | 6152 | F8V | H |
| 74824 | 135379 | $\cdots$ | C | 30.600 | 4.100 | 0.090 | $\cdots$ | A3V | S, H |
| 74975 | 136202 | $\cdots$ | A | 25.380 | 5.040 | 0.540 | 6119 | F8IV | H |
| 75458 | 137759 | $\cdots$ | C | 31.000 | 3.500 | 1.170 | $\cdots$ | K2III | E |
| 75695 | 137909 | $\cdots$ | C | 34.300 | 3.700 | 0.320 | $\cdots$ | F0p | H |
| 76267 | 139006 | $\cdots$ | C, A | 23.010 | 2.210 | 0.025 | 9584 | A0V | H |
| 76829 | 139664 | 594 | C, A | 17.440 | 4.630 | 0.413 | 6649 | F3/5V | H |
| 77070 | 140573 | 596.2 | C | 22.680 | 2.610 | 1.167 | 4548 | K2III | E |
| 77622 | 141795 | $\cdots$ | C, A | 21.600 | 3.710 | 0.147 | 8257 | $\cdots$ | H |
| 77952 | 141891 | 601A | S, C, A | 12.380 | 2.810 | 0.315 | 7109 | F0III/IV | S, H |
| 78527 | 144284 | 609.1 | C, A | 21.030 | 3.990 | 0.528 | 4642 | F8IV-V | B |
| 79822 | 148048 | 3950A | A | 29.730 | 4.950 | 0.360 | 6868 | F2V | H |
| 79882 | 146791 | $\cdots$ | C | 32.600 | 3.400 | 0.970 | $\cdots$ | G8III | E |
| 80179 | 147449 | $\cdots$ | A | 27.270 | 4.820 | 0.340 | 6981 | F0V | H |
| 80331 | 148387 | 624.1A | C | 28.230 | 2.730 | 0.910 | 4941 | G8III | B |

Table 4—Continued

| Hipp. No. | HD No. | Gliese No. | Target[a] List | Dist. (pc) | $V$ (mag) | $B–V$ (mag) | $T_{\text{eff}}$ (K) | Sp. T. | Notes[b] |
|---|---|---|---|---|---|---|---|---|---|
| 80337 | 147513 | 620.1A | A | 12.780 | 5.370 | 0.630 | 5930 | G5V | S |
| 80686 | 147584 | 624 | S, C, A | 12.120 | 4.900 | 0.555 | 6107 | G0V | S |
| 81693 | 150680 | 635A | S, C, A | 10.720 | 2.810 | 0.650 | 5820 | F9IV | B |
| 81833 | 150997 | $\cdots$ | C | 33.300 | 3.600 | 0.920 | $\cdots$ | G8III-IV | E |
| 82020 | 151613 | $\cdots$ | A | 26.730 | 4.840 | 0.380 | 6805 | F2V | H |
| 82396 | 151680 | 639.1 | C | 19.540 | 2.260 | 1.181 | 4703 | K2IIIB | E |
| 82587 | 152598 | $\cdots$ | A | 29.190 | 5.340 | 0.310 | 7136 | F0V | H |
| 82860 | 153597 | 648 | C, A | 15.260 | 4.880 | 0.481 | 6146 | F6Vvar | B |
| 83000 | 153210 | $\cdots$ | C | 28.040 | 3.180 | 1.158 | 4564 | K2IIIvar | E |
| 83431 | 153580 | $\cdots$ | A | 27.220 | 5.270 | 0.470 | 6501 | F5V | H, S |
| 84012 | 155125 | 656.1A | C, A | 27.090 | 2.430 | 0.059 | 8788 | A2.5VA | H |
| 84143 | 155203 | 657 | C, A | 22.530 | 3.310 | 0.423 | 6519 | F2V | H |
| 84379 | 156164 | $\cdots$ | C, A | 23.040 | 3.120 | 0.080 | 8879 | A3IVv | B, H |
| 84405 | 155885 | 663A | S, C, A | 5.950 | 4.330 | 0.855 | 5119 | K1.5V | B |
| 84709 | $\cdots$ | 667AB | S | 6.836 | 6.255 | 0.999 | 4810 | M1.5V | S |
| 84720 | $\cdots$ | 666AB | S, C | 8.800 | 5.520 | 0.791 | 5052 | M0V | S |
| 84893 | 156897 | 670A | C, A | 17.360 | 4.390 | 0.366 | 6704 | F2/3V | H |
| 85340 | 157792 | 673.1 | C, A | 25.500 | 4.150 | 0.283 | 7440 | A3 | H |
| 85667 | 158614 | 678A | S | 16.340 | 5.310 | 0.715 | 5538 | G6V | B |
| 86032 | 159561 | 681 | S, C | 14.900 | 2.080 | 0.155 | 8225 | A5III | H |
| 86036 | 160269 | 684A | A | 14.190 | 5.230 | 0.600 | 5898 | G0V | B |
| 86201 | 160922 | $\cdots$ | C | 23.160 | 4.770 | 0.430 | 6560 | F5V | H |
| 86486 | 160032 | 686.2 | C | 21.450 | 4.750 | 0.403 | 6678 | F2V | H |
| 86614 | 162003 | 694.1A | C | 22.840 | 4.550 | 0.433 | 6435 | F5IV-V | H |
| 86736 | 160915 | 692 | C | 17.650 | 4.860 | 0.469 | 6465 | F6/7V | H |
| 86742 | 161096 | $\cdots$ | C | 25.090 | 2.750 | 1.191 | 4571 | K2III | E |
| 86796 | 160691 | 691 | A | 15.510 | 5.120 | 0.690 | 5784 | G3IV-V | S |
| 87108 | 161868 | $\cdots$ | C | 31.500 | 3.800 | 0.040 | $\cdots$ | A0V | H |
| 87585 | 163588 | $\cdots$ | C | 34.500 | 3.900 | 1.180 | $\cdots$ | K2III | E |
| 88175 | 164259 | 699.2 | C, A | 23.550 | 4.620 | 0.367 | 6771 | F2IV | H |
| 88601 | 165341 | 702A | S, C, A | 5.100 | 4.030 | 0.860 | 5019 | K0V | E |
| 88635 | 165135 | $\cdots$ | C | 29.700 | 2.950 | 1.021 | 4914 | K0III | E |
| 88745 | 165908 | 704A | S, A | 15.640 | 5.070 | 0.504 | 5925 | F7V | B |
| 88771 | 165777 | $\cdots$ | C, A | 26.630 | 3.700 | 0.140 | 8400 | A4IVs | H |
| 89348 | 168151 | 708.1 | A | 22.920 | 4.990 | 0.430 | 6404 | F5V | H |
| 89937 | 170153 | 713AB | C, A | 8.060 | 3.560 | 0.489 | 6122 | F7Vvar | B |

Table 4—Continued

| Hipp. No. | HD No. | Gliese No. | Target[a] List | Dist. (pc) | $V$ (mag) | $B$–$V$ (mag) | $T_{\rm eff}$ (K) | Sp. T. | Notes[b] |
|---|---|---|---|---|---|---|---|---|---|
| 90139 | 169414 | $\cdots$ | C | 36.500 | 4.000 | 1.170 | $\cdots$ | K2III | E |
| 90496 | 169916 | 713.1 | C | 23.970 | 2.810 | 1.057 | 4809 | K1IIIB | E |
| 91262 | 172167 | 721 | S, C, A | 7.680 | 0.030 | −0.001 | 9519 | A0Vvar | H |
| 92024 | 172555 | $\cdots$ | A | 28.550 | 4.780 | 0.200 | 7846 | A7V | H, S |
| 92161 | 173880 | $\cdots$ | C, A | 28.890 | 4.340 | 0.127 | 8334 | A5III | H |
| 93017 | 176051 | 738A | S, A | 14.870 | 5.280 | 0.555 | 6064 | G0V | B |
| 93506 | 176687 | $\cdots$ | C | 27.040 | 2.600 | 0.062 | 8799 | A3IV | H |
| 93747 | 177724 | $\cdots$ | C, A | 25.460 | 2.990 | 0.014 | 9190 | A0Vn | H |
| 93825 | 177474 | 743.1A | C, A | 17.300 | 4.230 | 0.523 | 6202 | F8/G0V | B |
| 94083 | 180777 | 748.1 | A | 27.300 | 5.110 | 0.310 | 7129 | F0Vs | H |
| 94376 | $\cdots$ | $\cdots$ | C | 29.870 | 3.050 | 1.001 | 4966 | G9III | E |
| 95501 | 182640 | 760 | S, C, A | 15.530 | 3.360 | 0.319 | 7074 | F2IV | H |
| 97295 | 187013 | 767.1A | A | 21.230 | 5.000 | 0.470 | 6401 | F5.5IV-V | H, B |
| 97649 | 187642 | 768 | S, C, A | 5.120 | 0.760 | 0.221 | 7800 | A7IV-V | H |
| 97650 | 187532 | $\cdots$ | A | 27.870 | 5.380 | 0.350 | 6812 | F5V | H, B |
| 98066 | 188376 | 770.1 | A | 25.840 | 4.700 | 0.750 | 5425 | G5IV | B, $N_{\rm obs}$=13 |
| 98495 | 188228 | $\cdots$ | C | 32.200 | 4.000 | 0.030 | $\cdots$ | A0V | S, H |
| 99240 | 190248 | 780 | S, C, A | 6.110 | 3.530 | 0.765 | 5590 | G8.0IV | S |
| 101612 | 195627 | $\cdots$ | A | 27.790 | 4.750 | 0.290 | 7201 | F0V | H, S |
| 101983 | 196378 | 794.2 | A | 24.660 | 5.110 | 0.510 | 6040 | G0V | S |
| 102333 | 197157 | $\cdots$ | C, A | 24.170 | 4.500 | 0.278 | 7448 | A7III/IV | S, H |
| 102422 | 198149 | 807 | S, C | 14.270 | 3.410 | 0.912 | 4940 | K0IV | E |
| 102431 | 198084 | $\cdots$ | C, A | 27.290 | 4.520 | 0.535 | 6138 | F8IV-V | B |
| 102485 | 197692 | 805 | S, C, A | 14.680 | 4.130 | 0.426 | 6633 | F5V | H |
| 102488 | 197989 | 806.1A | C | 22.290 | 2.450 | 1.021 | 4799 | K0III | E |
| 104858 | 202275 | 822A | C, A | 18.490 | 4.470 | 0.529 | 6238 | F5V | H |
| 104887 | 202444 | 822.1A | C, A | 20.340 | 3.740 | 0.393 | 6621 | F1IV | H |
| 105199 | 203280 | 826 | S, C, A | 15.040 | 2.430 | 0.243 | 7773 | A7IV-V | H |
| 105858 | 203608 | 827 | S, C, A | 9.260 | 4.220 | 0.469 | 6205 | F7V | S |
| 107089 | 205478 | 835.1 | C | 21.200 | 3.730 | 1.017 | 4769 | K0III | S |
| 107310 | 206826 | 836.6A | C, A | 22.240 | 4.690 | 0.454 | 6309 | F6V | B |
| 107556 | $\cdots$ | $\cdots$ | S, C, A | 11.870 | 2.850 | 0.305 | 7301 | A5mF2 | H |
| 107649 | 207129 | 838 | S | 15.990 | 5.570 | 0.601 | 5889 | G0V | Y |
| 108036 | 207958 | 838.5 | A | 26.610 | 5.080 | 0.380 | 6799 | F2V | H |
| 108870 | 209100 | 845 | S, C, A | 3.620 | 4.690 | 1.056 | 4683 | K4V | Y, S |
| 108917 | $\cdots$ | $\cdots$ | C, A | 29.590 | 4.400 | 0.341 | 6964 | Am | H |

Table 4—Continued

| Hipp. No. | HD No. | Gliese No. | Target[a] List | Dist. (pc) | $V$ (mag) | $B–V$ (mag) | $T_{\rm eff}$ (K) | Sp. T. | Notes[b] |
|---|---|---|---|---|---|---|---|---|---|
| 109176 | 210027 | 848 | S, C, A | 11.730 | 3.770 | 0.435 | 6442 | F5V | H |
| 109268 | 209952 | $\cdots$ | C | 31.000 | 1.700 | 0.070 | $\cdots$ | B7IV | H |
| 109427 | 210418 | $\cdots$ | C, A | 28.300 | 3.520 | 0.086 | 8569 | A2V | H |
| 109857 | 211336 | $\cdots$ | C, A | 26.200 | 4.170 | 0.278 | 7283 | F0IV | H |
| 110109 | 211415 | 853A | S, A | 13.790 | 5.360 | 0.614 | 5837 | G3V | S |
| 110618 | 211998 | 855.1A | A | 28.700 | 5.280 | 0.630 | 5486 | G9V | S |
| 110649 | 212330 | 857 | A | 20.560 | 5.310 | 0.670 | 5739 | G2IV-V | S |
| 110960 | $\cdots$ | $\cdots$ | C | 28.170 | 3.650 | 0.406 | 6619 | F3III-IV | H, E |
| 111169 | 213558 | $\cdots$ | C | 31.500 | 3.800 | 0.030 | $\cdots$ | A1V | H |
| 111449 | 213845 | 863.2 | A | 22.680 | 5.210 | 0.450 | 6597 | F5V | H |
| 112724 | 216228 | $\cdots$ | C | 35.300 | 3.700 | 1.050 | $\cdots$ | K0III | E |
| 112748 | 216131 | $\cdots$ | C | 32.500 | 3.700 | 0.930 | $\cdots$ | M2III | E |
| 112935 | 216385 | 9801A | A | 27.280 | 5.160 | 0.470 | 6250 | F6V | H |
| 113368 | 216956 | 881A | S, C, A | 7.700 | 1.230 | 0.140 | 8399 | A3V | H |
| 113638 | 217364 | $\cdots$ | C | 33.400 | 4.300 | 0.960 | $\cdots$ | G8III | S |
| 113860 | 217792 | 886.2 | A | 29.400 | 5.120 | 0.280 | 7143 | F1V | H, S |
| 114570 | 219080 | 891.1 | C, A | 24.590 | 4.520 | 0.302 | 7176 | F0V | H |
| 114996 | 219571 | $\cdots$ | C, A | 23.060 | 3.990 | 0.410 | 6618 | F3IV/V | S, H |
| 115126 | 219834 | $\cdots$ | A | 21.050 | 5.200 | 0.790 | 5461 | G8.5IV | |
| 116584 | 222107 | $\cdots$ | C | 26.410 | 3.850 | 0.987 | 4636 | G8III-IV | B |
| 116727 | 222404 | 903 | C | 14.100 | 3.210 | 1.031 | 4761 | K1IV | E |
| 118268 | 224617 | $\cdots$ | C | 32.000 | 4.100 | 0.420 | $\cdots$ | F4IV | H |

[a]Target list code: S = Starshade study mission target, C = Coronagraph study mission target, A = AFTA study mission target.

[b]Stars were not observed by Lick and Keck Doppler programs because of these (non-exhaustive) list of reasons: star too hot (H), typically earlier than F8V; star too far south (S); star is evolved (E) into a giant or subgiant; star too young (Y), with chromospheric activity substantially increasing jitter; or binary (B) or higher stellar multiple noted in the literature and/or our RVs. These reasons for a lack of observations were inferred in 2014 based on stellar properties and not based on a target down-selections when observing lists were created.

## C.    Completeness of Individual Stars

In this appendix show the results of automated searches for planets in our Doppler data. This search methodology is described fully in Sec. 5.1. We also show the completeness limits for each star computed by injection-recovery tests (Sec. 5.3). The figures below show these results in graphical form for the 76 stars for which we have Doppler data. Each figure caption lists the HD number, Hipparcos number, and the codes for the imaging program target lists (S = starshade, C = coronagraph, A = AFTA).
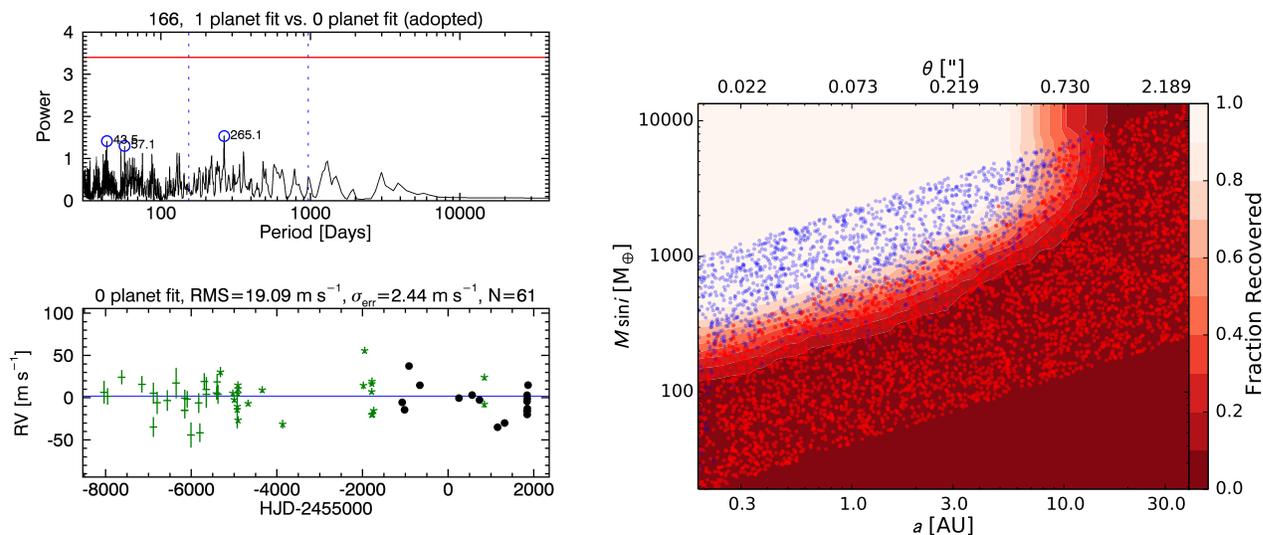


Fig. 14.— Results from an automated search for planets orbiting the star HD 166 (HIP 544; program(s) = S) based on RVs from Lick and/or Keck Observatory. The set of plots on the left (analogous to Figs. 3 and 4) show the planet search results and the plot on the right shows the completeness limits (analogous to Fig. 6). See the captions of those figures for detailed descriptions.
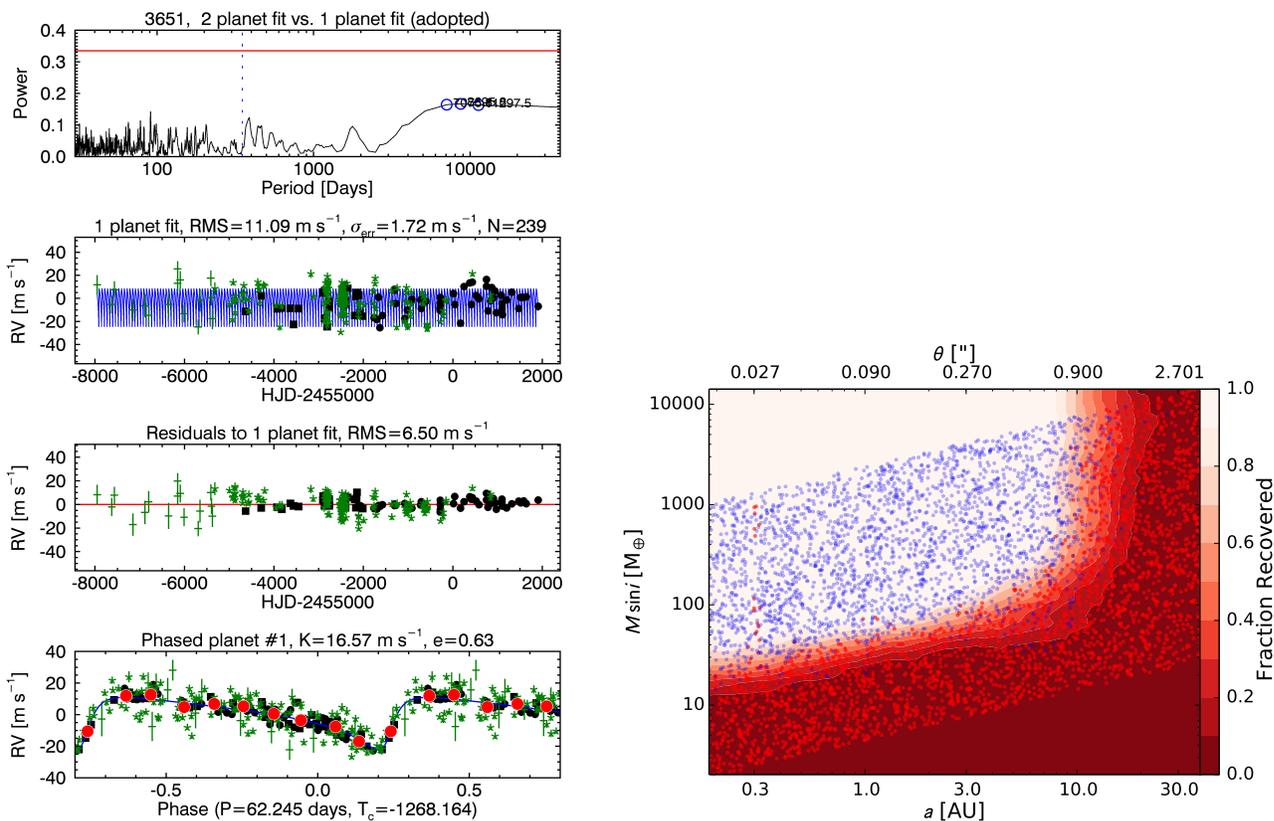
Fig. 15.— Results from an automated search for planets orbiting the star HD 3651 (HIP 3093; program(s) = S) based on RVs from Lick and/or Keck Observatory. The set of plots on the left (analogous to Figs. 3 and 4) show the planet search results and the plot on the right shows the completeness limits (analogous to Fig. 6). See the captions of those figures for detailed descriptions. This star has one known planet.
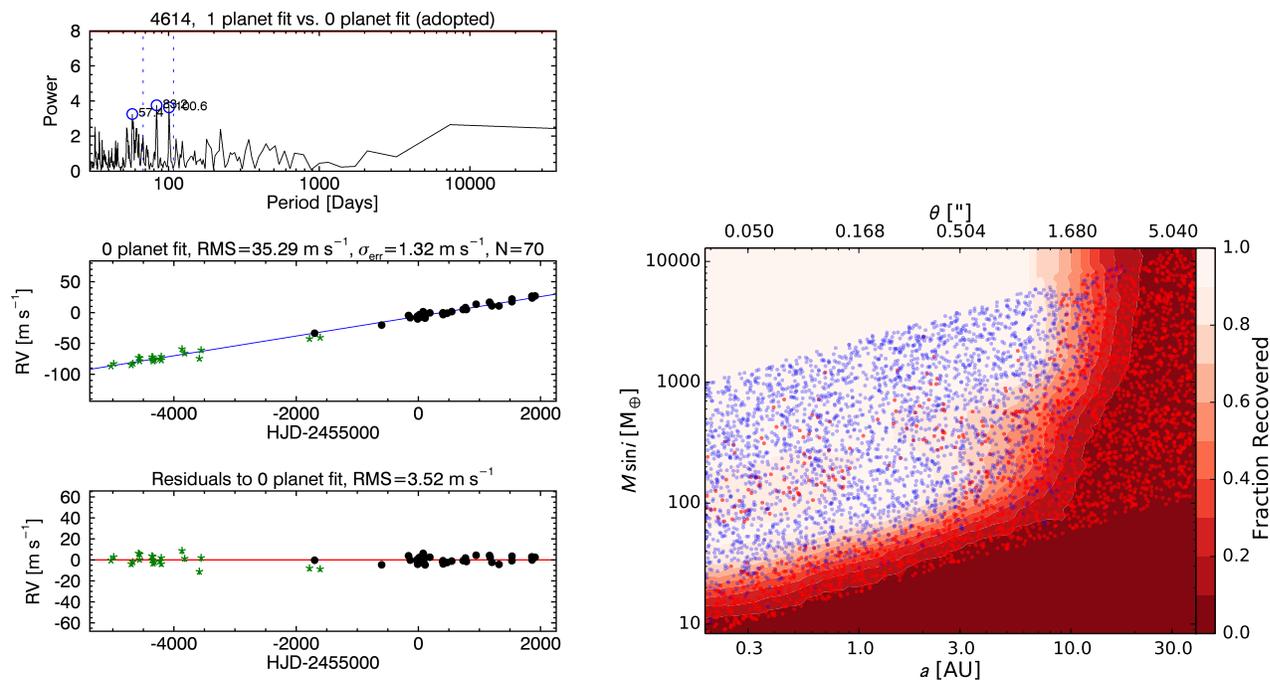
Fig. 16.— Results from an automated search for planets orbiting the star HD 4614 (HIP 3821; program(s) = S, C, A) based on RVs from Lick and/or Keck Observatory. The set of plots on the left (analogous to Figs. 3 and 4) show the planet search results and the plot on the right shows the completeness limits (analogous to Fig. 6). See the captions of those figures for detailed descriptions. This star shows a significant linear trend with no detectable curvature, presumably due to its known stellar companion.
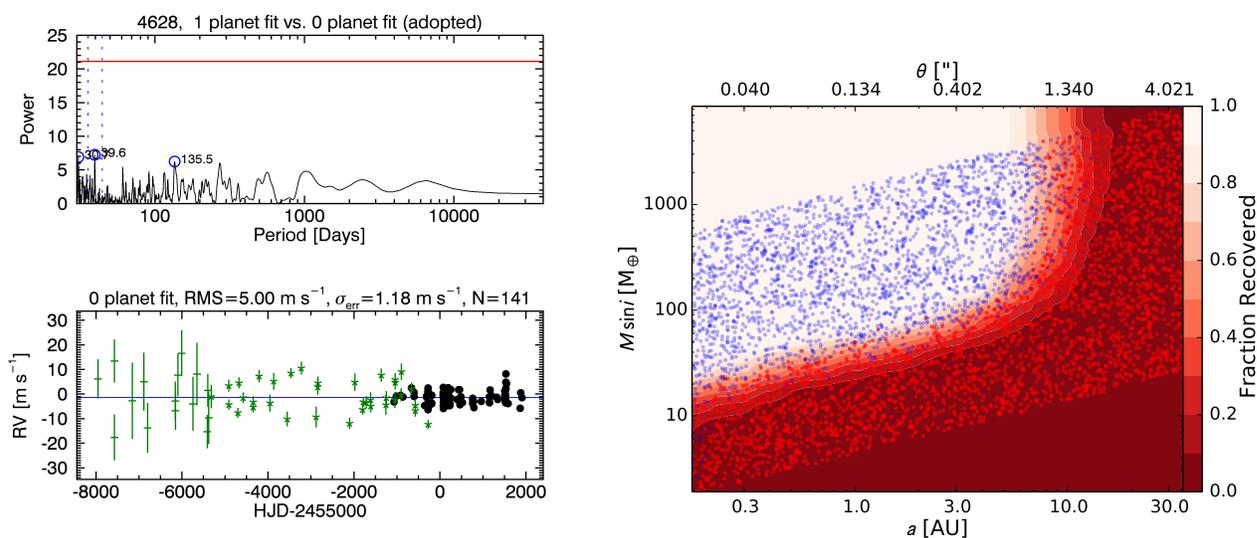
Fig. 17.— Results from an automated search for planets orbiting the star HD 4628 (HIP 3765; program(s) = S, C) based on RVs from Lick and/or Keck Observatory. The set of plots on the left (analogous to Figs. 3 and 4) show the planet search results and the plot on the right shows the completeness limits (analogous to Fig. 6). See the captions of those figures for detailed descriptions.
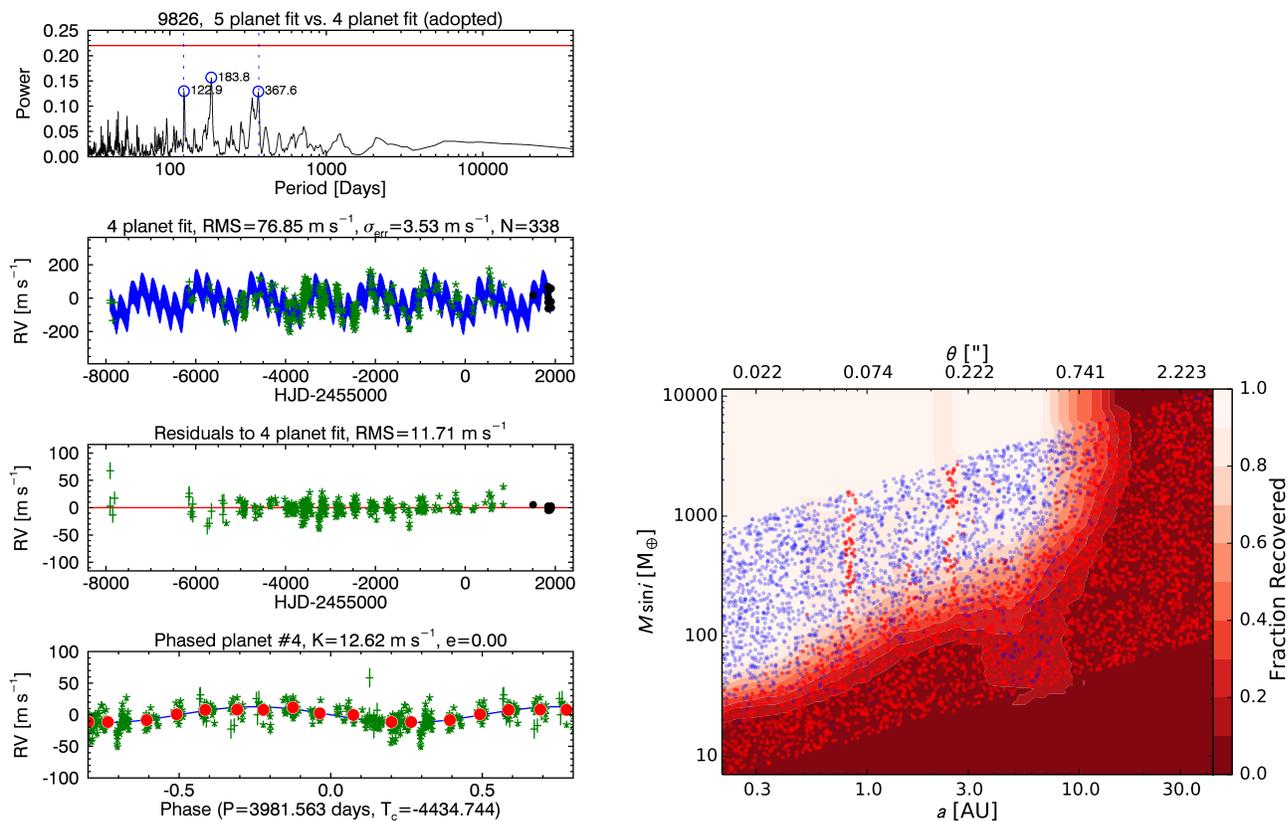
Fig. 18.— Results from an automated search for planets orbiting the star HD 9826 (HIP 7513; program(s) = C, A) based on RVs from Lick and/or Keck Observatory. The set of plots on the left (analogous to Figs. 3 and 4) show the planet search results and the plot on the right shows the completeness limits (analogous to Fig. 6). See the captions of those figures for detailed descriptions. This star has three known planets. We detect an additional periodicity at ∼4000 days and interpret this as the signature of a stellar magnetic activity cycle.
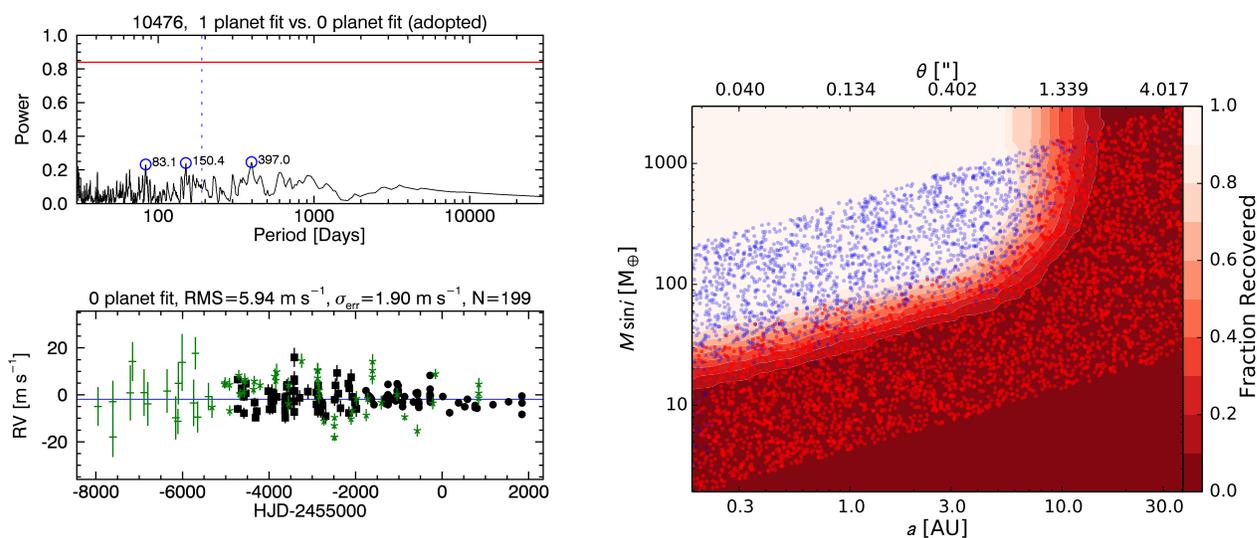
Fig. 19.— Results from an automated search for planets orbiting the star HD 10476 (HIP 7981; program(s) = S, C, A) based on RVs from Lick and/or Keck Observatory. The set of plots on the left (analogous to Figs. 3 and 4) show the planet search results and the plot on the right shows the completeness limits (analogous to Fig. 6). See the captions of those figures for detailed descriptions.
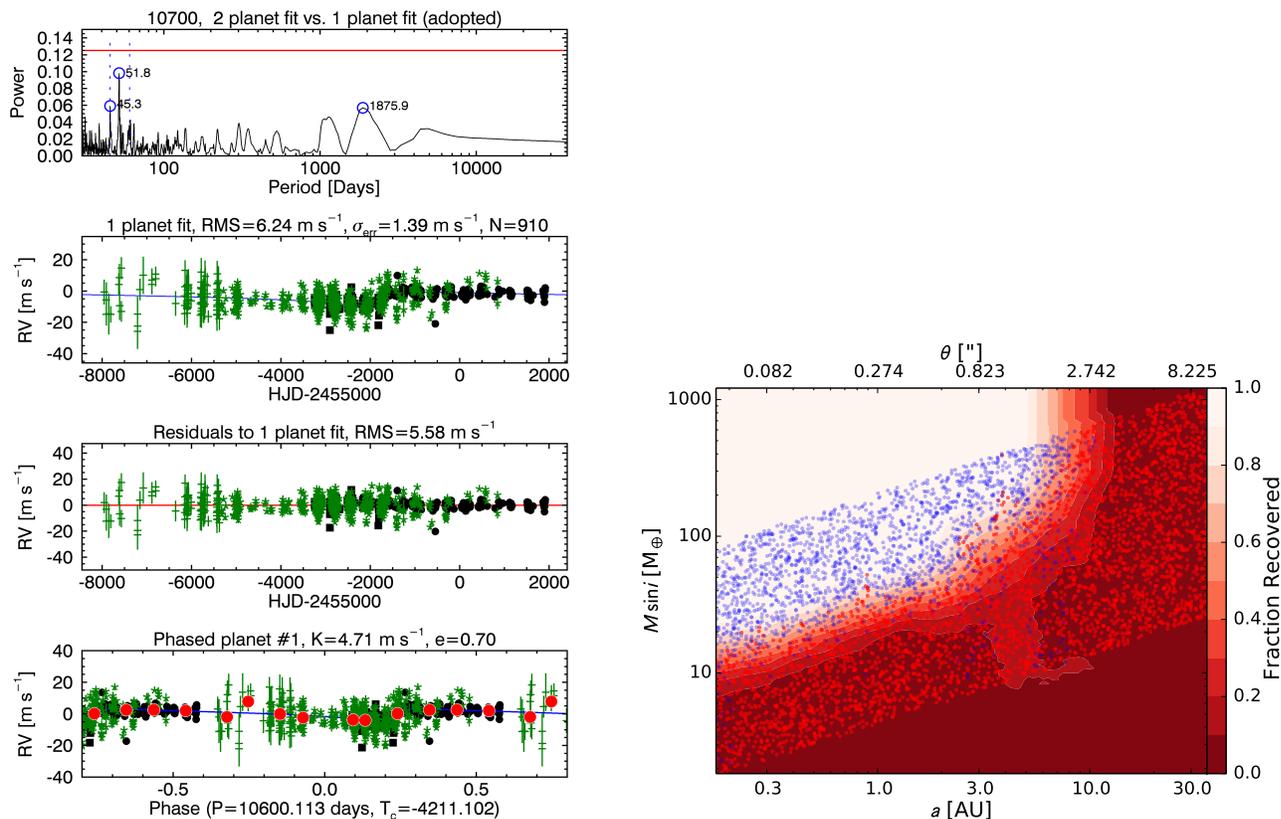
Fig. 20.— Results from an automated search for planets orbiting the star HD 10700 (HIP 8102; program(s) = S, C, A) based on RVs from Lick and/or Keck Observatory. The set of plots on the left (analogous to Figs. 3 and 4) show the planet search results and the plot on the right shows the completeness limits (analogous to Fig. 6). See the captions of those figures for detailed descriptions. The automated pipeline detects a long-period signal but it appears to be caused by a poorly constrained offset between datasets. We do not detect to five controversial, low-mass planets claimed by Tuomi et al. (2013).
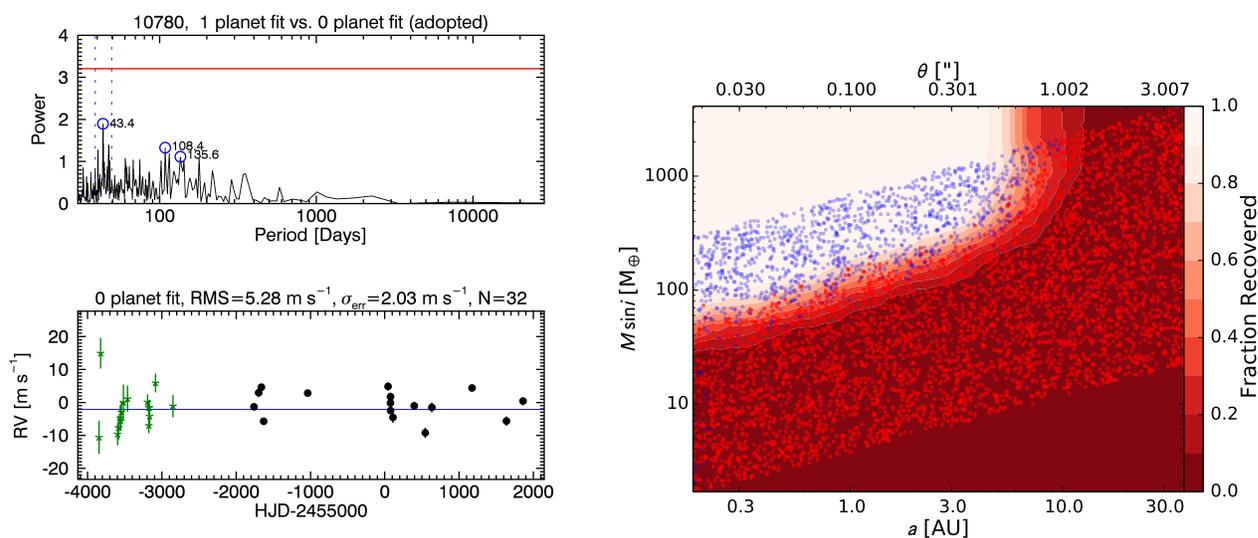
Fig. 21.— Results from an automated search for planets orbiting the star HD 10780 (HIP 8362; program(s) = S) based on RVs from Lick and/or Keck Observatory. The set of plots on the left (analogous to Figs. 3 and 4) show the planet search results and the plot on the right shows the completeness limits (analogous to Fig. 6). See the captions of those figures for detailed descriptions.
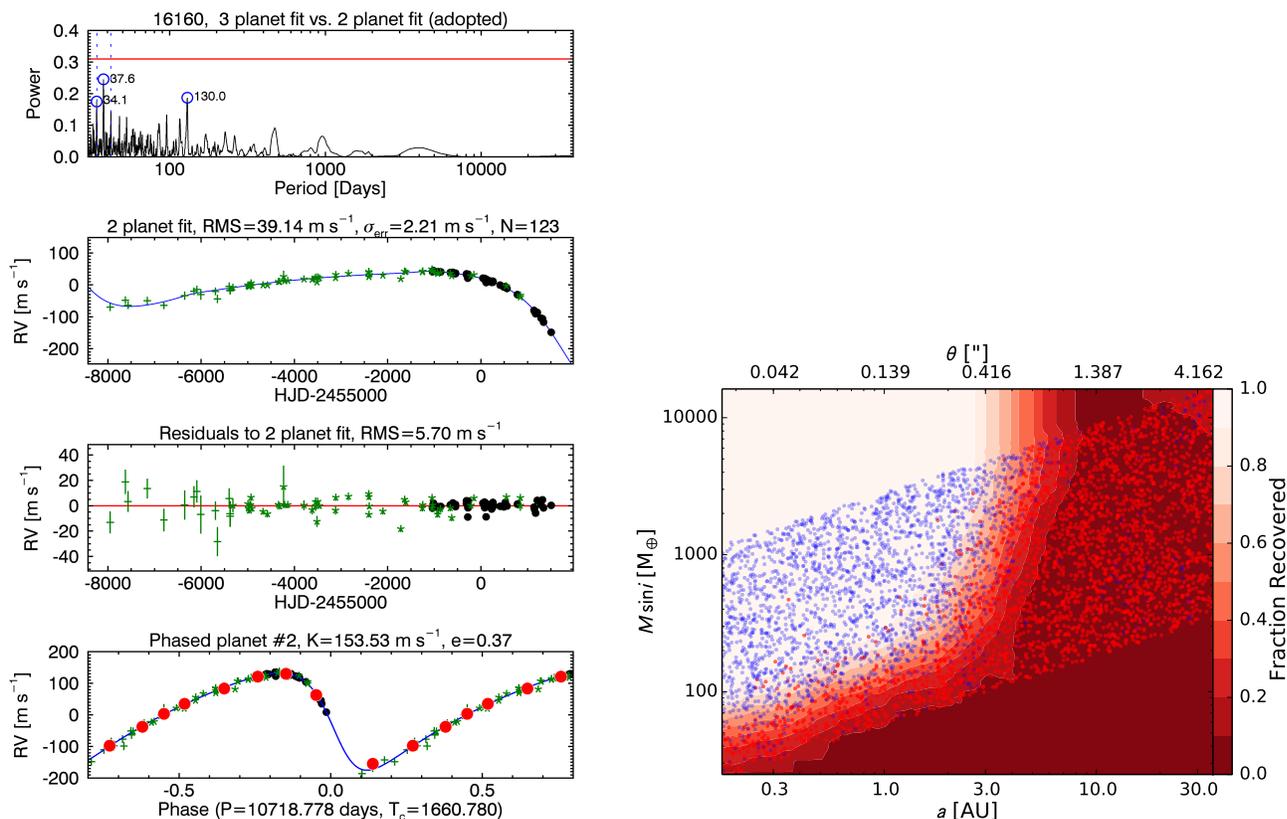
Fig. 22.— Results from an automated search for planets orbiting the star HD 16160 (HIP 12114; program(s) = S) based on RVs from Lick and/or Keck Observatory. The set of plots on the left (analogous to Figs. 3 and 4) show the planet search results and the plot on the right shows the completeness limits (analogous to Fig. 6). See the captions of those figures for detailed descriptions. The RV time-series for this star shows significant curvature from a late M-type companion. The RV curvature makes it difficult to detect long-period planets in this system.
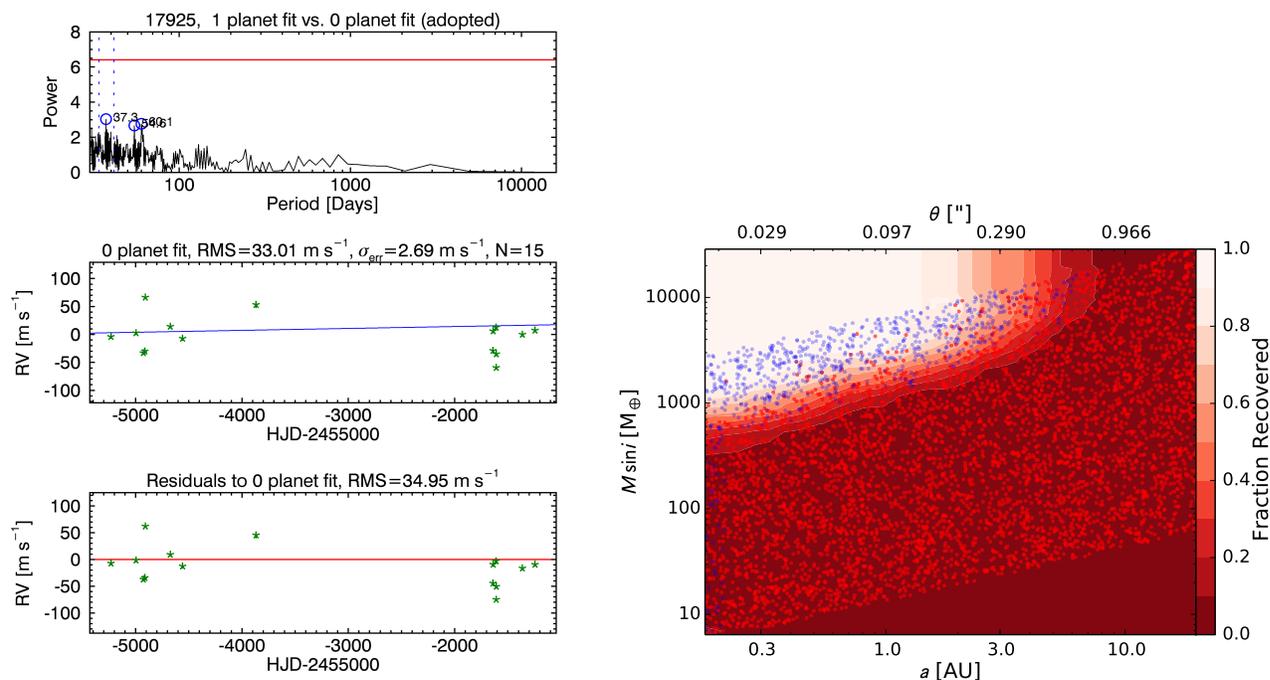
Fig. 23.— Results from an automated search for planets orbiting the star HD 17925 (HIP 13402; program(s) = S) based on RVs from Lick and/or Keck Observatory. The set of plots on the left (analogous to Figs. 3 and 4) show the planet search results and the plot on the right shows the completeness limits (analogous to Fig. 6). See the captions of those figures for detailed descriptions. The automated pipeline detects a marginally significant linear trend in the RV time series.
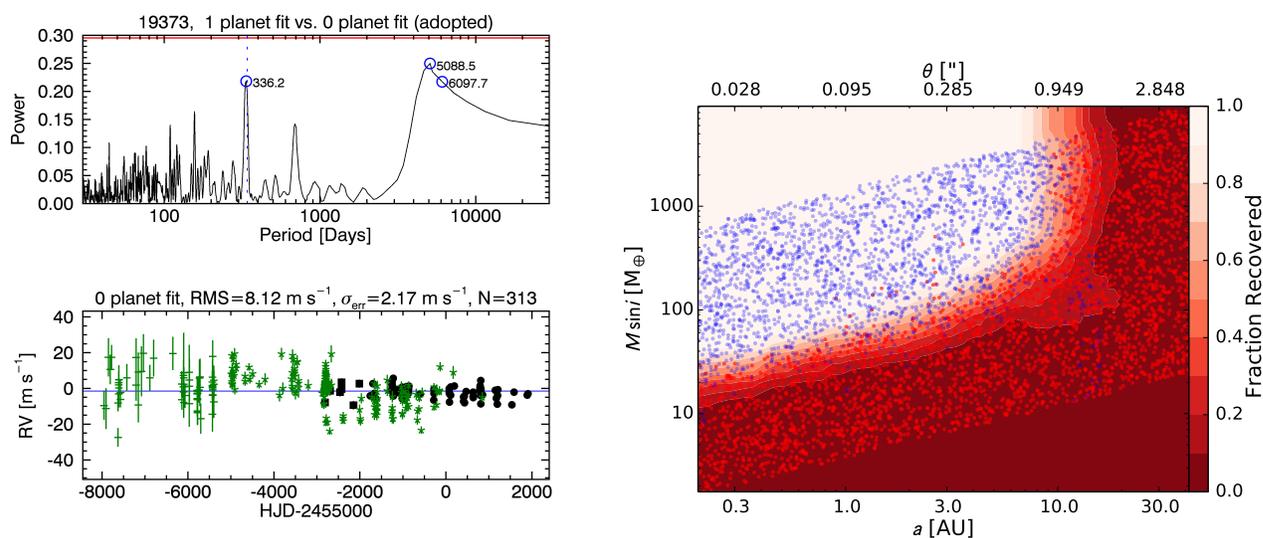
Fig. 24.— Results from an automated search for planets orbiting the star HD 19373 (HIP 14632; program(s) = S, C, A) based on RVs from Lick and/or Keck Observatory. The set of plots on the left (analogous to Figs. 3 and 4) show the planet search results and the plot on the right shows the completeness limits (analogous to Fig. 6). See the captions of those figures for detailed descriptions.
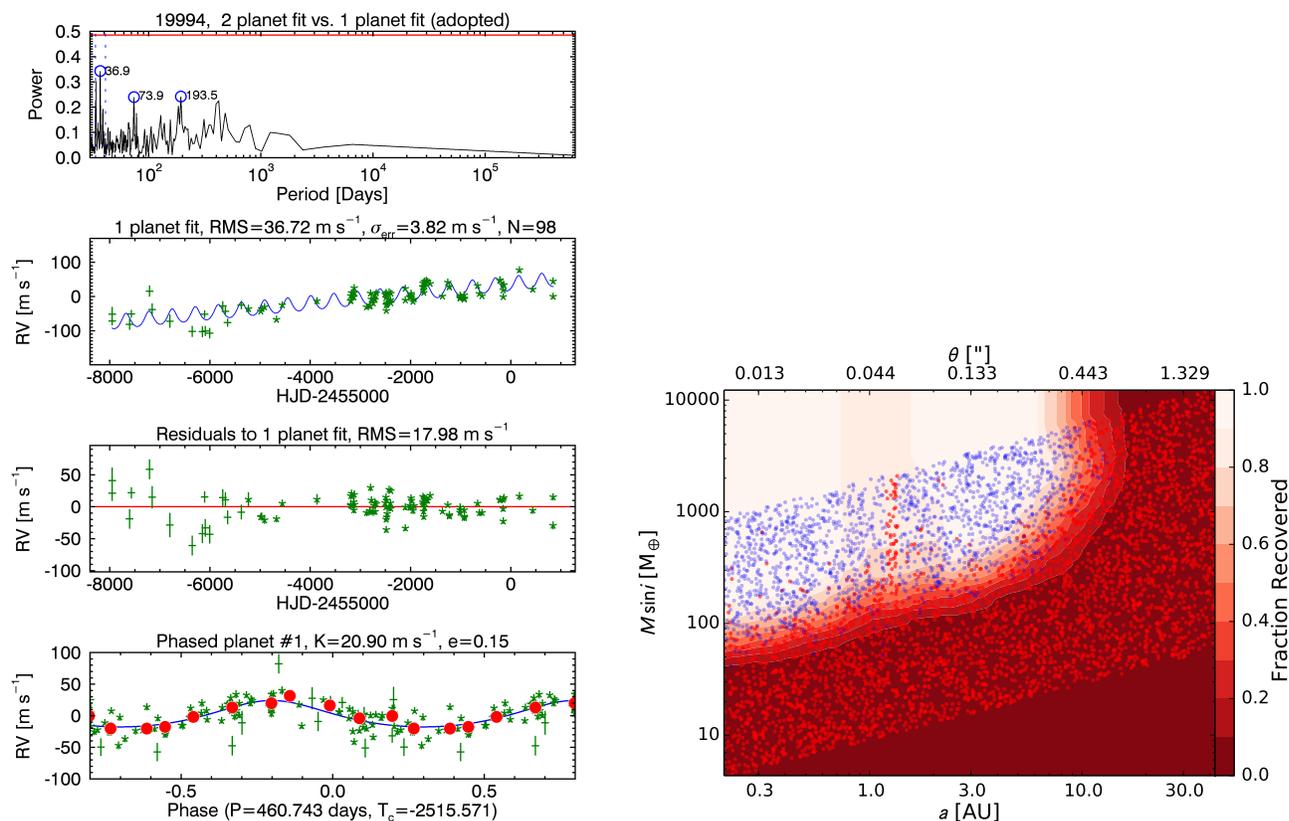
Fig. 25.— Results from an automated search for planets orbiting the star HD 19994 (HIP 14954; program(s) = A) based on RVs from Lick and/or Keck Observatory. The set of plots on the left (analogous to Figs. 3 and 4) show the planet search results and the plot on the right shows the completeness limits (analogous to Fig. 6). See the captions of those figures for detailed descriptions. This star has one known planet. The pipeline also detects a linear trend in the RV time series.
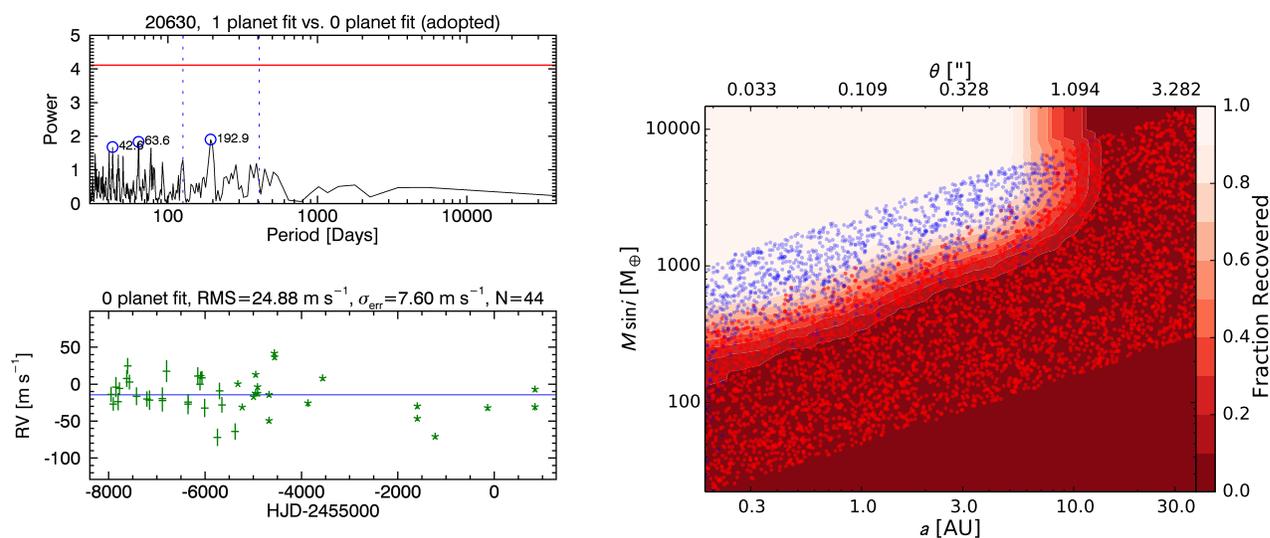
Fig. 26.— Results from an automated search for planets orbiting the star HD 20630 (HIP 15457; program(s) = S, C, A) based on RVs from Lick and/or Keck Observatory. The set of plots on the left (analogous to Figs. 3 and 4) show the planet search results and the plot on the right shows the completeness limits (analogous to Fig. 6). See the captions of those figures for detailed descriptions.
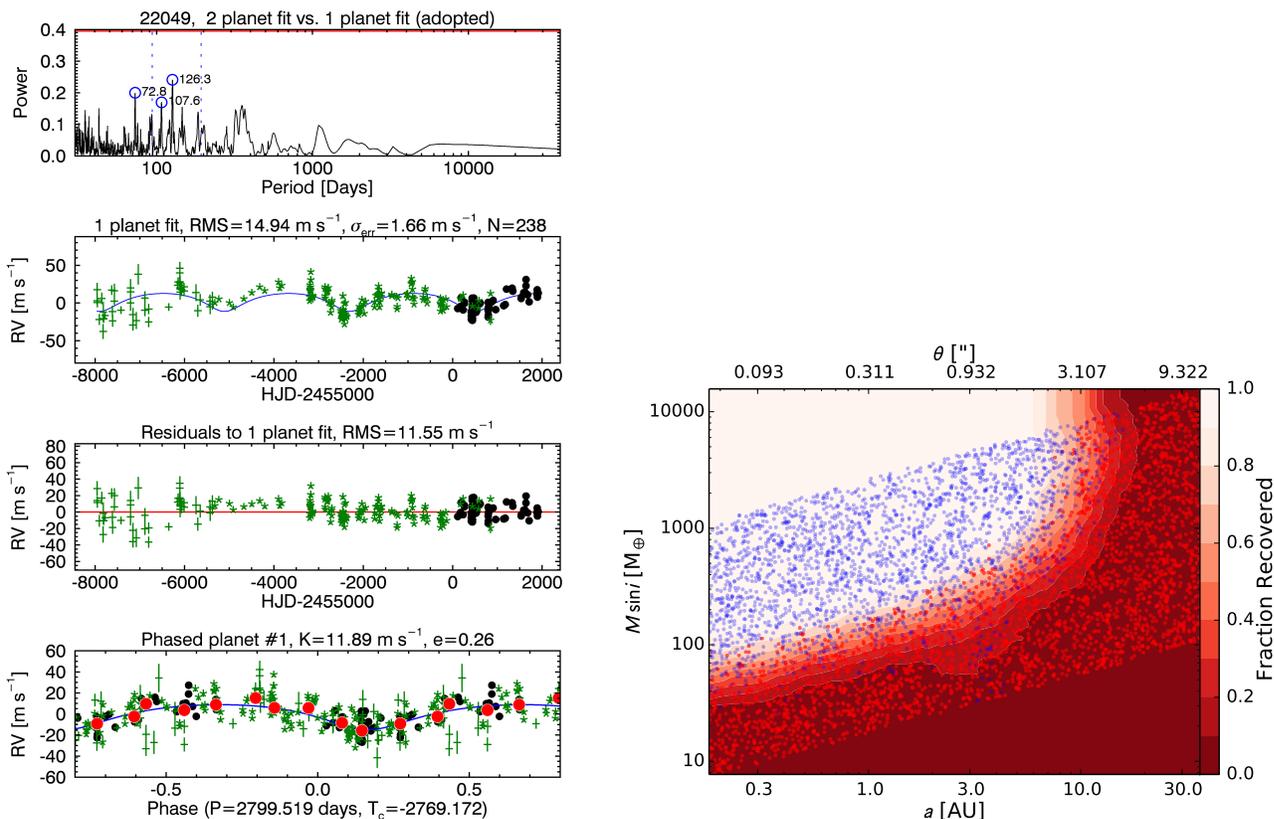
Fig. 27.— Results from an automated search for planets orbiting the star HD 22049 (HIP 16537; program(s) = C, A) based on RVs from Lick and/or Keck Observatory. The set of plots on the left (analogous to Figs. 3 and 4) show the planet search results and the plot on the right shows the completeness limits (analogous to Fig. 6). See the captions of those figures for detailed descriptions. This star has one known, long-period planet, which we clearly detect in the Rv time series. This claim has been controversial because the host star is young and active. However, our measurements of the activity-sensitive Ca II H & K lines in Keck spectra do not correlate with the RVs.
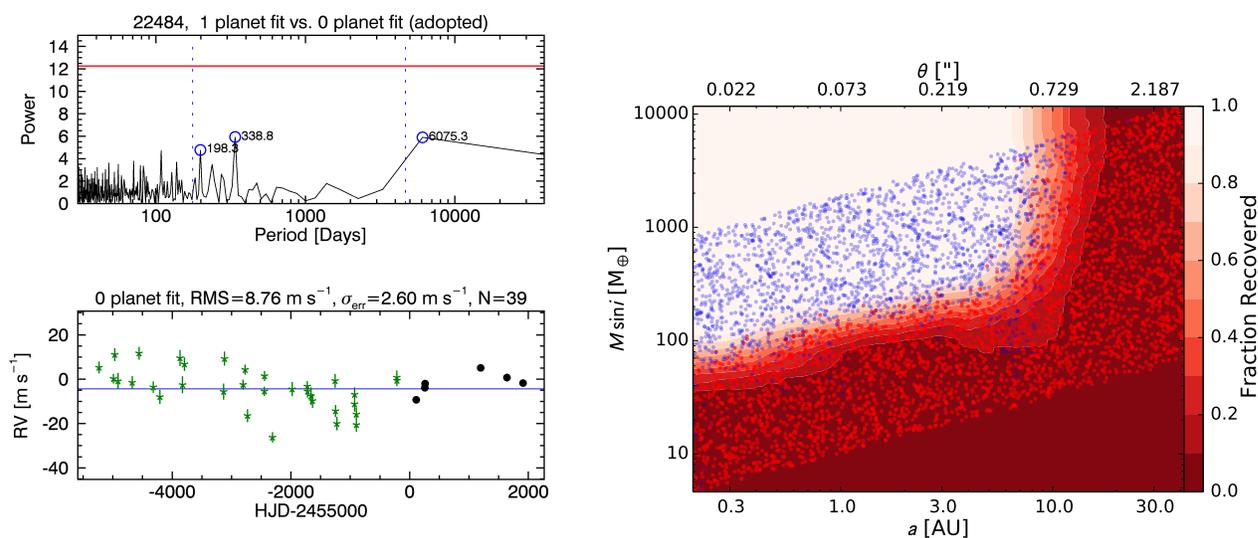
Fig. 28.— Results from an automated search for planets orbiting the star HD 22484 (HIP 16852; program(s) = S, C, A) based on RVs from Lick and/or Keck Observatory. The set of plots on the left (analogous to Figs. 3 and 4) show the planet search results and the plot on the right shows the completeness limits (analogous to Fig. 6). See the captions of those figures for detailed descriptions.
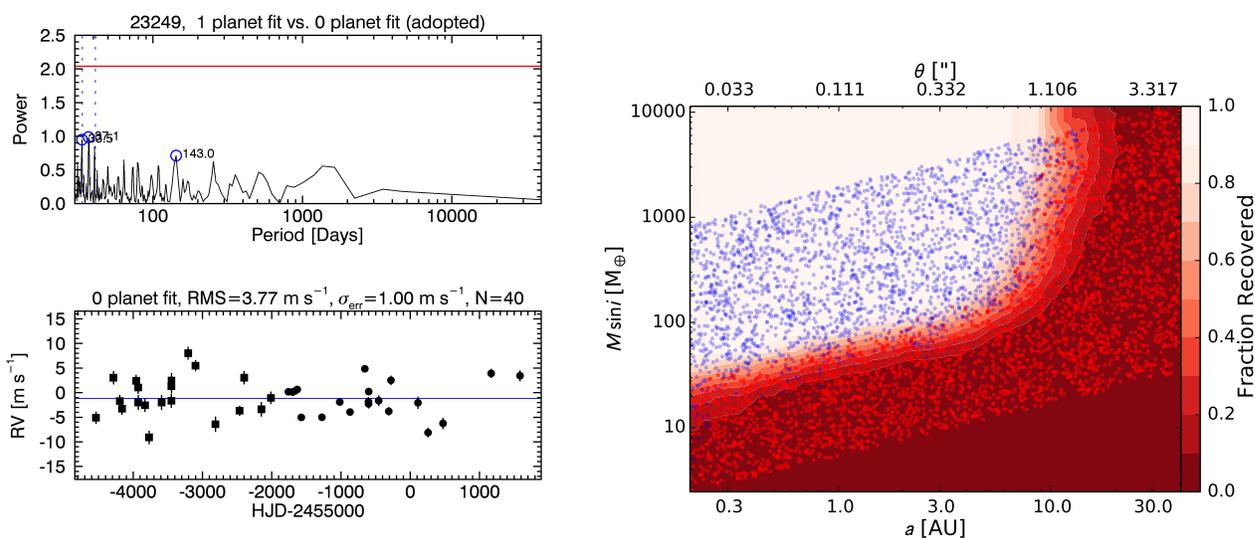
Fig. 29.— Results from an automated search for planets orbiting the star HD 23249 (HIP 17378; program(s) = S, C) based on RVs from Lick and/or Keck Observatory. The set of plots on the left (analogous to Figs. 3 and 4) show the planet search results and the plot on the right shows the completeness limits (analogous to Fig. 6). See the captions of those figures for detailed descriptions.
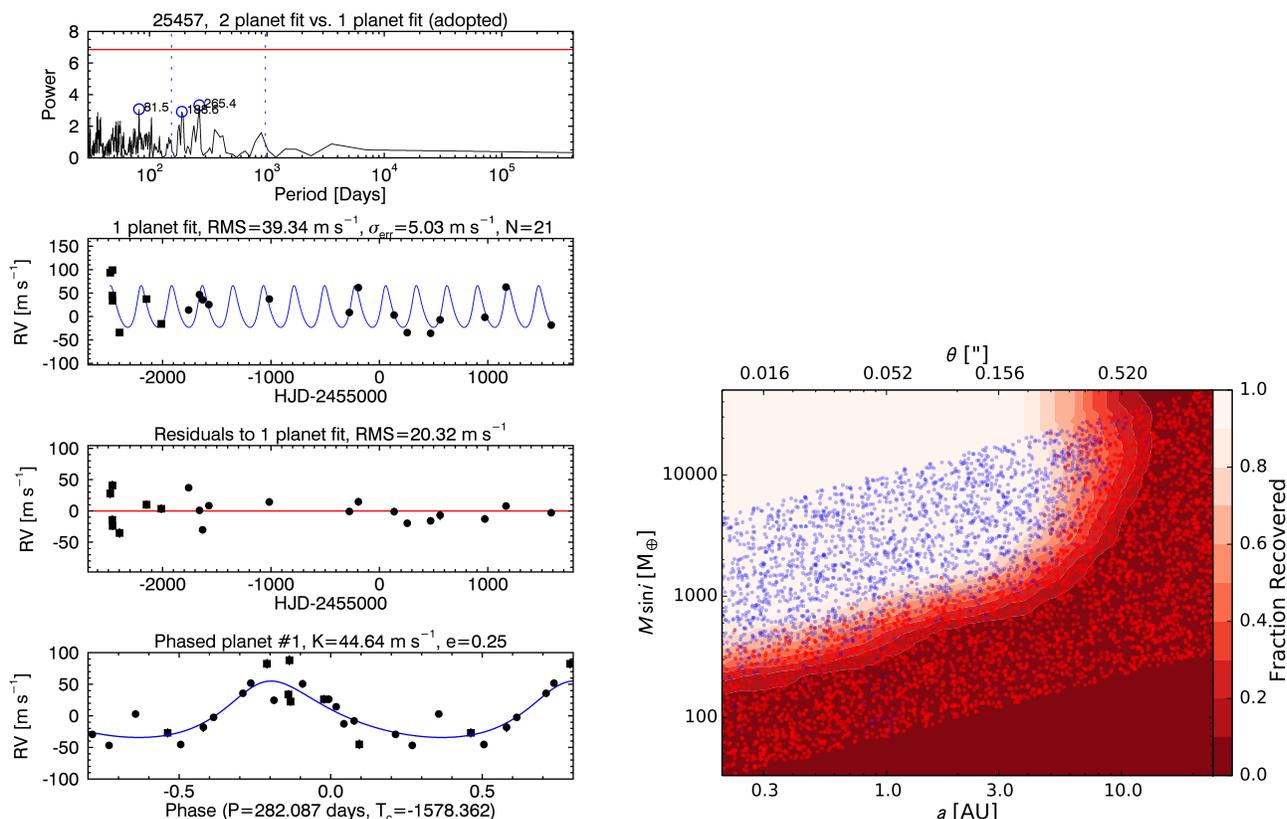
Fig. 30.— Results from an automated search for planets orbiting the star HD 25457 (HIP 18859; program(s) = A) based on RVs from Lick and/or Keck Observatory. The set of plots on the left (analogous to Figs. 3 and 4) show the planet search results and the plot on the right shows the completeness limits (analogous to Fig. 6). See the captions of those figures for detailed descriptions. The automated pipeline formally identifies a planet candidate based on 21 Keck RVs. Given the high jitter and small number of observations, we deem this candidate not credible with the current data.
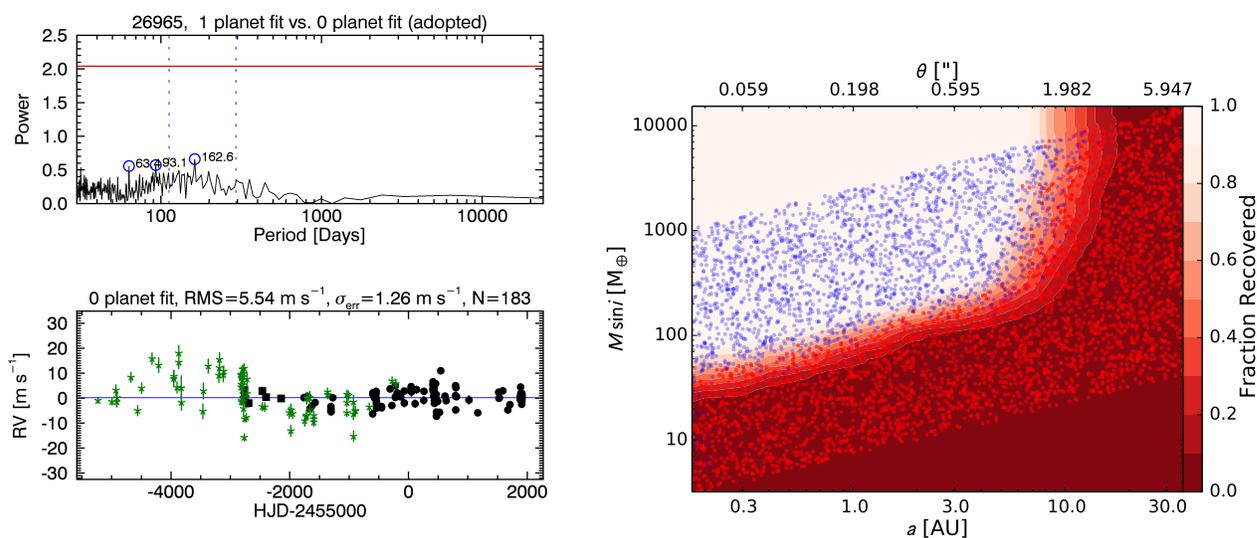
Fig. 31.— Results from an automated search for planets orbiting the star HD 26965 (HIP 19849; program(s) = S, C, A) based on RVs from Lick and/or Keck Observatory. The set of plots on the left (analogous to Figs. 3 and 4) show the planet search results and the plot on the right shows the completeness limits (analogous to Fig. 6). See the captions of those figures for detailed descriptions.
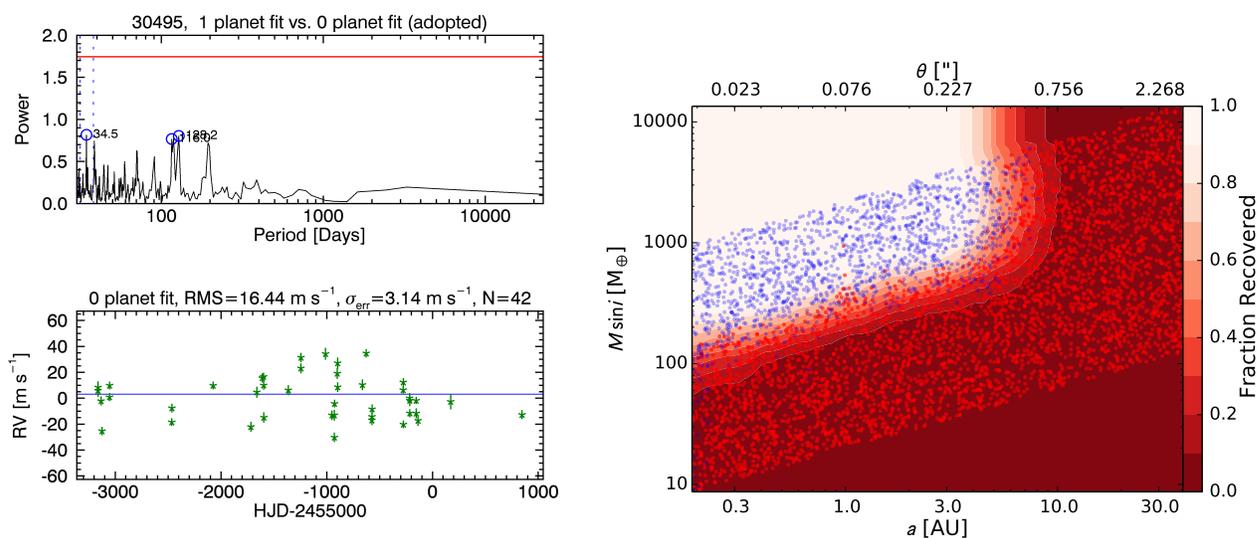
Fig. 32.— Results from an automated search for planets orbiting the star HD 30495 (HIP 22263; program(s) = S) based on RVs from Lick and/or Keck Observatory. The set of plots on the left (analogous to Figs. 3 and 4) show the planet search results and the plot on the right shows the completeness limits (analogous to Fig. 6). See the captions of those figures for detailed descriptions.
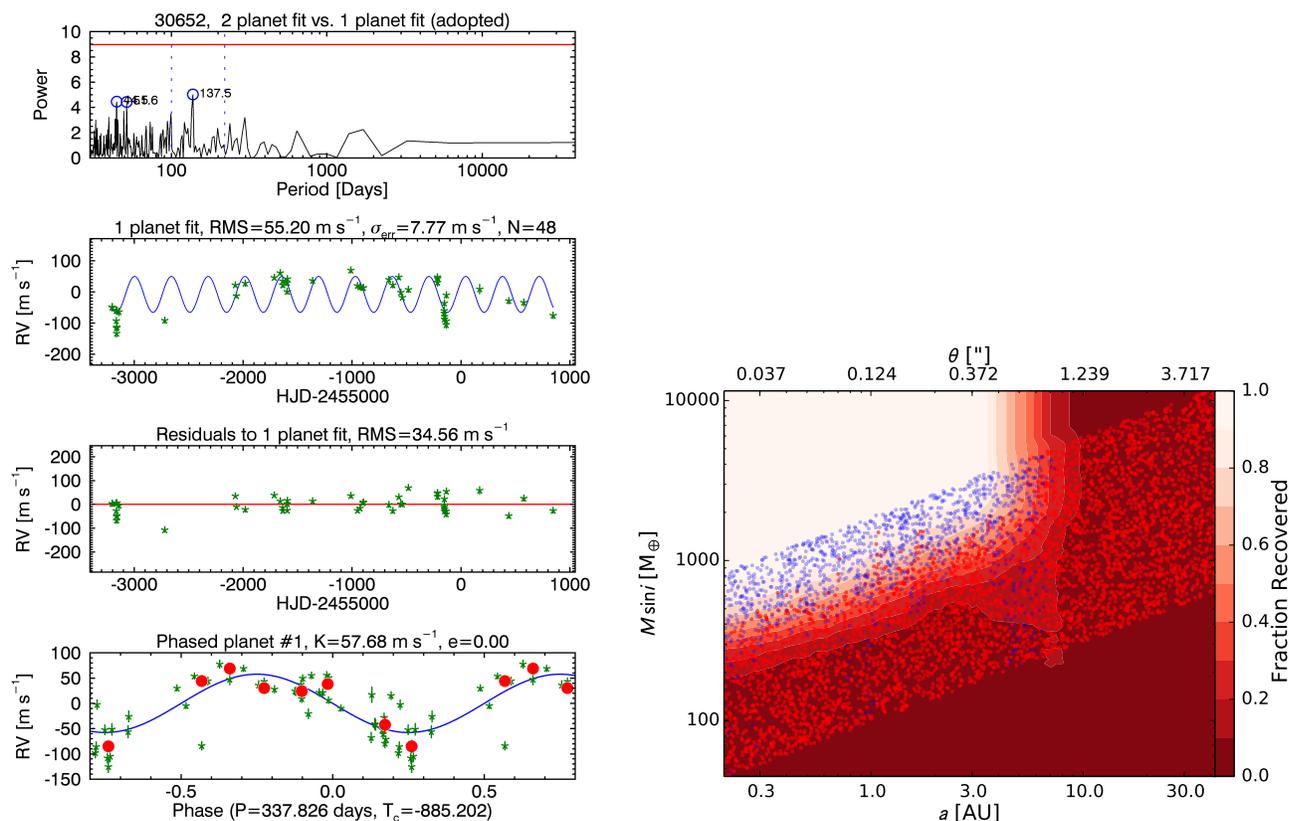
Fig. 33.— Results from an automated search for planets orbiting the star HD 30652 (HIP 22449; program(s) = S, C, A) based on RVs from Lick and/or Keck Observatory. The set of plots on the left (analogous to Figs. 3 and 4) show the planet search results and the plot on the right shows the completeness limits (analogous to Fig. 6). See the captions of those figures for detailed descriptions. We detect a marginally significant periodic signal with a period of 338 days. However, the poor observing history and the proximity of the period to one year, we conclude that this signal is not caused by a real planetary companion. The nature of the signal is most likely non-astrophysical in nature.
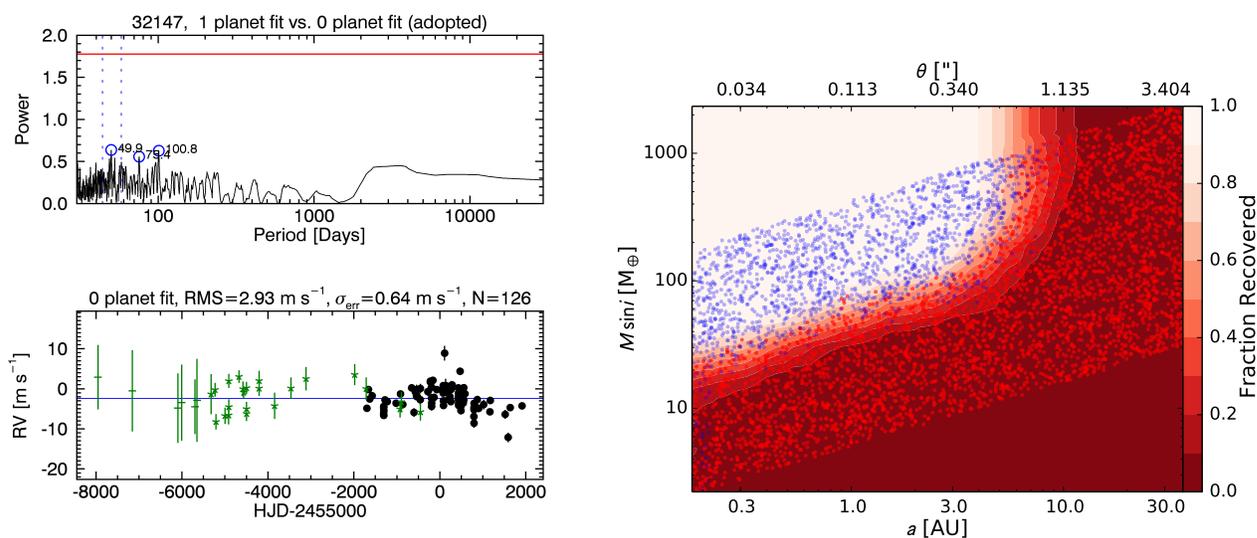
Fig. 34.— Results from an automated search for planets orbiting the star HD 32147 (HIP 23311; program(s) = S) based on RVs from Lick and/or Keck Observatory. The set of plots on the left (analogous to Figs. 3 and 4) show the planet search results and the plot on the right shows the completeness limits (analogous to Fig. 6). See the captions of those figures for detailed descriptions.
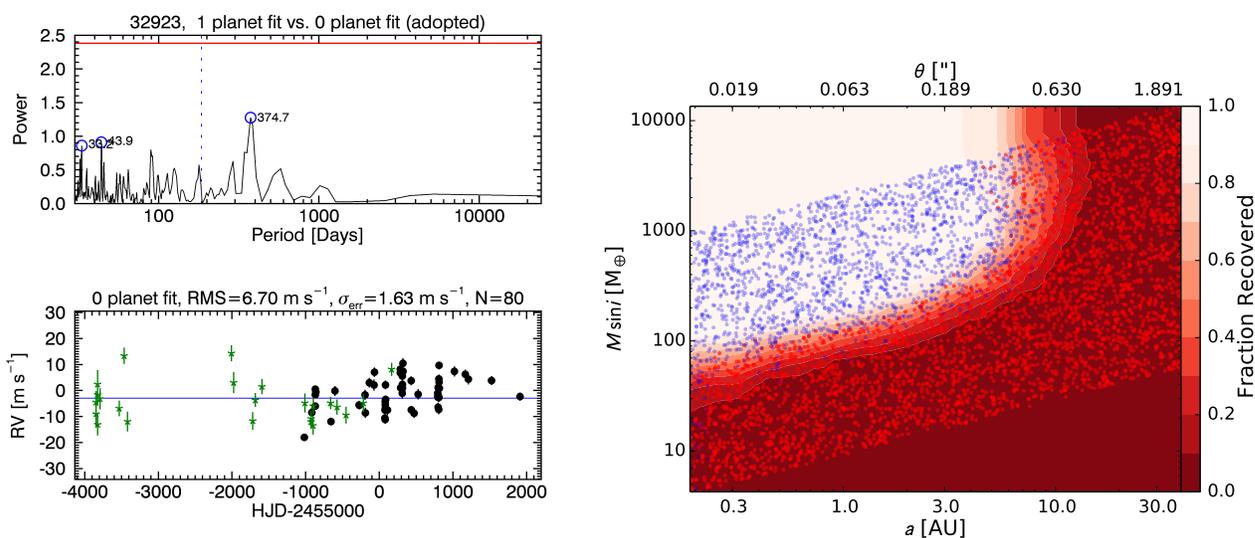
Fig. 35.— Results from an automated search for planets orbiting the star HD 32923 (HIP 23835; program(s) = S, C, A) based on RVs from Lick and/or Keck Observatory. The set of plots on the left (analogous to Figs. 3 and 4) show the planet search results and the plot on the right shows the completeness limits (analogous to Fig. 6). See the captions of those figures for detailed descriptions.
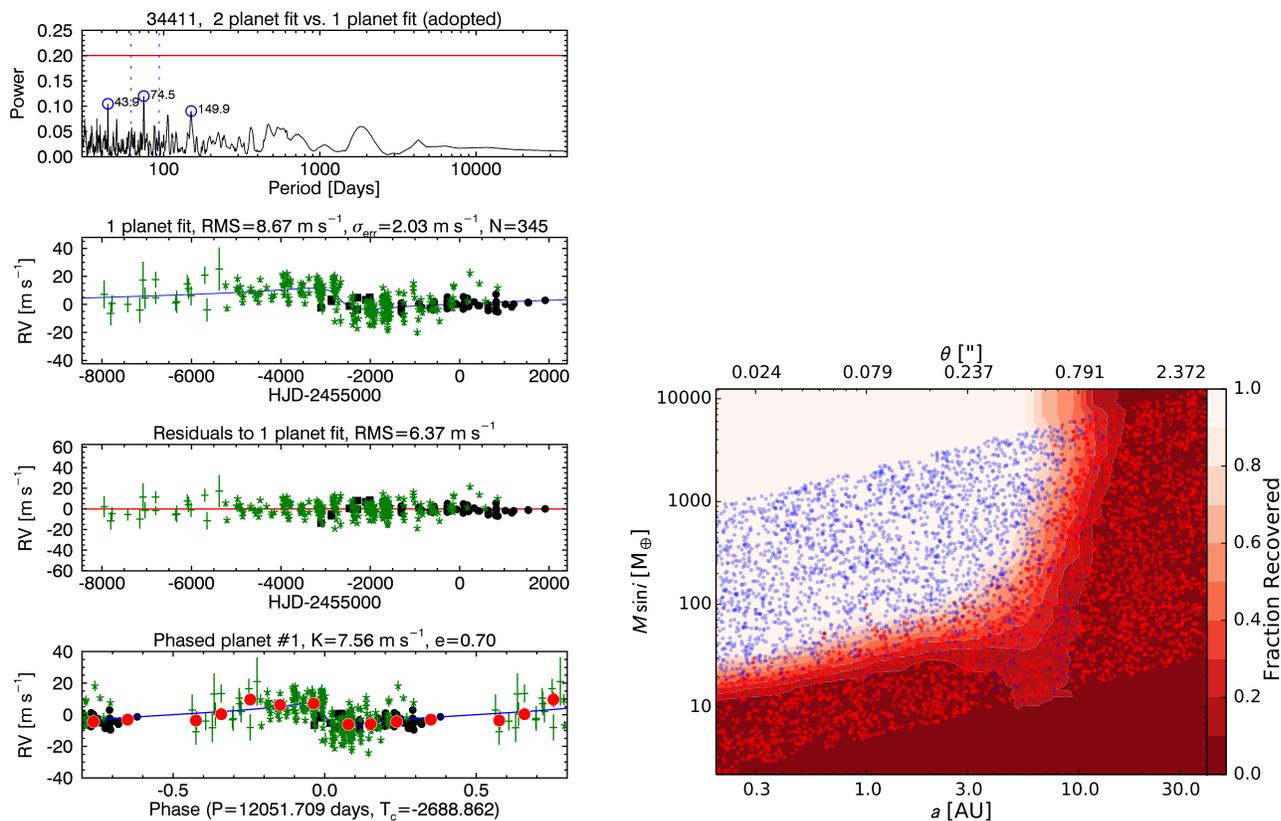
Fig. 36.— Results from an automated search for planets orbiting the star HD 34411 (HIP 24813; program(s) = S, C, A) based on RVs from Lick and/or Keck Observatory. The set of plots on the left (analogous to Figs. 3 and 4) show the planet search results and the plot on the right shows the completeness limits (analogous to Fig. 6). See the captions of those figures for detailed descriptions. The automated pipeline picks up a long-period, high-eccentricity signal that is likely due to poorly constrained offsets between instruments
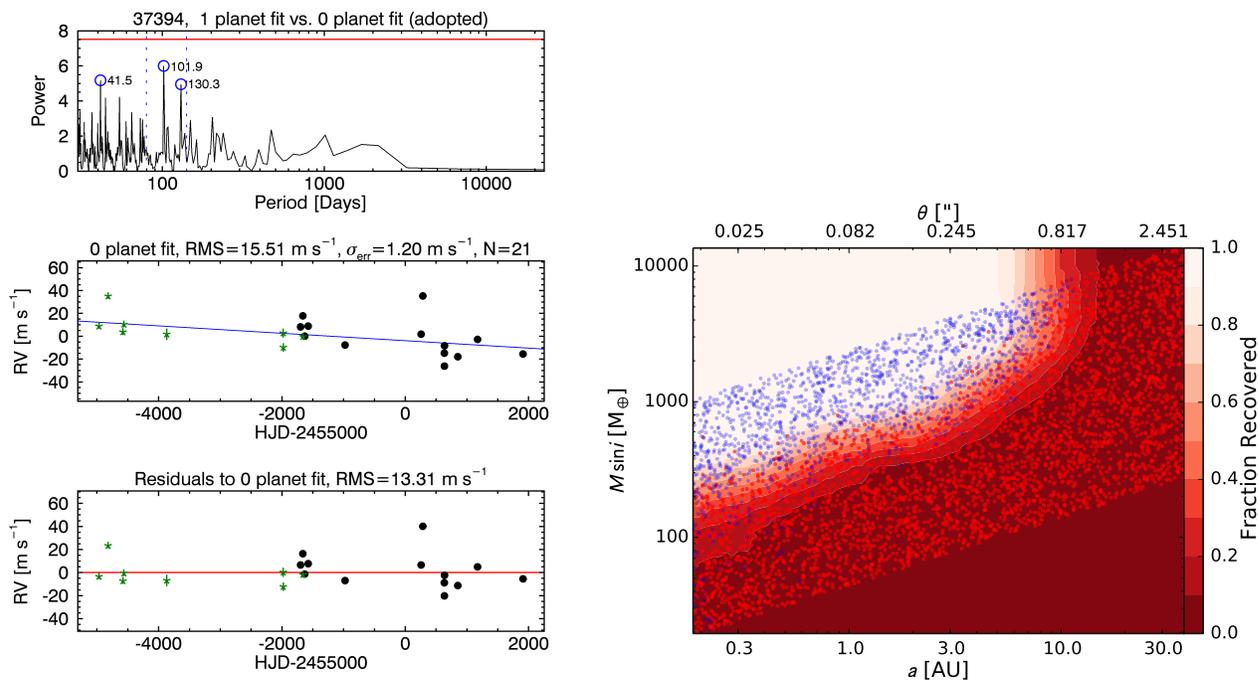
Fig. 37.— Results from an automated search for planets orbiting the star HD 37394 (HIP 26779; program(s) = S) based on RVs from Lick and/or Keck Observatory. The set of plots on the left (analogous to Figs. 3 and 4) show the planet search results and the plot on the right shows the completeness limits (analogous to Fig. 6). See the captions of those figures for detailed descriptions. This young, active star shows a small, marginally significant linear trend.
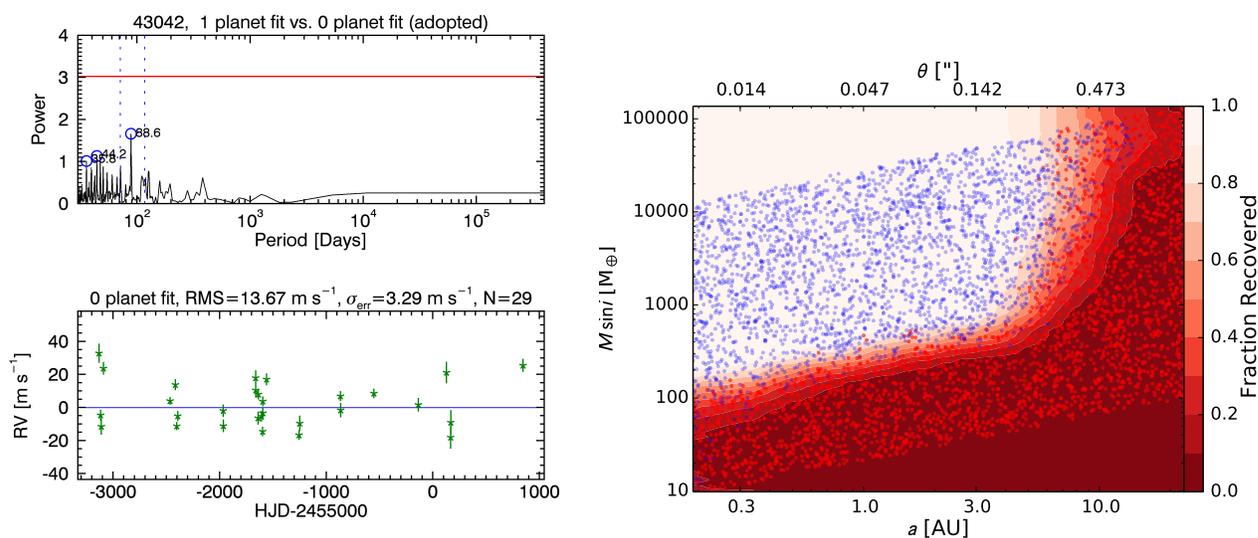
Fig. 38.— Results from an automated search for planets orbiting the star HD 43042 (HIP 29650; program(s) = A) based on RVs from Lick and/or Keck Observatory. The set of plots on the left (analogous to Figs. 3 and 4) show the planet search results and the plot on the right shows the completeness limits (analogous to Fig. 6). See the captions of those figures for detailed descriptions.
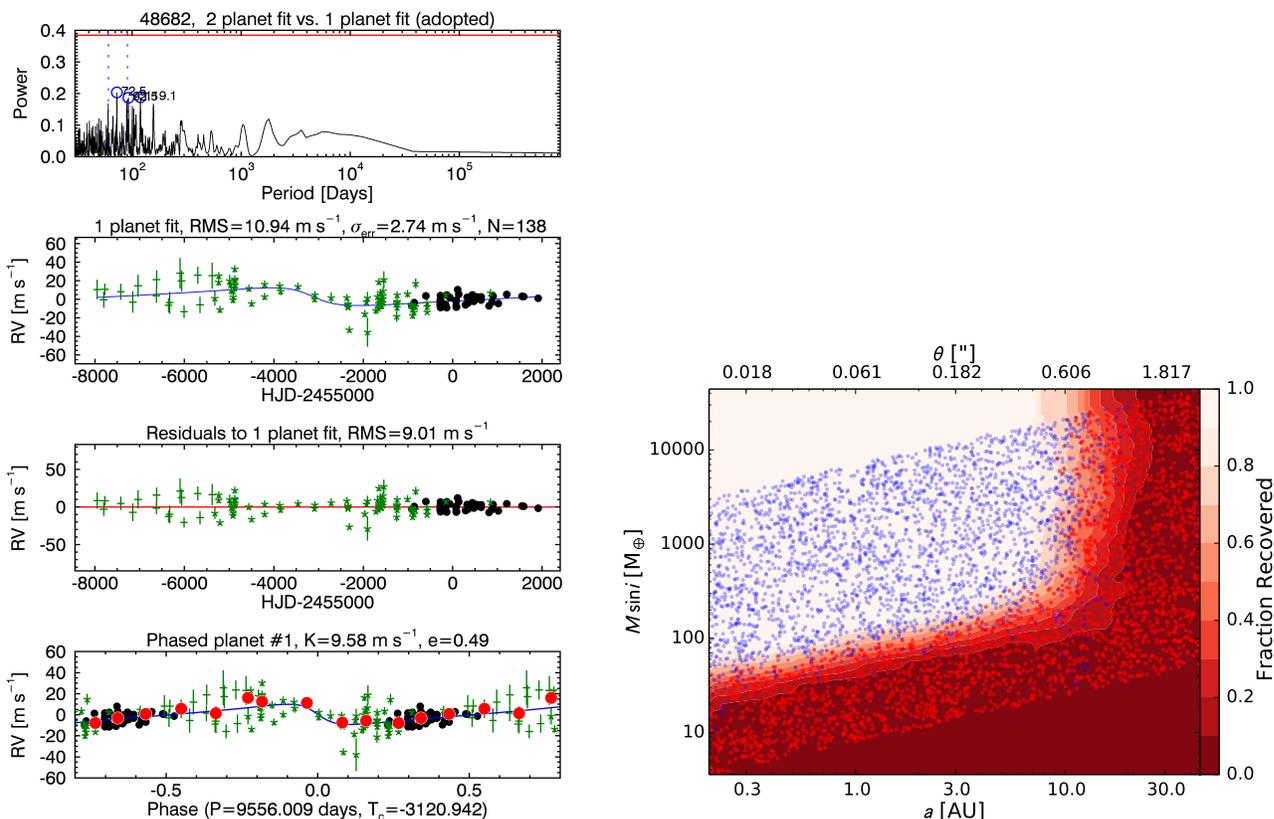
Fig. 39.— Results from an automated search for planets orbiting the star HD 48682 (HIP 32480; program(s) = A) based on RVs from Lick and/or Keck Observatory. The set of plots on the left (analogous to Figs. 3 and 4) show the planet search results and the plot on the right shows the completeness limits (analogous to Fig. 6). See the captions of those figures for detailed descriptions. This star has a formally adopted signal that appears to be due to uncorrected zero-point offsets in the Lick RVs and not due a planet.
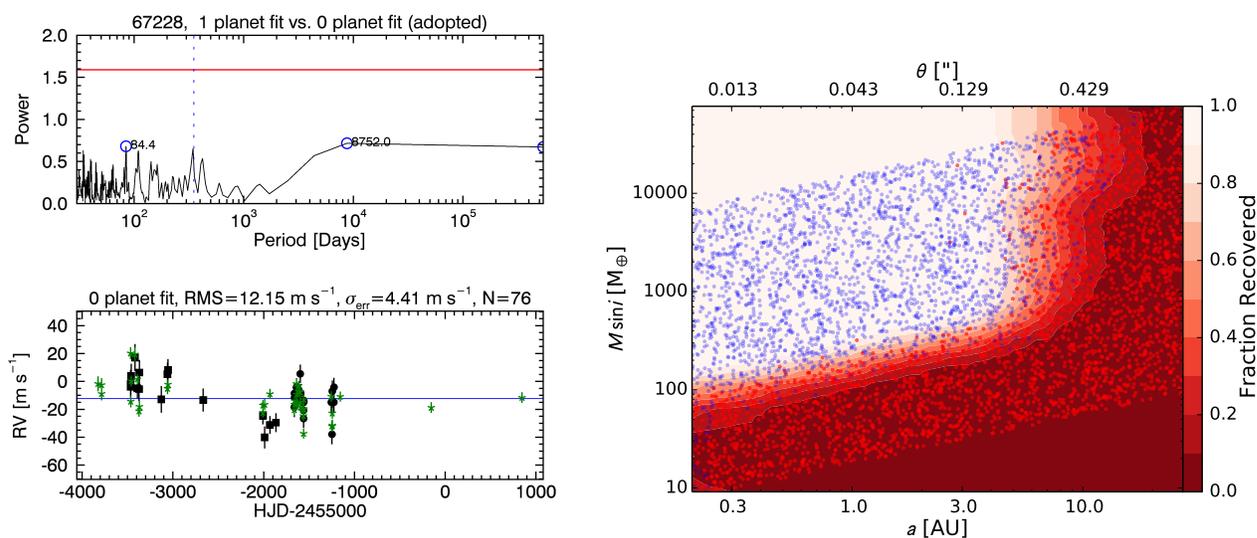
Fig. 40.— Results from an automated search for planets orbiting the star HD 67228 (HIP 39780; program(s) = A) based on RVs from Lick and/or Keck Observatory. The set of plots on the left (analogous to Figs. 3 and 4) show the planet search results and the plot on the right shows the completeness limits (analogous to Fig. 6). See the captions of those figures for detailed descriptions.
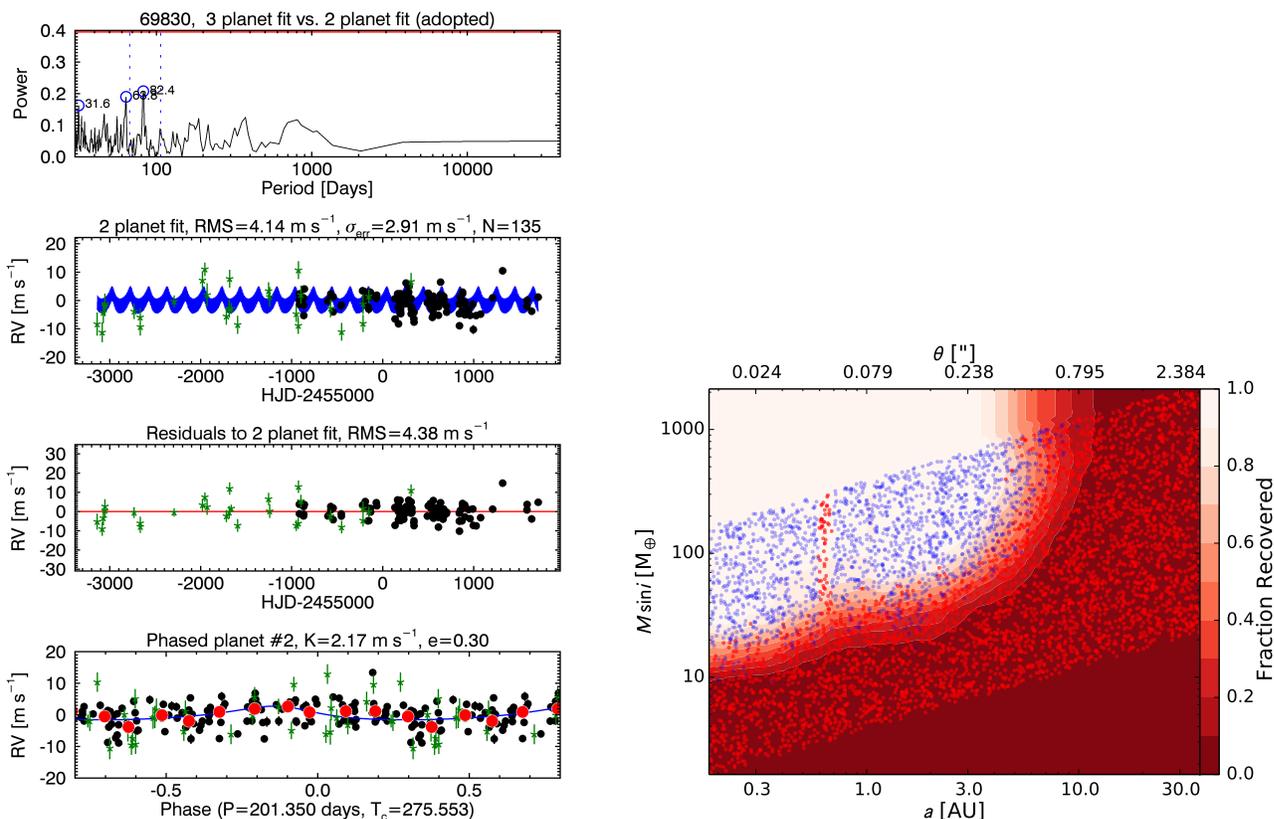
Fig. 41.— Results from an automated search for planets orbiting the star HD 69830 (HIP 40693; program(s) = S) based on RVs from Lick and/or Keck Observatory. The set of plots on the left (analogous to Figs. 3 and 4) show the planet search results and the plot on the right shows the completeness limits (analogous to Fig. 6). See the captions of those figures for detailed descriptions. This star hosts three Neptune-mass planets, two of which we detect with our Keck and Lick RVs. While we do not detect the 31.6 day signal, we have not performed an analysis to show that our non-detection is dispositive.
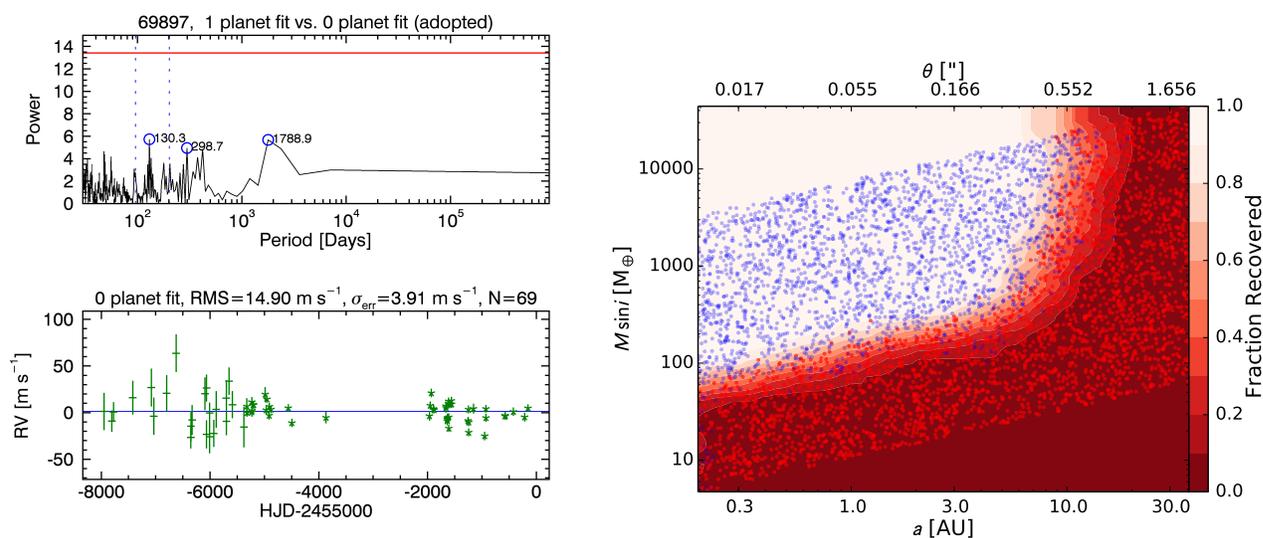
Fig. 42.— Results from an automated search for planets orbiting the star HD 69897 (HIP 40843; program(s) = A) based on RVs from Lick and/or Keck Observatory. The set of plots on the left (analogous to Figs. 3 and 4) show the planet search results and the plot on the right shows the completeness limits (analogous to Fig. 6). See the captions of those figures for detailed descriptions.
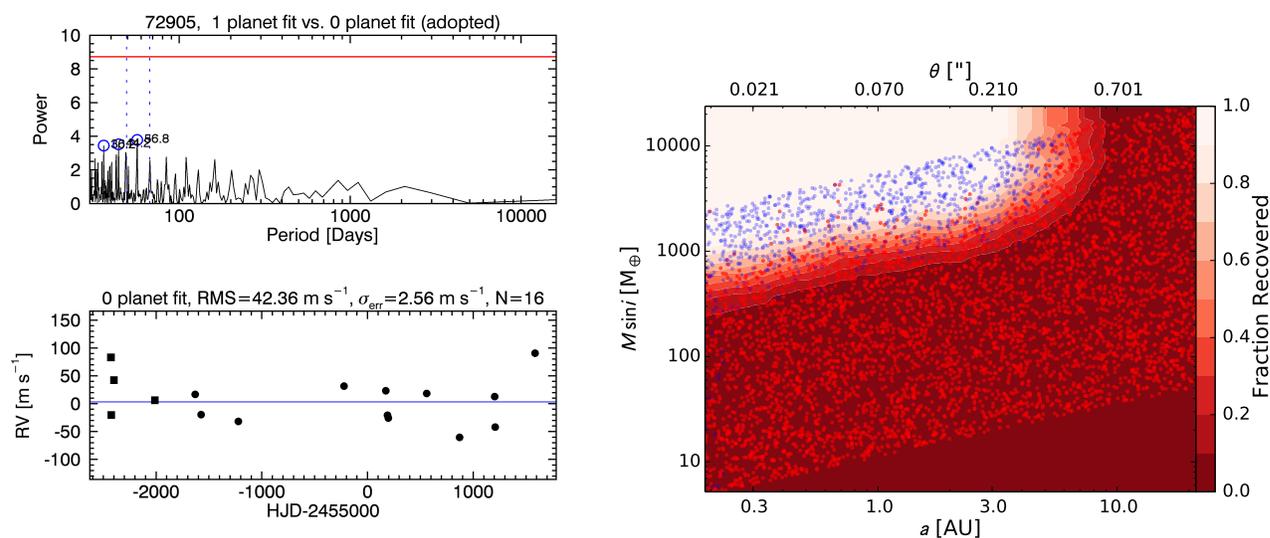
Fig. 43.— Results from an automated search for planets orbiting the star HD 72905 (HIP 42438; program(s) = S) based on RVs from Lick and/or Keck Observatory. The set of plots on the left (analogous to Figs. 3 and 4) show the planet search results and the plot on the right shows the completeness limits (analogous to Fig. 6). See the captions of those figures for detailed descriptions.
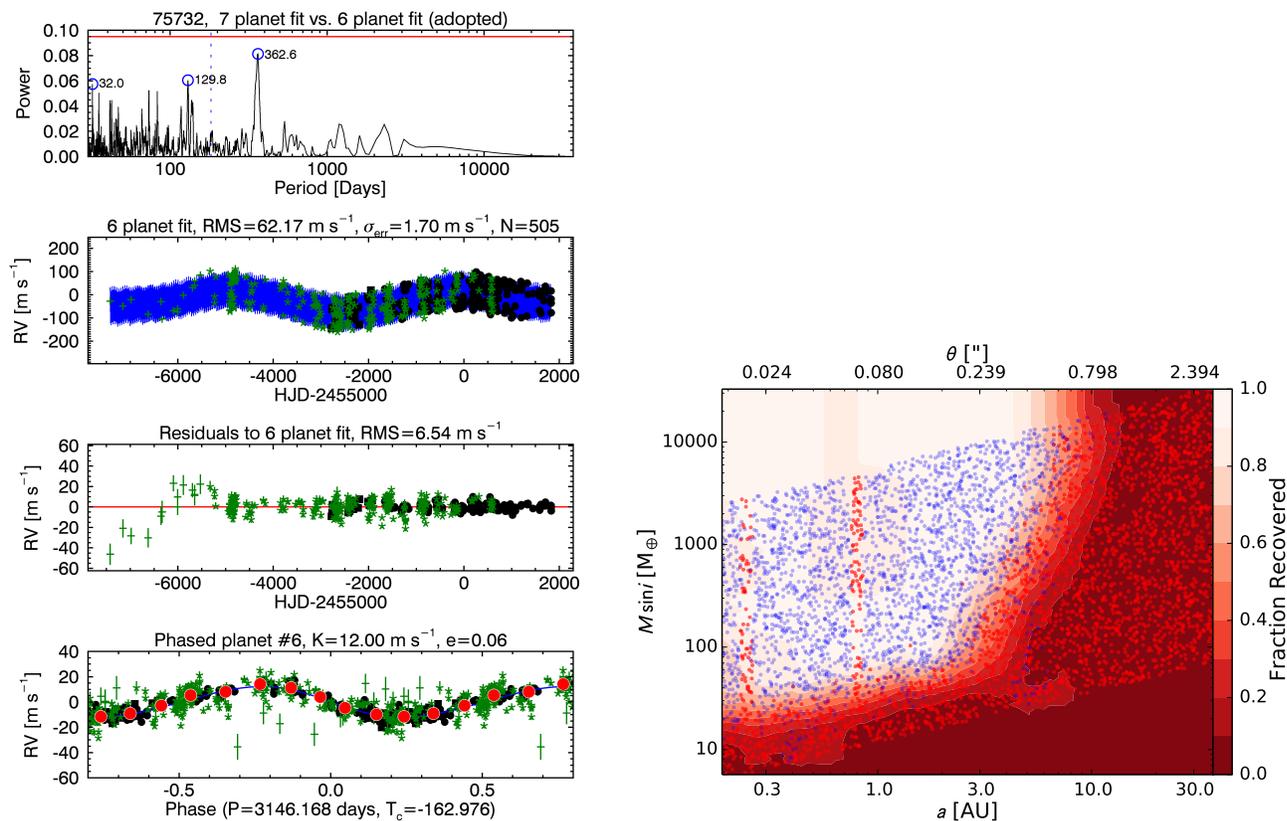
Fig. 44.— Results from an automated search for planets orbiting the star HD 75732 (HIP 43587; program(s) = S) based on RVs from Lick and/or Keck Observatory. The set of plots on the left (analogous to Figs. 3 and 4) show the planet search results and the plot on the right shows the completeness limits (analogous to Fig. 6). See the captions of those figures for detailed descriptions. This star hosts five known planets.
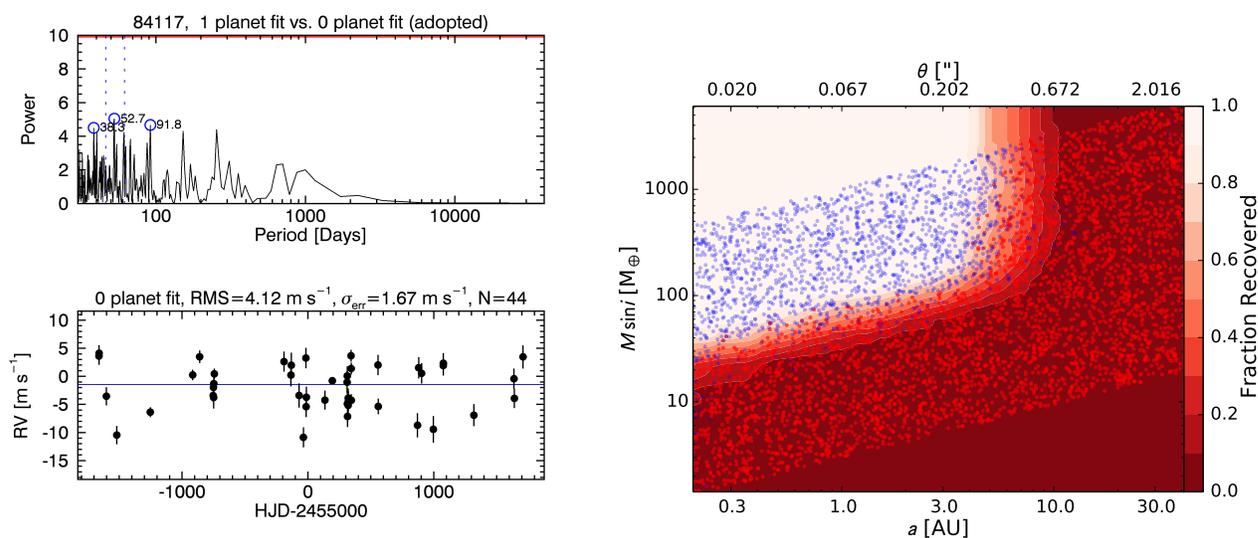
Fig. 45.— Results from an automated search for planets orbiting the star HD 84117 (HIP 47592; program(s) = S, C, A) based on RVs from Lick and/or Keck Observatory. The set of plots on the left (analogous to Figs. 3 and 4) show the planet search results and the plot on the right shows the completeness limits (analogous to Fig. 6). See the captions of those figures for detailed descriptions.
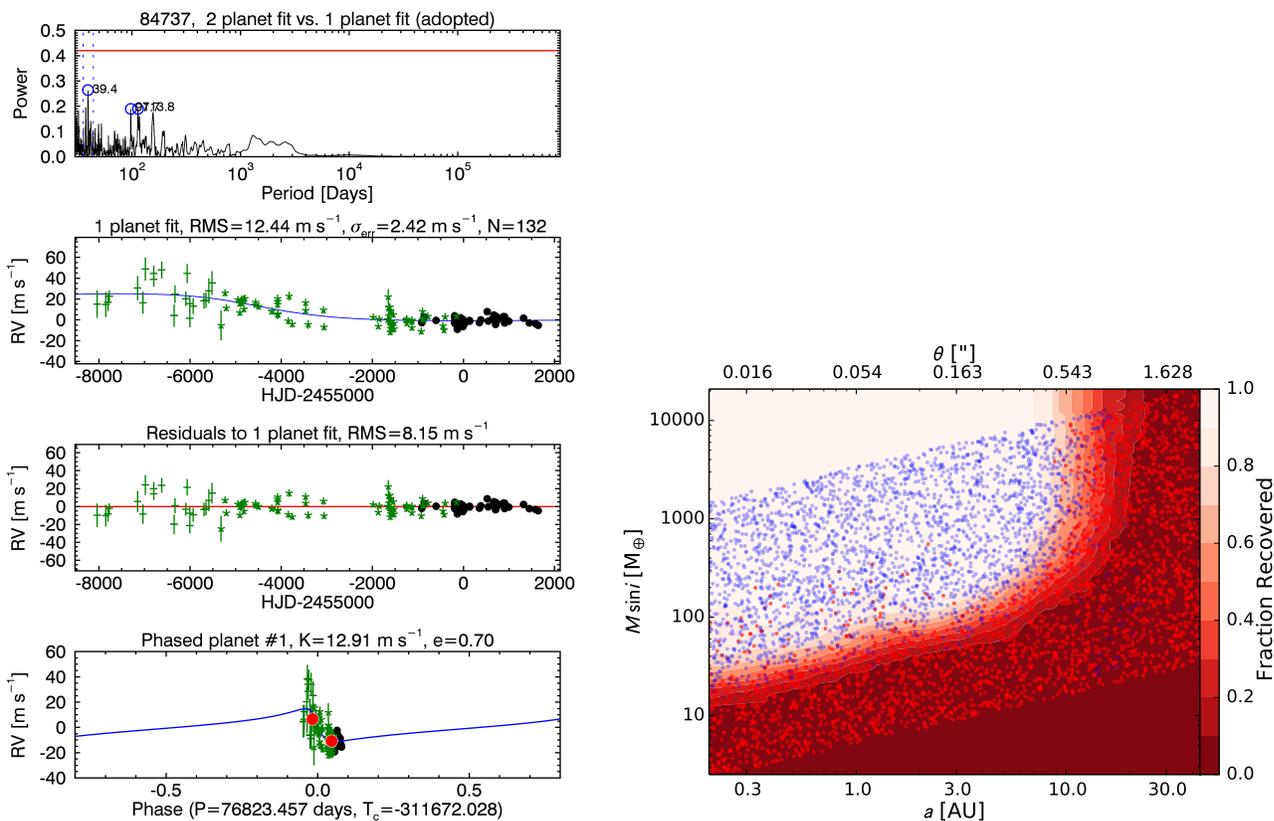
Fig. 46.— Results from an automated search for planets orbiting the star HD 84737 (HIP 48113; program(s) = A) based on RVs from Lick and/or Keck Observatory. The set of plots on the left (analogous to Figs. 3 and 4) show the planet search results and the plot on the right shows the completeness limits (analogous to Fig. 6). See the captions of those figures for detailed descriptions. This star has a formally adopted signal that appears to be due to uncorrected zero-point offsets in the Lick RVs and not due a planet.
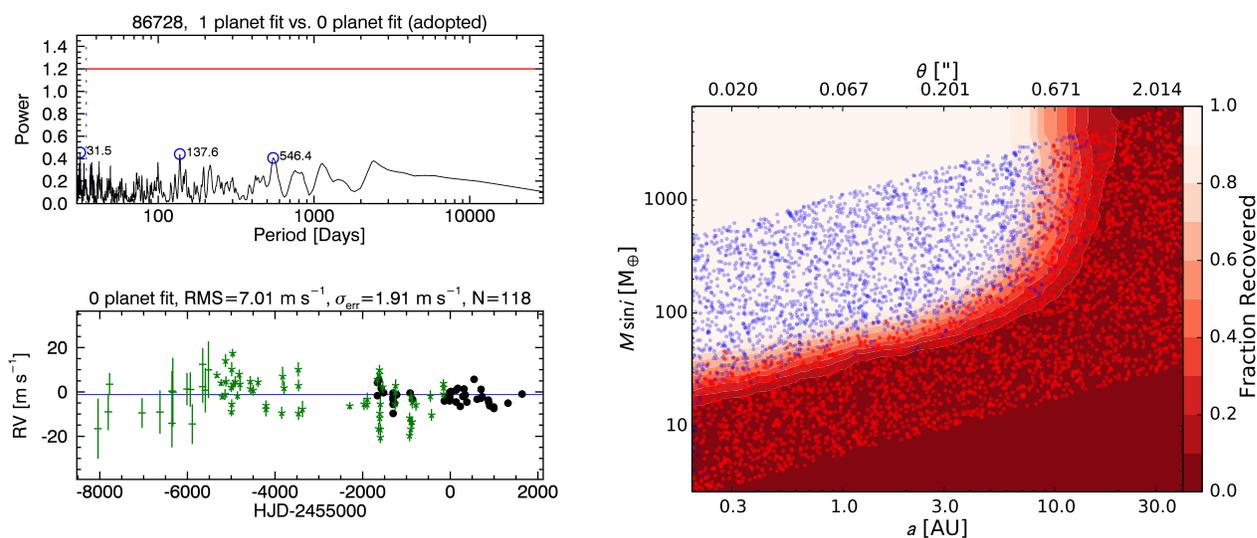
Fig. 47.— Results from an automated search for planets orbiting the star HD 86728 (HIP 49081; program(s) = S, A) based on RVs from Lick and/or Keck Observatory. The set of plots on the left (analogous to Figs. 3 and 4) show the planet search results and the plot on the right shows the completeness limits (analogous to Fig. 6). See the captions of those figures for detailed descriptions.
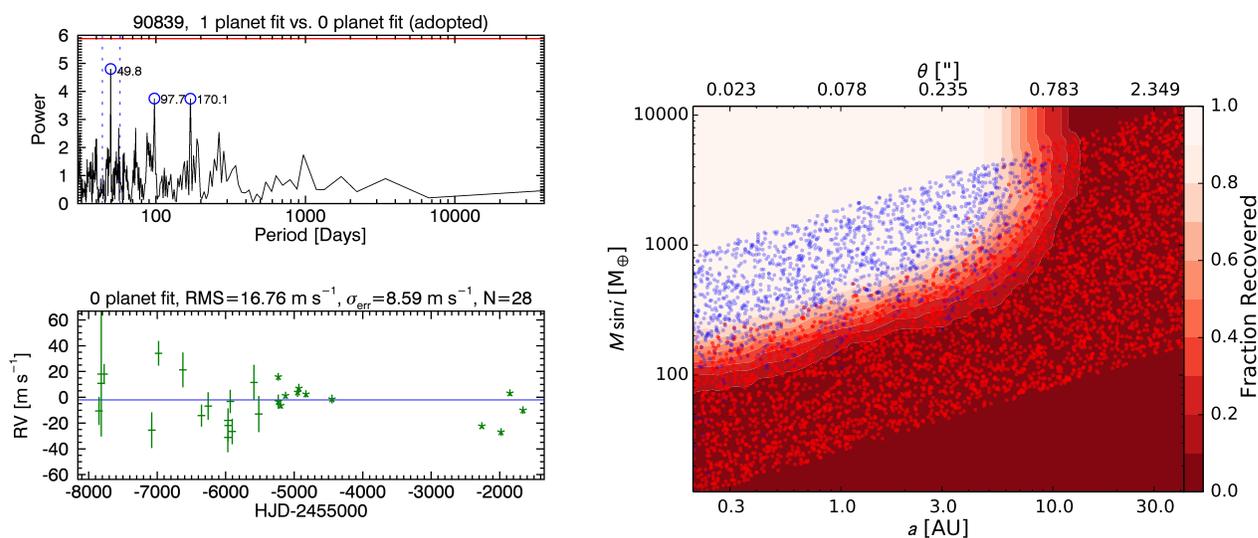
Fig. 48.— Results from an automated search for planets orbiting the star HD 90839 (HIP 51459; program(s) = S, C, A) based on RVs from Lick and/or Keck Observatory. The set of plots on the left (analogous to Figs. 3 and 4) show the planet search results and the plot on the right shows the completeness limits (analogous to Fig. 6). See the captions of those figures for detailed descriptions.
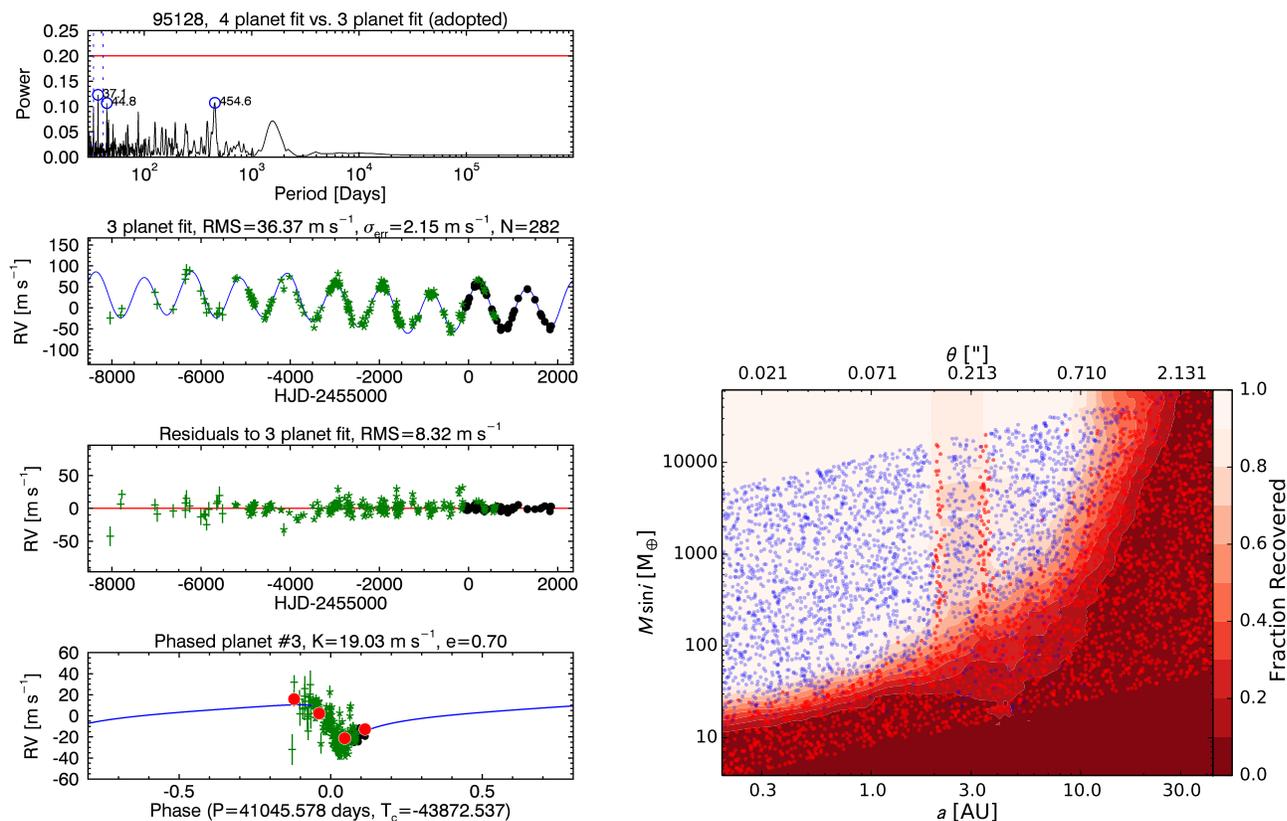
Fig. 49.— Results from an automated search for planets orbiting the star HD 95128 (HIP 53721; program(s) = A) based on RVs from Lick and/or Keck Observatory. The set of plots on the left (analogous to Figs. 3 and 4) show the planet search results and the plot on the right shows the completeness limits (analogous to Fig. 6). See the captions of those figures for detailed descriptions. This star hosts two well-known giant planets with semi-major axes of 2 and 3.6 AU, and possibly a third planet at ~11 AU. Our automated search prefers a model with three planets, although the outer most planet has a poorly constrained orbit.
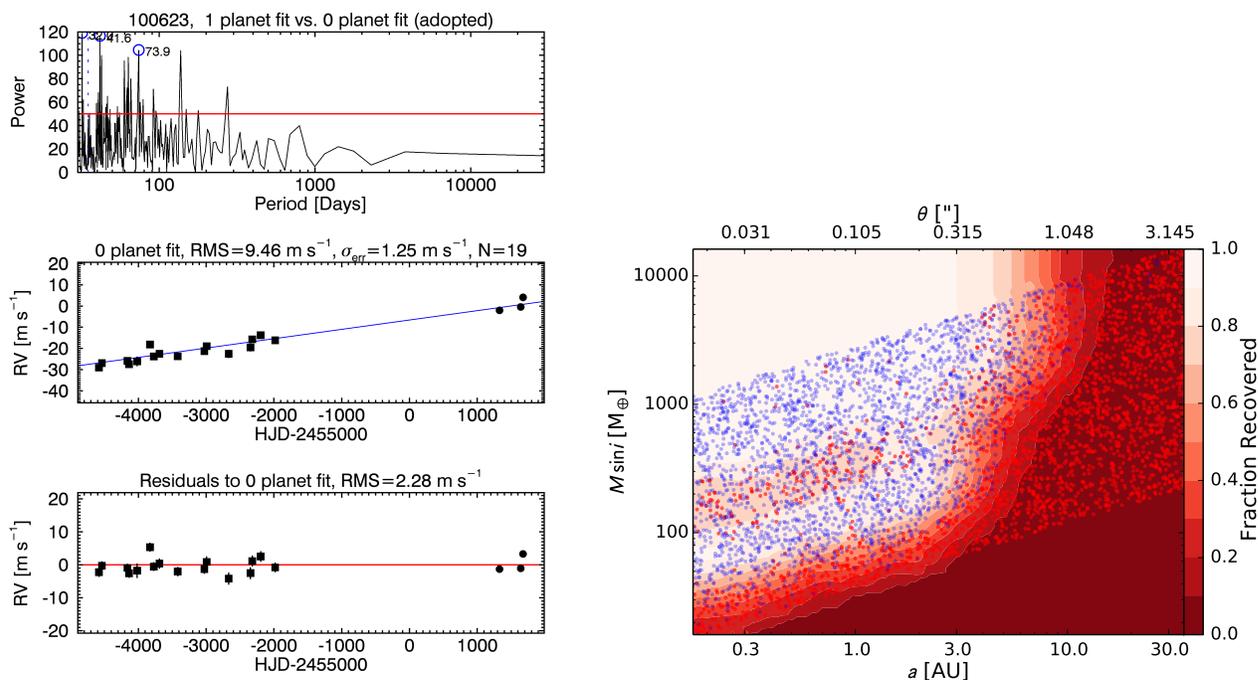
Fig. 50.— Results from an automated search for planets orbiting the star HD 100623 (HIP 56452; program(s) = S) based on RVs from Lick and/or Keck Observatory. The set of plots on the left (analogous to Figs. 3 and 4) show the planet search results and the plot on the right shows the completeness limits (analogous to Fig. 6). See the captions of those figures for detailed descriptions. This star shows a significant linear trend with no detectable curvature.
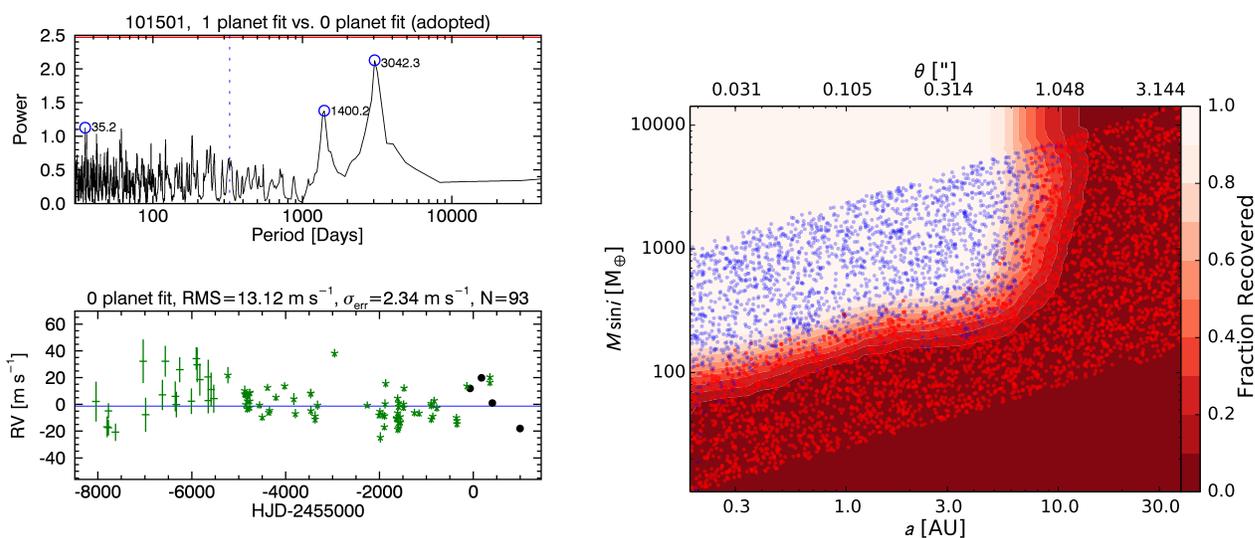
Fig. 51.— Results from an automated search for planets orbiting the star HD 101501 (HIP 56997; program(s) = S, C, A) based on RVs from Lick and/or Keck Observatory. The set of plots on the left (analogous to Figs. 3 and 4) show the planet search results and the plot on the right shows the completeness limits (analogous to Fig. 6). See the captions of those figures for detailed descriptions.
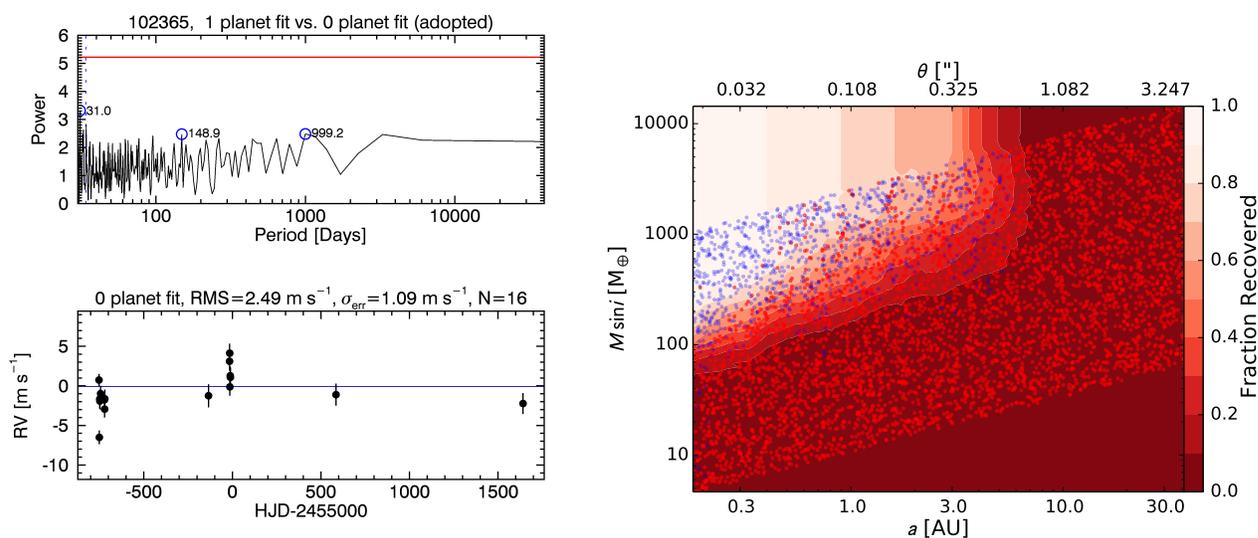
Fig. 52.— Results from an automated search for planets orbiting the star HD 102365 (HIP 57443; program(s) = S, C, A) based on RVs from Lick and/or Keck Observatory. The set of plots on the left (analogous to Figs. 3 and 4) show the planet search results and the plot on the right shows the completeness limits (analogous to Fig. 6). See the captions of those figures for detailed descriptions.
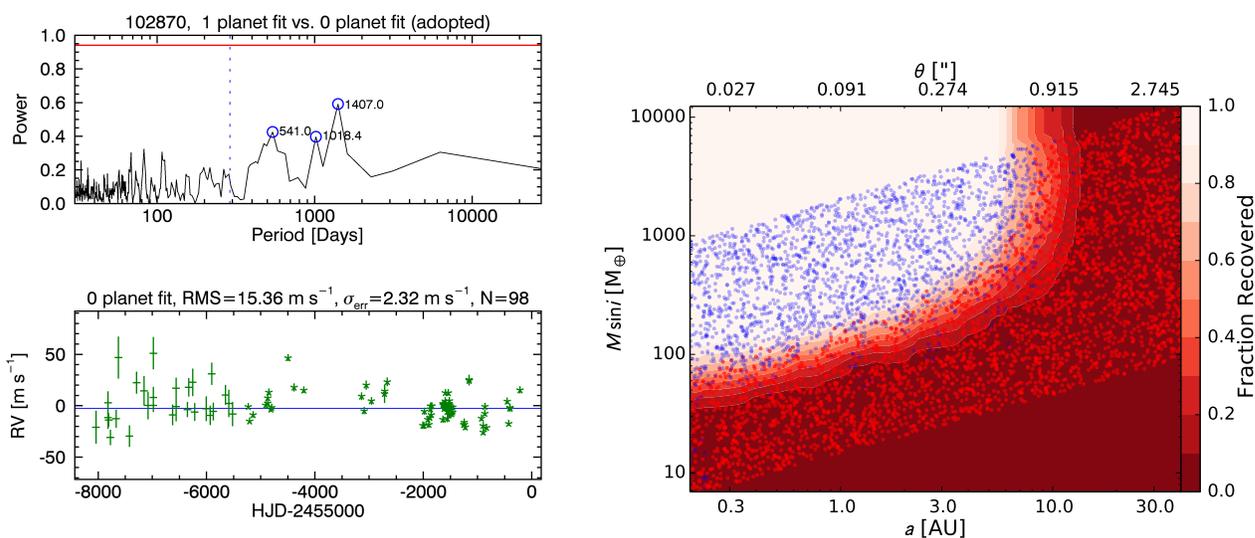
Fig. 53.— Results from an automated search for planets orbiting the star HD 102870 (HIP 57757; program(s) = S, C, A) based on RVs from Lick and/or Keck Observatory. The set of plots on the left (analogous to Figs. 3 and 4) show the planet search results and the plot on the right shows the completeness limits (analogous to Fig. 6). See the captions of those figures for detailed descriptions.
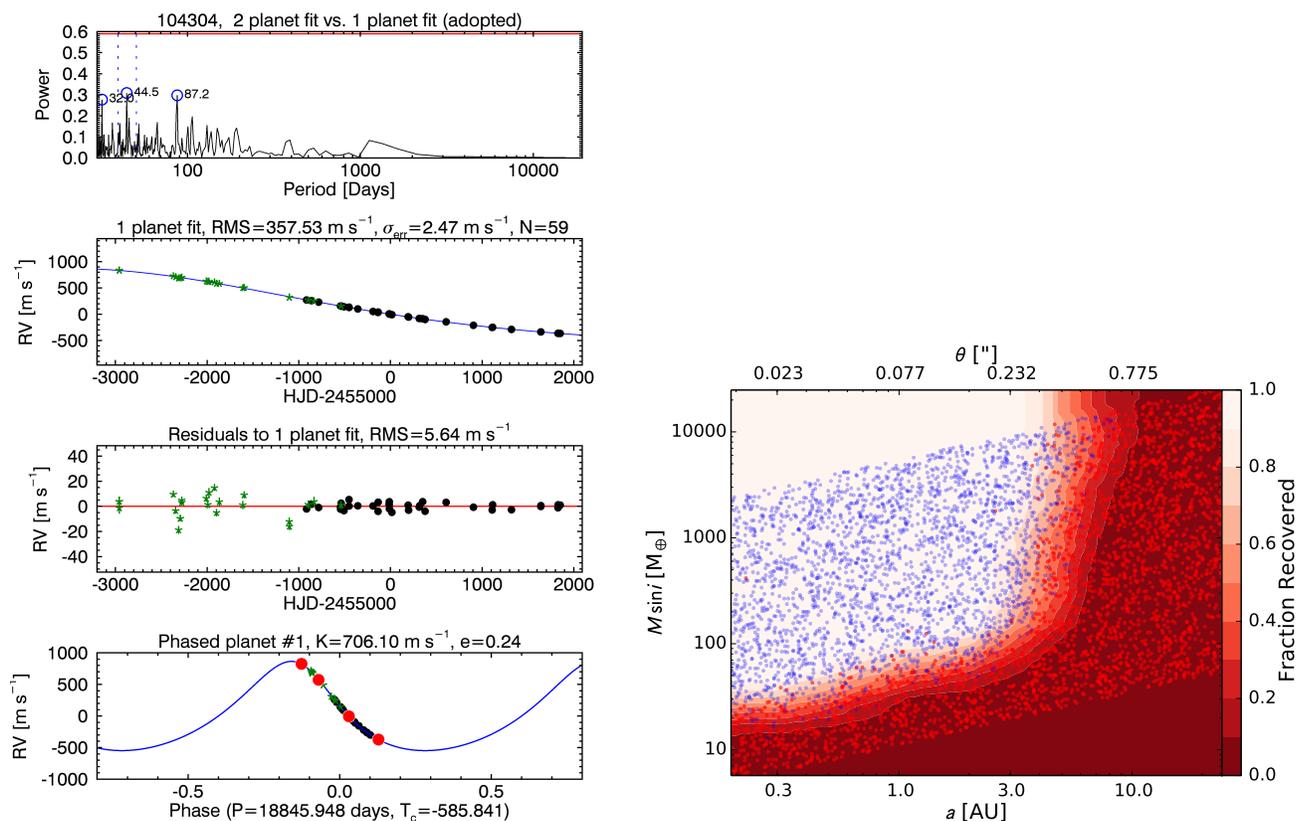
Fig. 54.— Results from an automated search for planets orbiting the star HD 104304 (HIP 58576; program(s) = S) based on RVs from Lick and/or Keck Observatory. The set of plots on the left (analogous to Figs. 3 and 4) show the planet search results and the plot on the right shows the completeness limits (analogous to Fig. 6). See the captions of those figures for detailed descriptions. This system shows a strong long-term linear trend with curvature, likely due to a detected low-mass, stellar companion. Our automated search prefers a model with a linear velocity trend (constant acceleration) in addition to the orbit segment from the companion (three bodies total), with considerable model degeneracy.
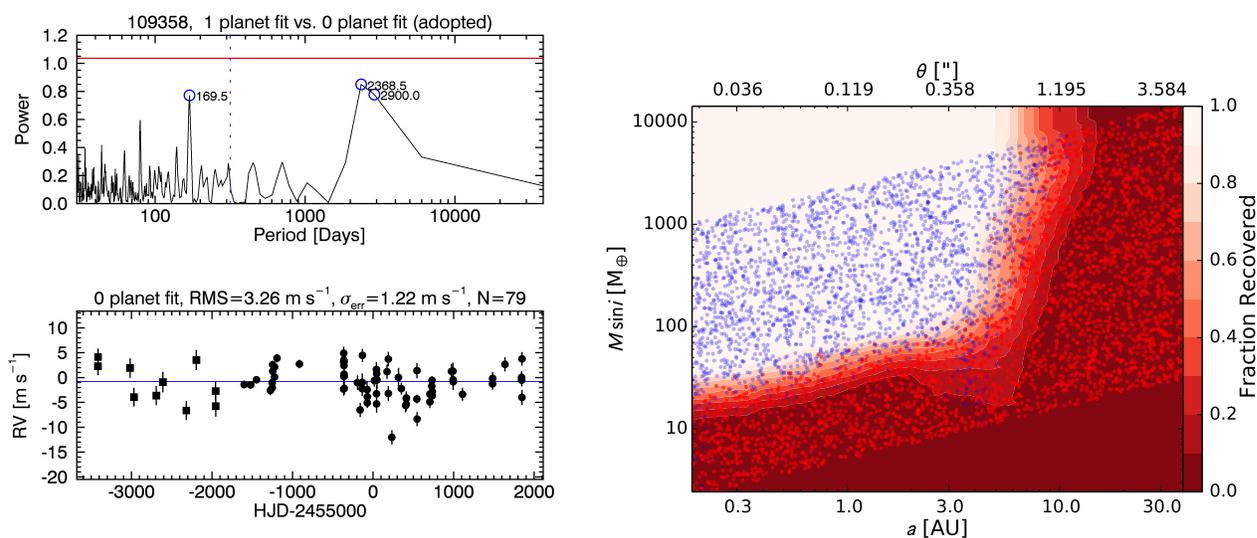
Fig. 55.— Results from an automated search for planets orbiting the star HD 109358 (HIP 61317; program(s) = S, C, A) based on RVs from Lick and/or Keck Observatory. The set of plots on the left (analogous to Figs. 3 and 4) show the planet search results and the plot on the right shows the completeness limits (analogous to Fig. 6). See the captions of those figures for detailed descriptions.
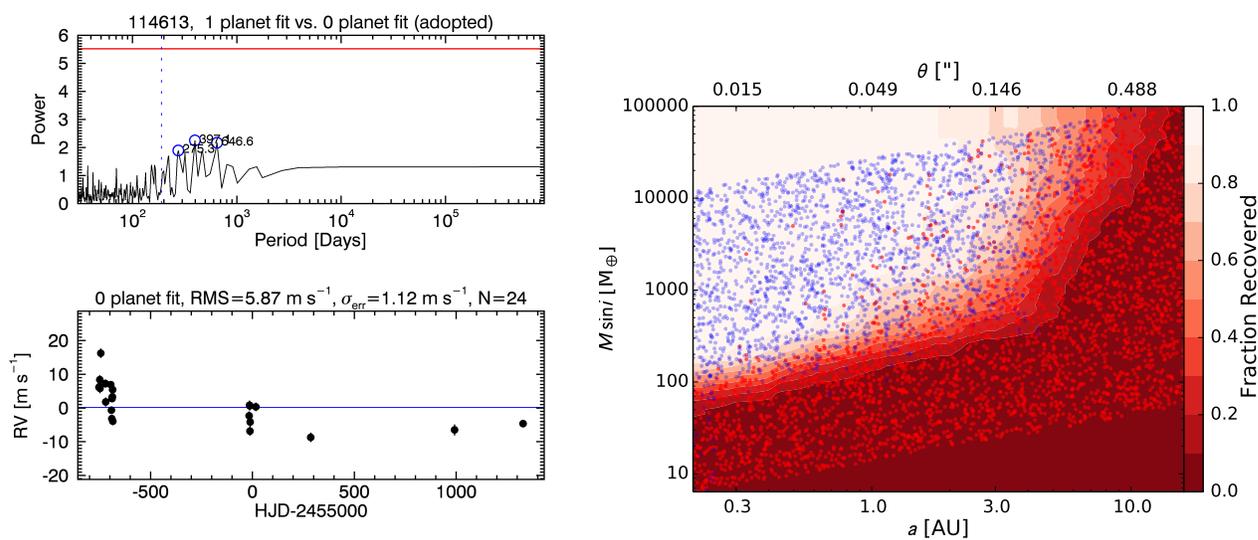
Fig. 56.— Results from an automated search for planets orbiting the star HD 114613 (HIP 64408; program(s) = A) based on RVs from Lick and/or Keck Observatory. The set of plots on the left (analogous to Figs. 3 and 4) show the planet search results and the plot on the right shows the completeness limits (analogous to Fig. 6). See the captions of those figures for detailed descriptions.
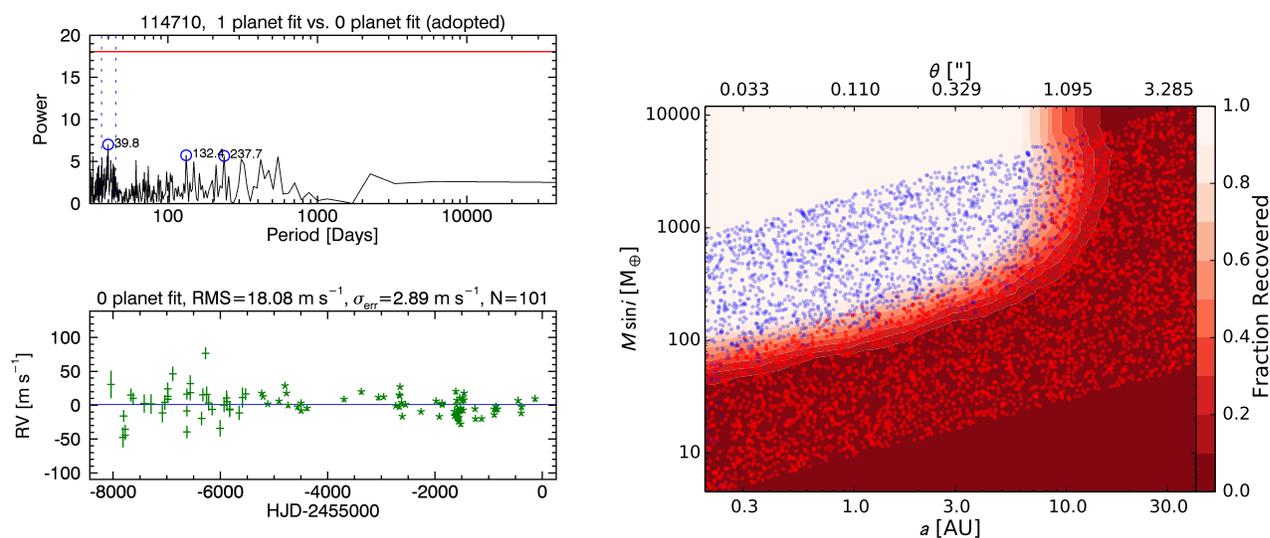
Fig. 57.— Results from an automated search for planets orbiting the star HD 114710 (HIP 64394; program(s) = S, C, A) based on RVs from Lick and/or Keck Observatory. The set of plots on the left (analogous to Figs. 3 and 4) show the planet search results and the plot on the right shows the completeness limits (analogous to Fig. 6). See the captions of those figures for detailed descriptions.
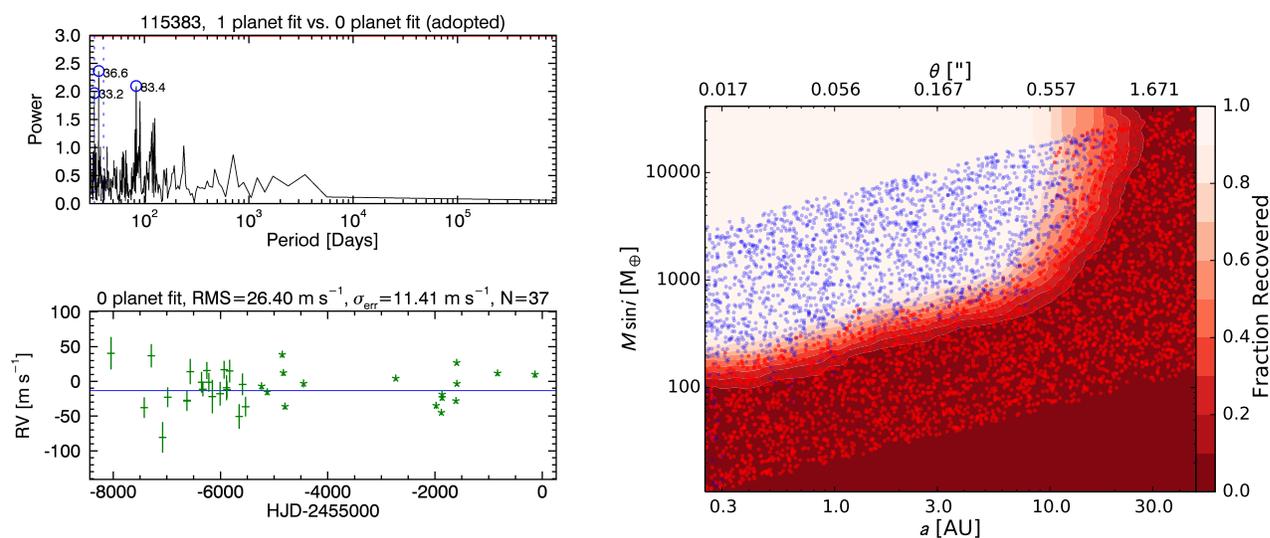
Fig. 58.— Results from an automated search for planets orbiting the star HD 115383 (HIP 64792; program(s) = A) based on RVs from Lick and/or Keck Observatory. The set of plots on the left (analogous to Figs. 3 and 4) show the planet search results and the plot on the right shows the completeness limits (analogous to Fig. 6). See the captions of those figures for detailed descriptions.
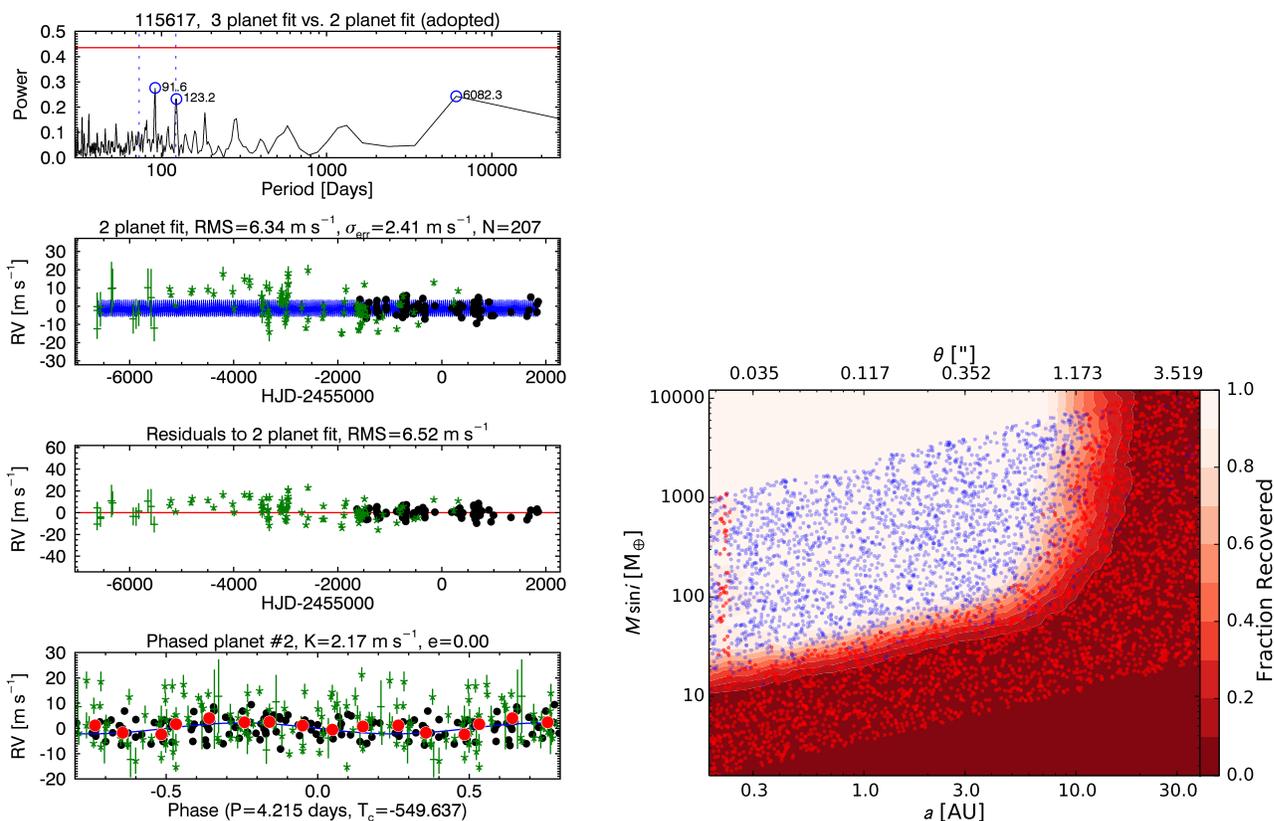
Fig. 59.— Results from an automated search for planets orbiting the star HD 115617 (HIP 64924; program(s) = S, C, A) based on RVs from Lick and/or Keck Observatory. The set of plots on the left (analogous to Figs. 3 and 4) show the planet search results and the plot on the right shows the completeness limits (analogous to Fig. 6). See the captions of those figures for detailed descriptions. This star has three reported small planets, two of which we detect in our Keck RVs.
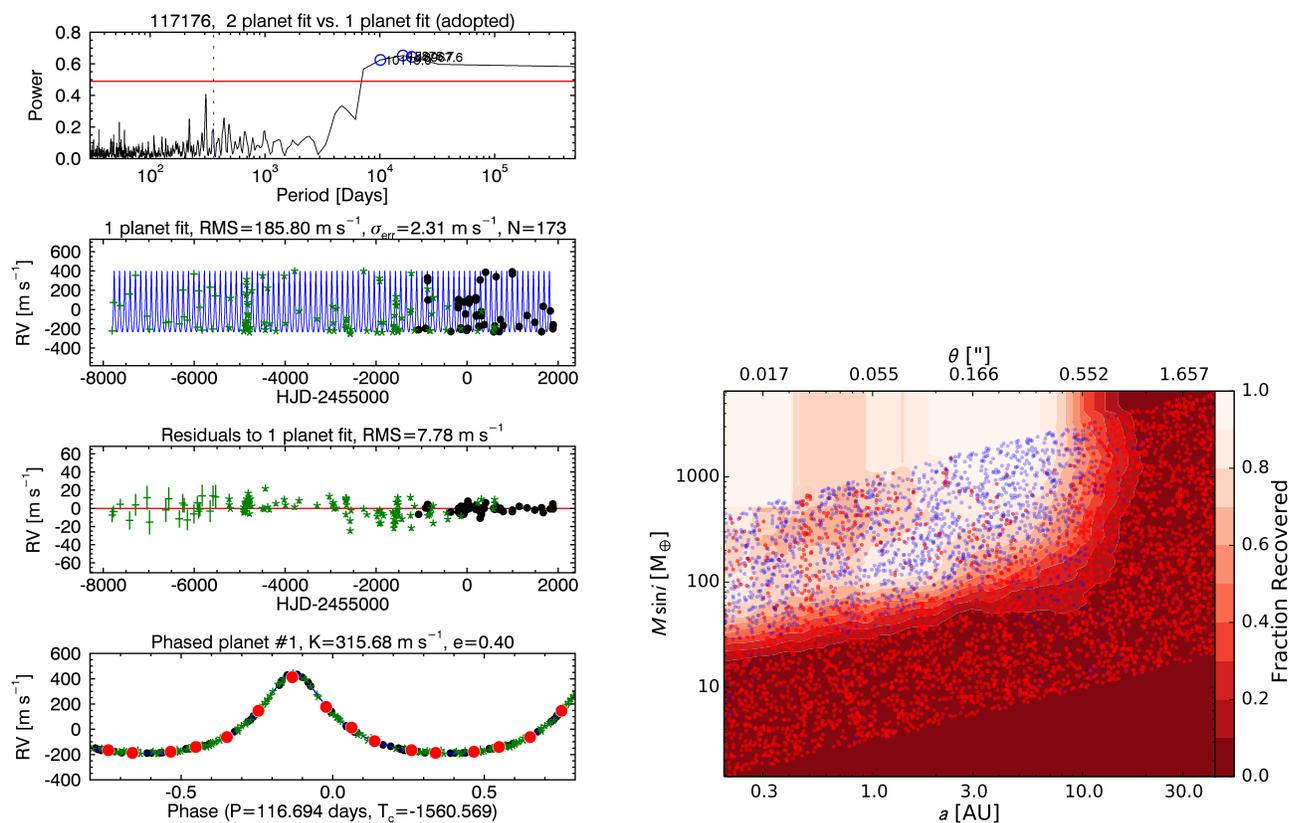
Fig. 60.— Results from an automated search for planets orbiting the star HD 117176 (HIP 65721; program(s) = A) based on RVs from Lick and/or Keck Observatory. The set of plots on the left (analogous to Figs. 3 and 4) show the planet search results and the plot on the right shows the completeness limits (analogous to Fig. 6). See the captions of those figures for detailed descriptions. This star hosts a giant planet.
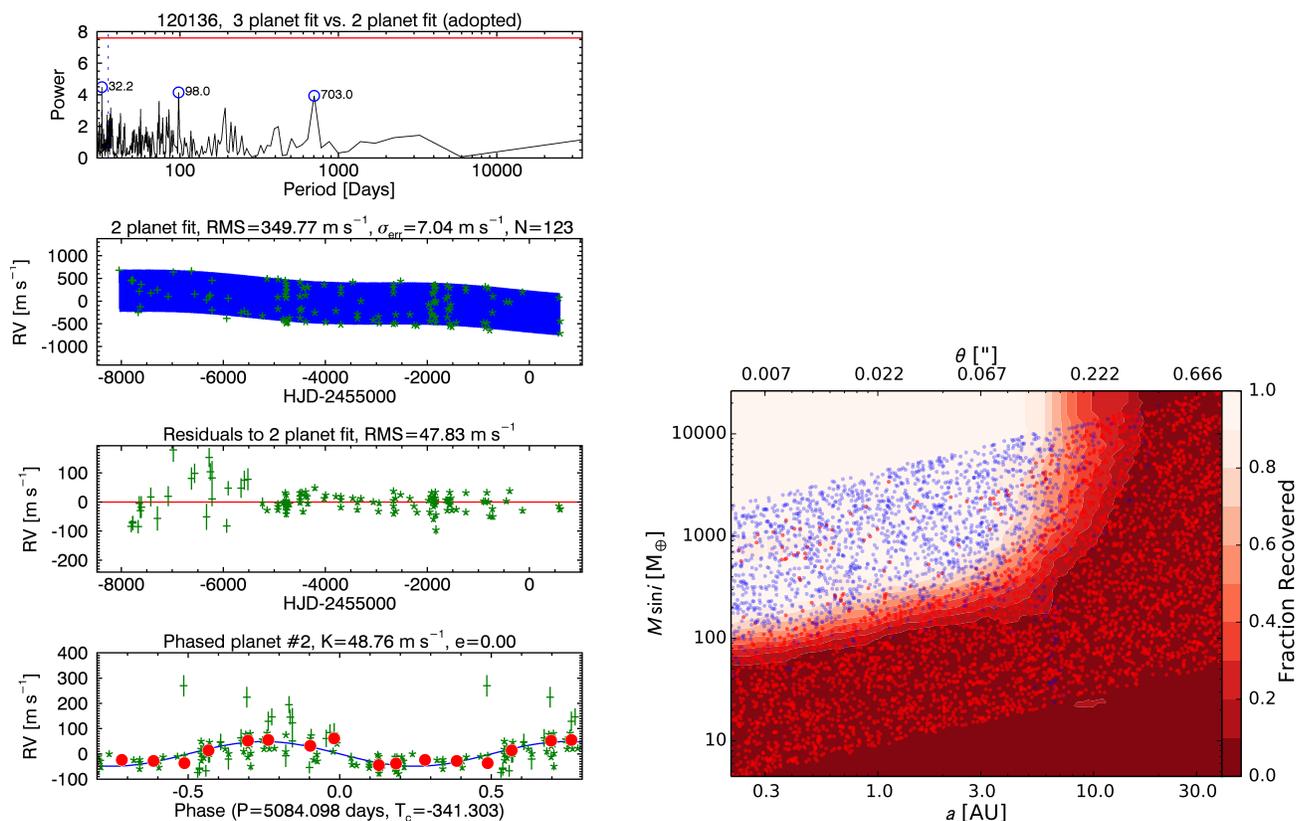
Fig. 61.— Results from an automated search for planets orbiting the star HD 120136 (HIP 67275; program(s) = S, C, A) based on RVs from Lick and/or Keck Observatory. The set of plots on the left (analogous to Figs. 3 and 4) show the planet search results and the plot on the right shows the completeness limits (analogous to Fig. 6). See the captions of those figures for detailed descriptions. This star hosts a massive, hot Jupiter planet. We also detect a significant linear trend in the RV time series and a periodicity at ∼5000 days. The trend is likely real, but the 5000 day periodicity could be due to instrumental offsets in the Lick-only data or a stellar magnetic activity cycle.
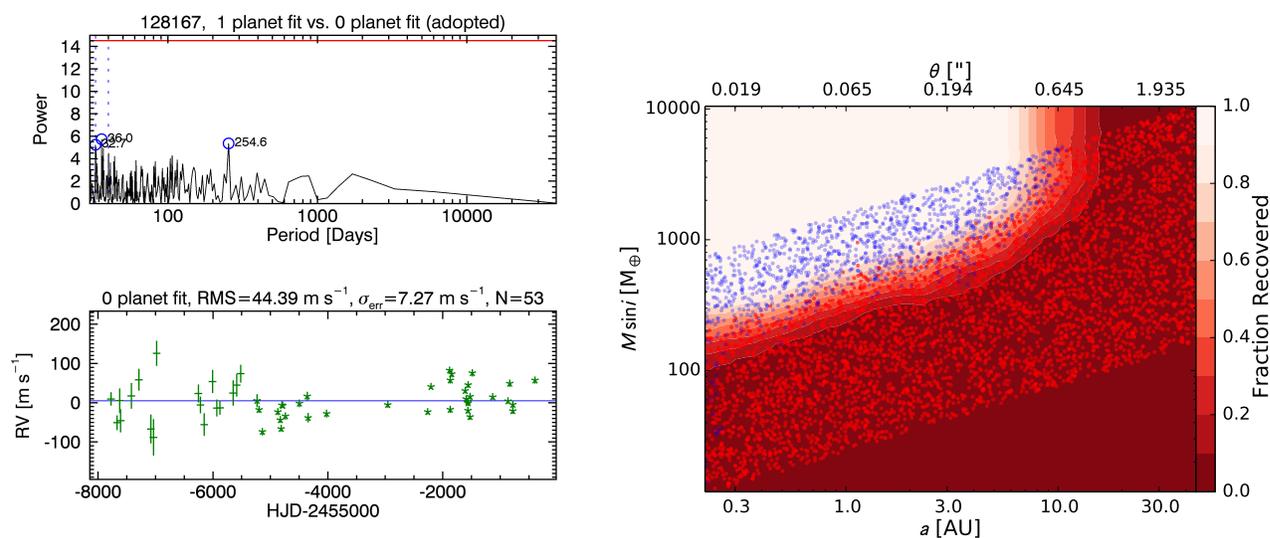
Fig. 62.— Results from an automated search for planets orbiting the star HD 128167 (HIP 71284; program(s) = S, C, A) based on RVs from Lick and/or Keck Observatory. The set of plots on the left (analogous to Figs. 3 and 4) show the planet search results and the plot on the right shows the completeness limits (analogous to Fig. 6). See the captions of those figures for detailed descriptions.
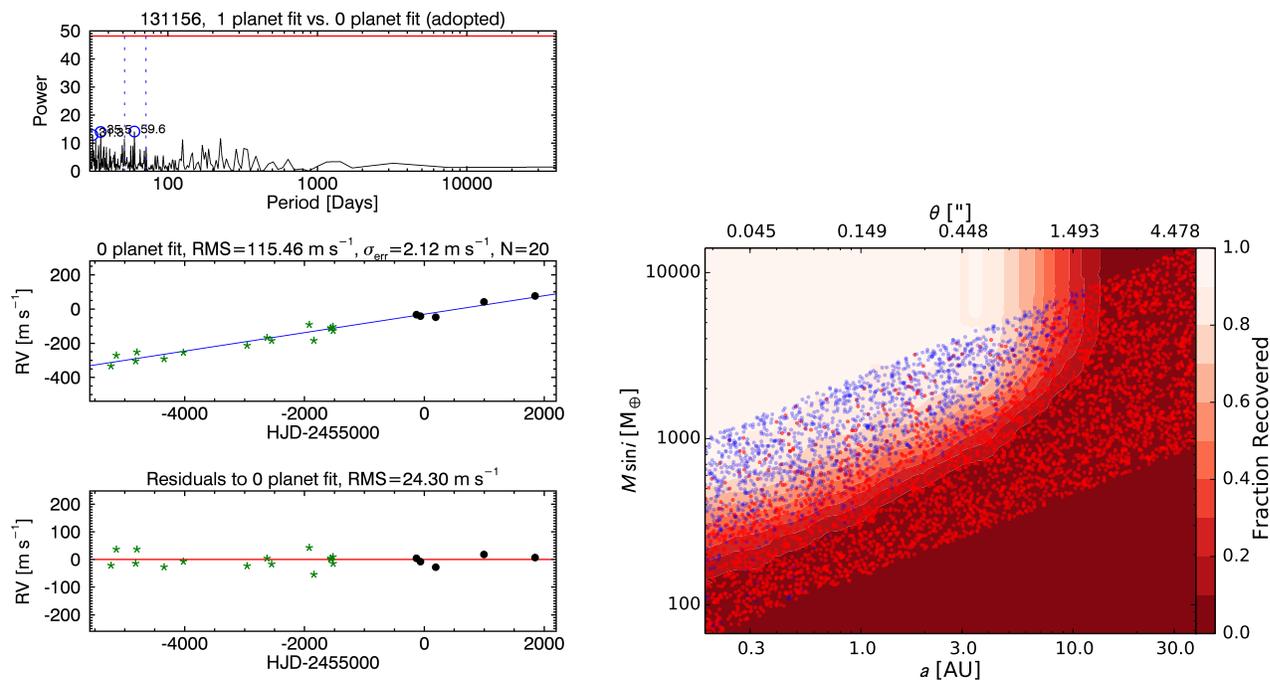
Fig. 63.— Results from an automated search for planets orbiting the star HD 131156 (HIP 72659; program(s) = S, C, A) based on RVs from Lick and/or Keck Observatory. The set of plots on the left (analogous to Figs. 3 and 4) show the planet search results and the plot on the right shows the completeness limits (analogous to Fig. 6). See the captions of those figures for detailed descriptions. This star has a significant linear trend in the RV time series, likely due to a binary companion.
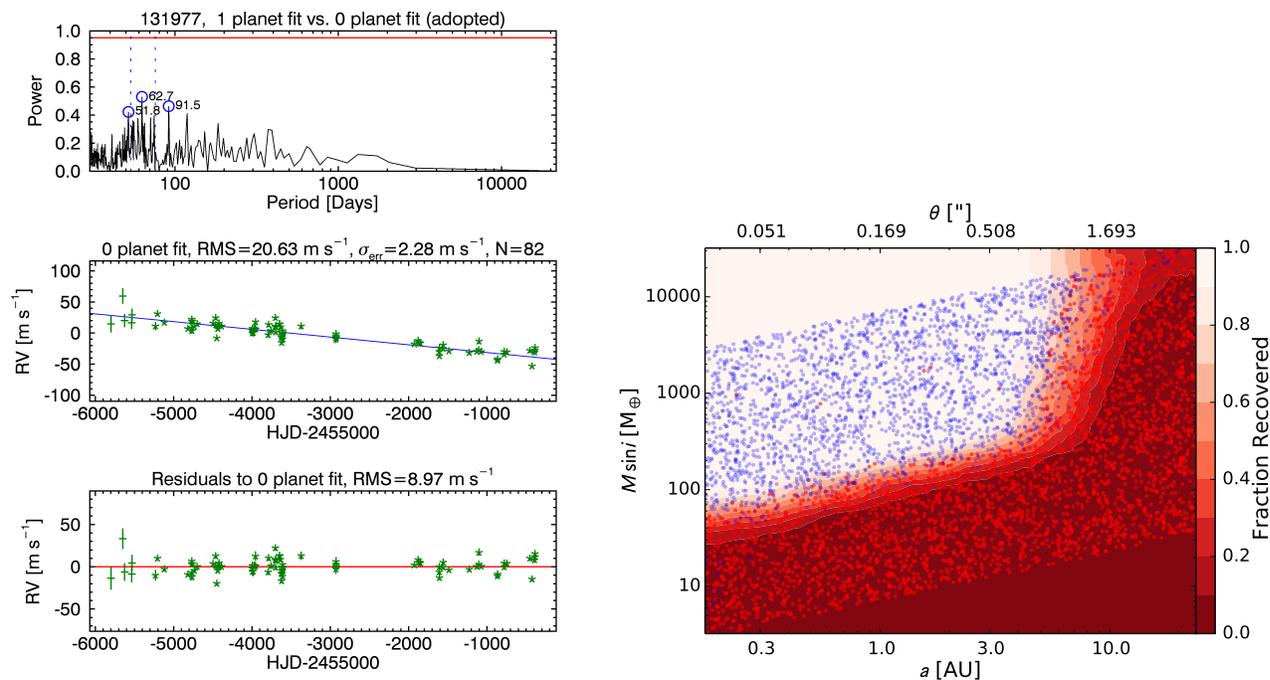
Fig. 64.— Results from an automated search for planets orbiting the star HD 131977 (HIP 73184; program(s) = S, C) based on RVs from Lick and/or Keck Observatory. The set of plots on the left (analogous to Figs. 3 and 4) show the planet search results and the plot on the right shows the completeness limits (analogous to Fig. 6). See the captions of those figures for detailed descriptions. This star has a significant linear trend in the RV time series, likely due to a binary companion.
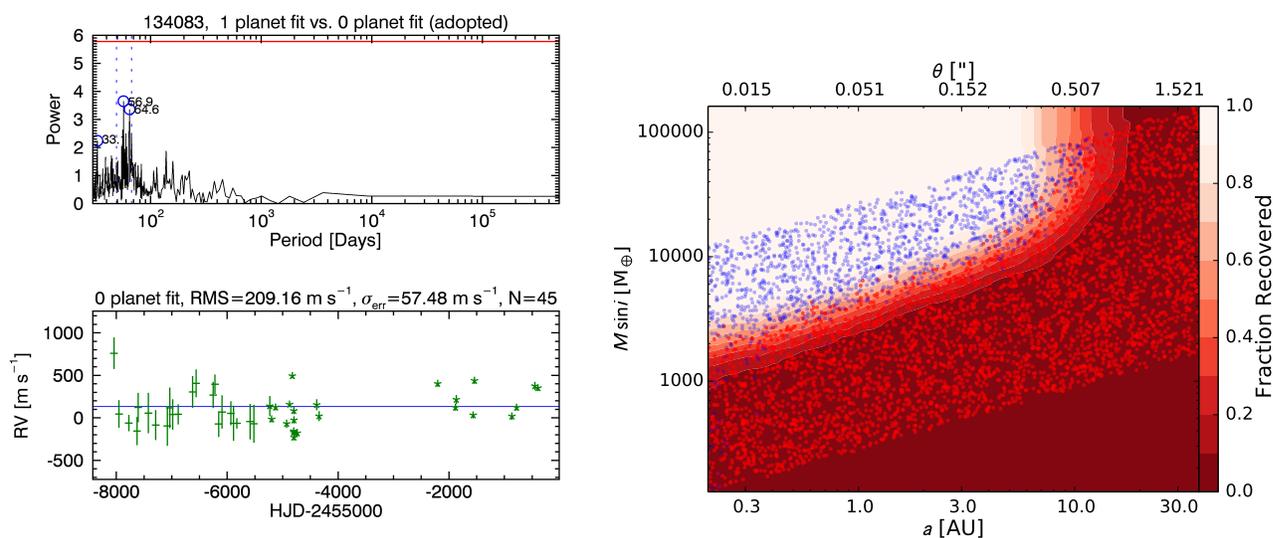
Fig. 65.— Results from an automated search for planets orbiting the star HD 134083 (HIP 73996; program(s) = A) based on RVs from Lick and/or Keck Observatory. The set of plots on the left (analogous to Figs. 3 and 4) show the planet search results and the plot on the right shows the completeness limits (analogous to Fig. 6). See the captions of those figures for detailed descriptions.
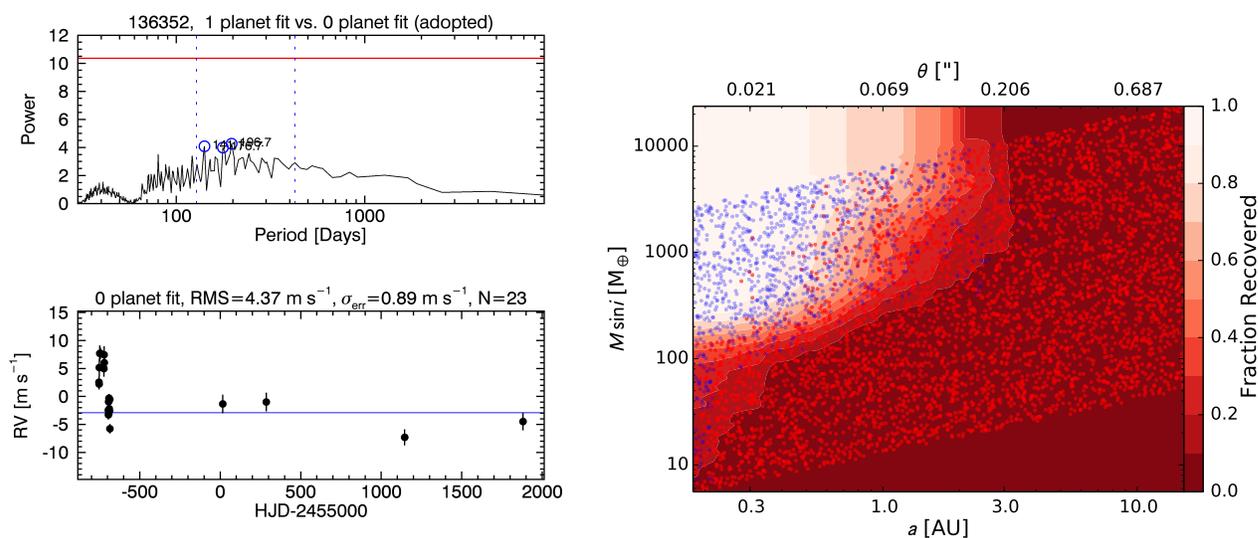
Fig. 66.— Results from an automated search for planets orbiting the star HD 136352 (HIP 75181; program(s) = S) based on RVs from Lick and/or Keck Observatory. The set of plots on the left (analogous to Figs. 3 and 4) show the planet search results and the plot on the right shows the completeness limits (analogous to Fig. 6). See the captions of those figures for detailed descriptions.
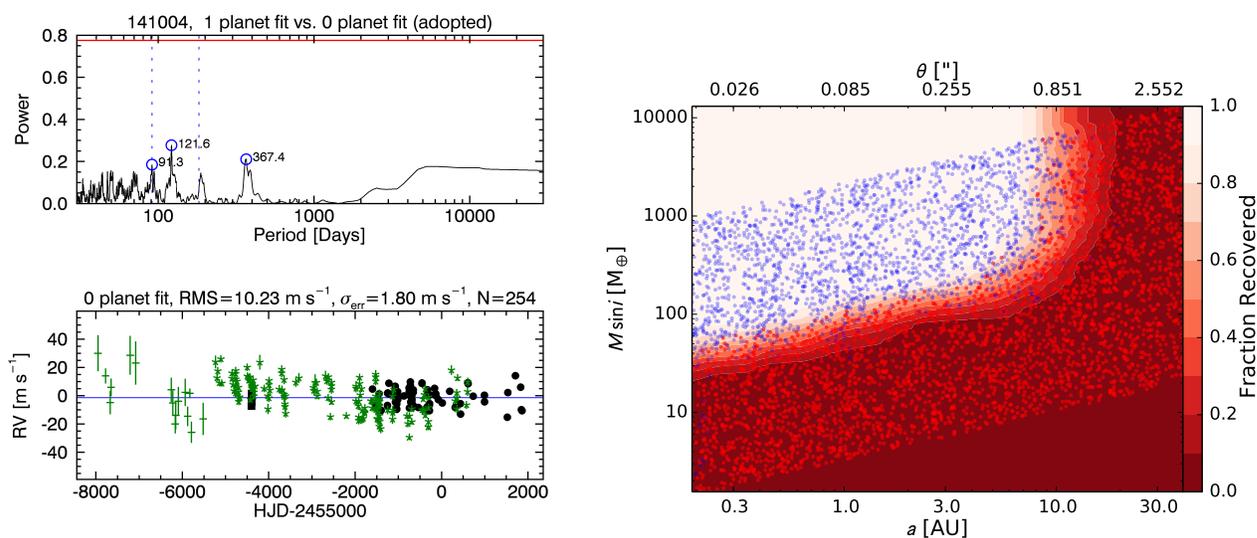
Fig. 67.— Results from an automated search for planets orbiting the star HD 141004 (HIP 77257; program(s) = S, C, A) based on RVs from Lick and/or Keck Observatory. The set of plots on the left (analogous to Figs. 3 and 4) show the planet search results and the plot on the right shows the completeness limits (analogous to Fig. 6). See the captions of those figures for detailed descriptions.
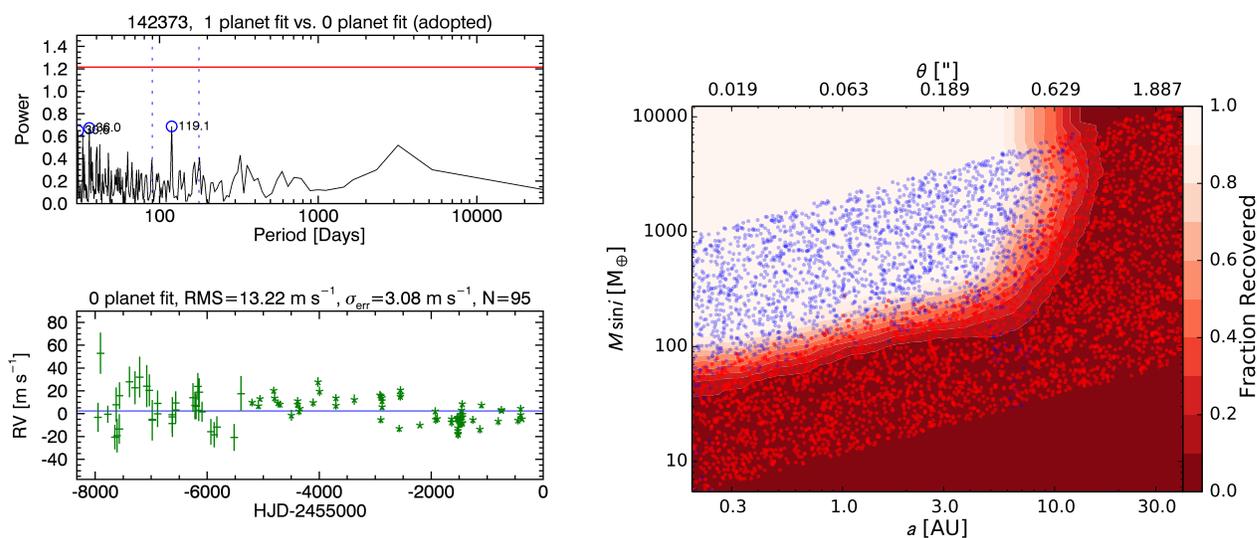
Fig. 68.— Results from an automated search for planets orbiting the star HD 142373 (HIP 77760; program(s) = S, C, A) based on RVs from Lick and/or Keck Observatory. The set of plots on the left (analogous to Figs. 3 and 4) show the planet search results and the plot on the right shows the completeness limits (analogous to Fig. 6). See the captions of those figures for detailed descriptions.
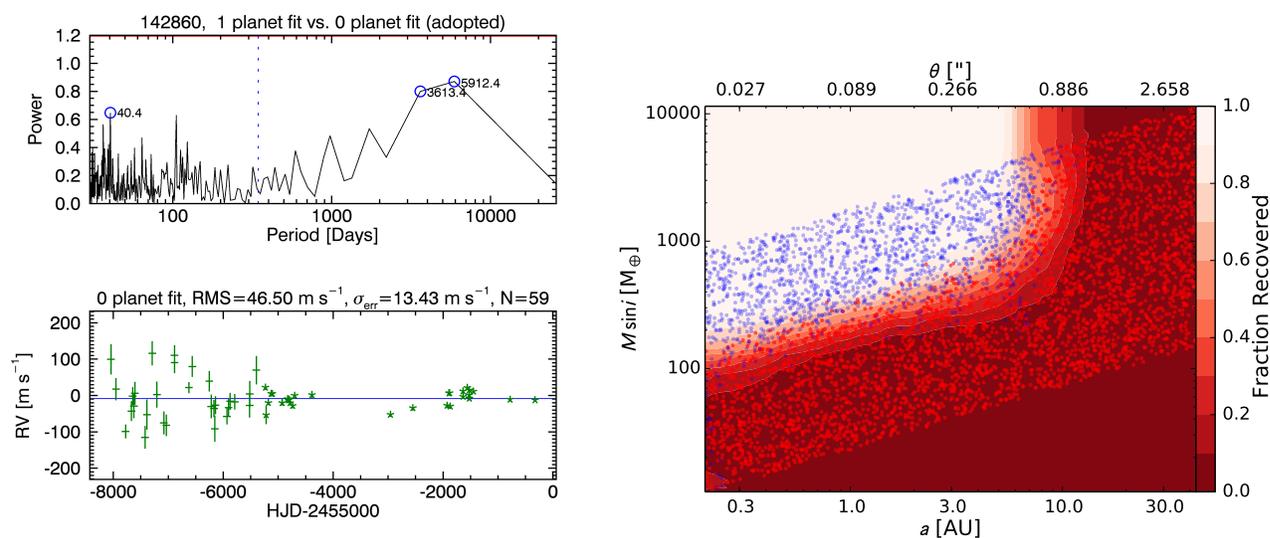
Fig. 69.— Results from an automated search for planets orbiting the star HD 142860 (HIP 78072; program(s) = S, C, A) based on RVs from Lick and/or Keck Observatory. The set of plots on the left (analogous to Figs. 3 and 4) show the planet search results and the plot on the right shows the completeness limits (analogous to Fig. 6). See the captions of those figures for detailed descriptions.
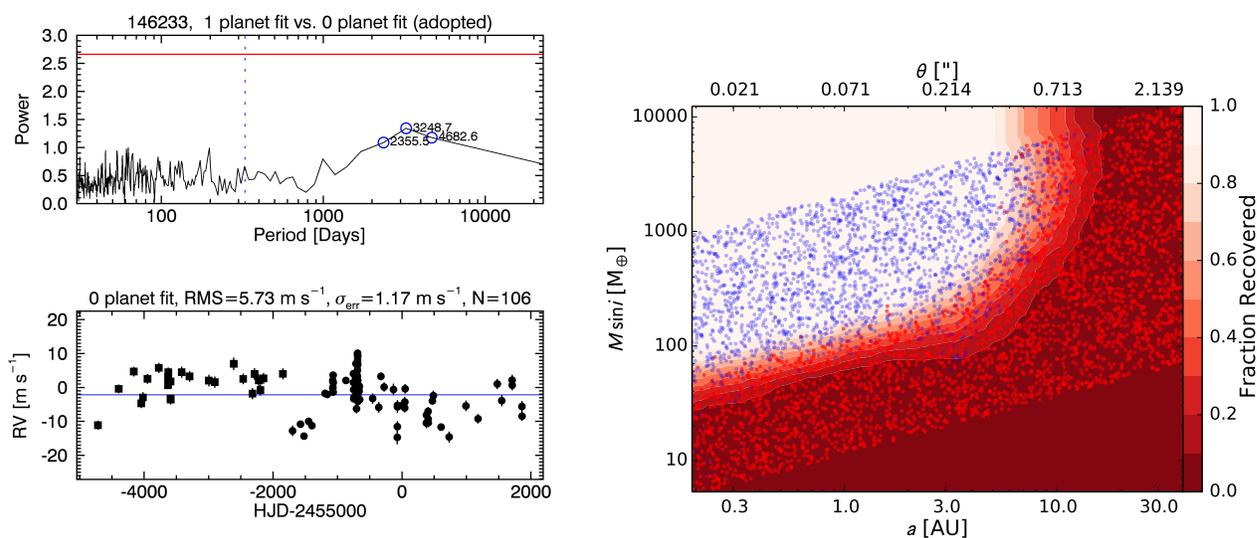
Fig. 70.— Results from an automated search for planets orbiting the star HD 146233 (HIP 79672; program(s) = S) based on RVs from Lick and/or Keck Observatory. The set of plots on the left (analogous to Figs. 3 and 4) show the planet search results and the plot on the right shows the completeness limits (analogous to Fig. 6). See the captions of those figures for detailed descriptions.
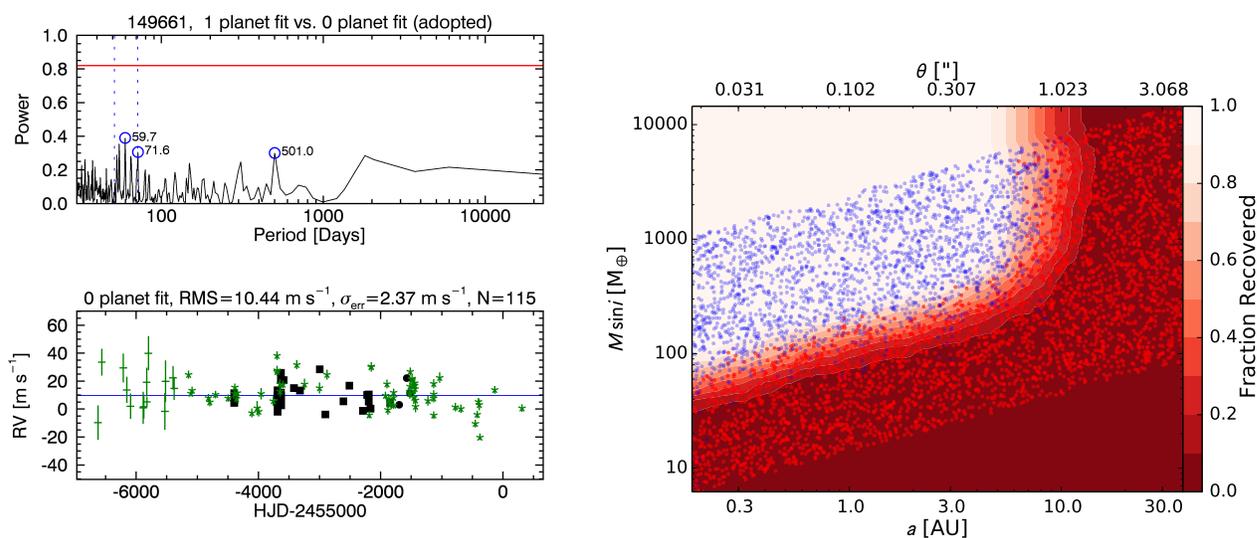
Fig. 71.— Results from an automated search for planets orbiting the star HD 149661 (HIP 81300; program(s) = S) based on RVs from Lick and/or Keck Observatory. The set of plots on the left (analogous to Figs. 3 and 4) show the planet search results and the plot on the right shows the completeness limits (analogous to Fig. 6). See the captions of those figures for detailed descriptions.
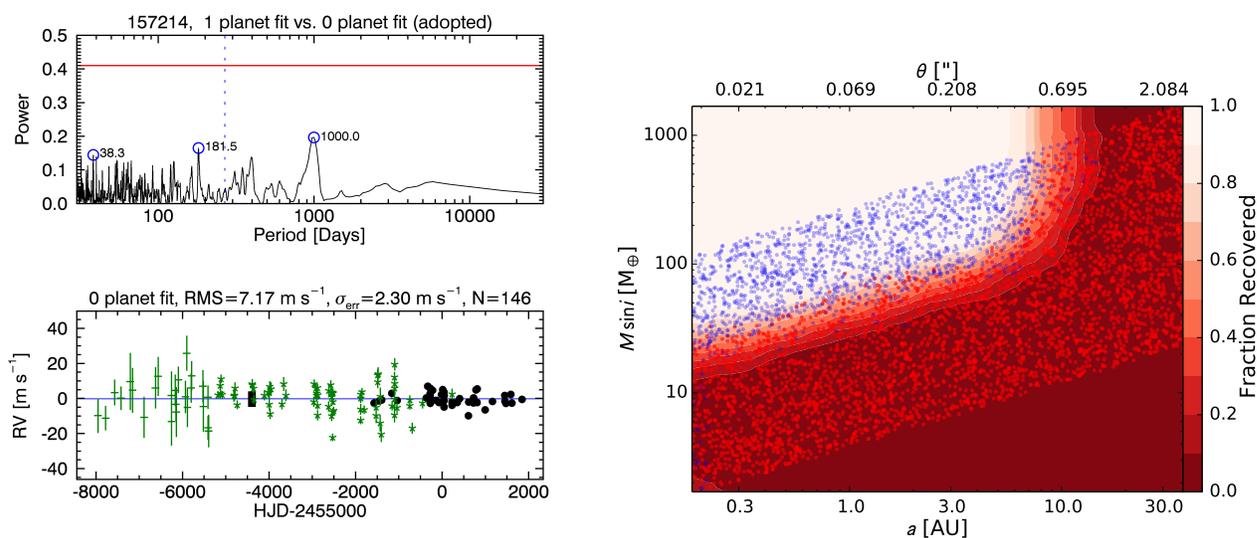
Fig. 72.— Results from an automated search for planets orbiting the star HD 157214 (HIP 84862; program(s) = S, A) based on RVs from Lick and/or Keck Observatory. The set of plots on the left (analogous to Figs. 3 and 4) show the planet search results and the plot on the right shows the completeness limits (analogous to Fig. 6). See the captions of those figures for detailed descriptions.
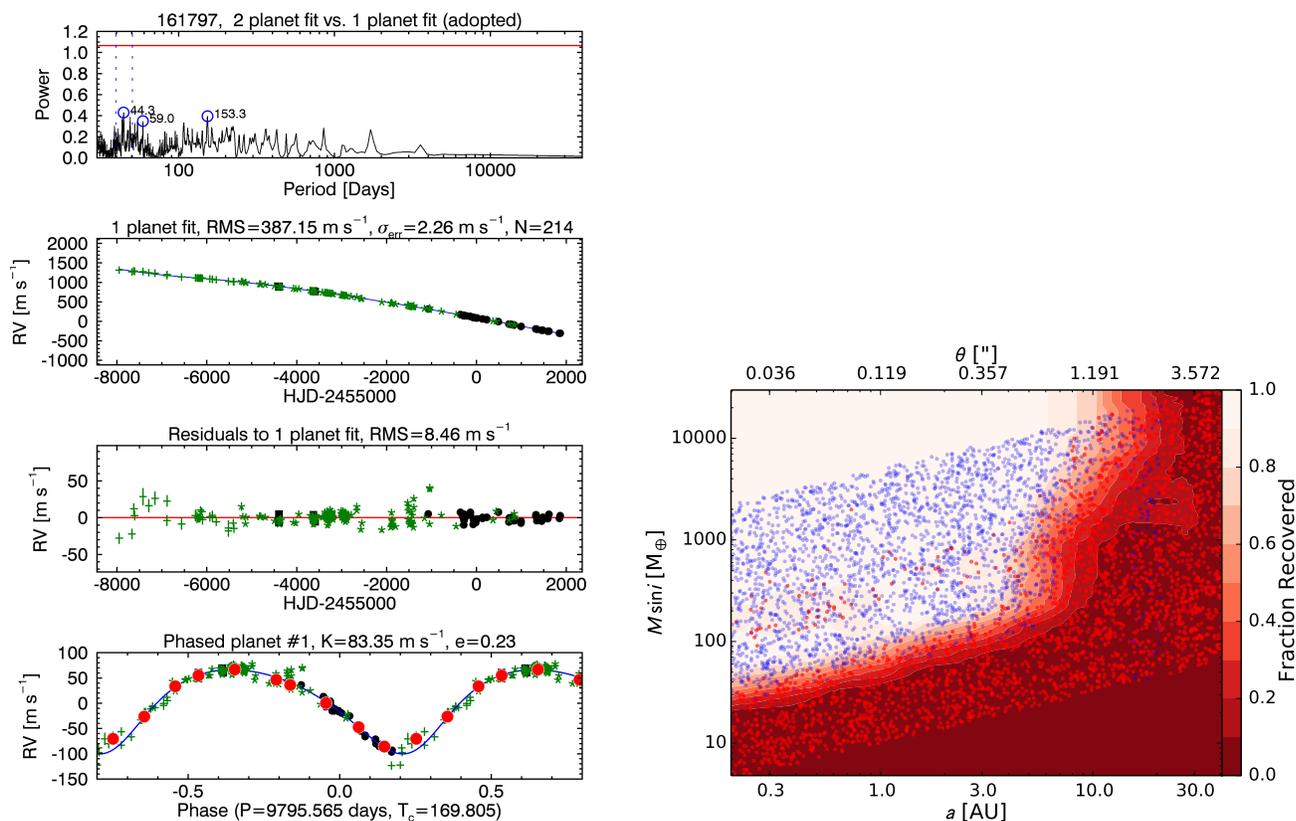
Fig. 73.— Results from an automated search for planets orbiting the star HD 161797 (HIP 86974; program(s) = S, C, A) based on RVs from Lick and/or Keck Observatory. The set of plots on the left (analogous to Figs. 3 and 4) show the planet search results and the plot on the right shows the completeness limits (analogous to Fig. 6). See the captions of those figures for detailed descriptions. This star is in a hierarchical triple system and shows a strong linear trend and significant curvature or a possibly closed orbit in the RV time series.
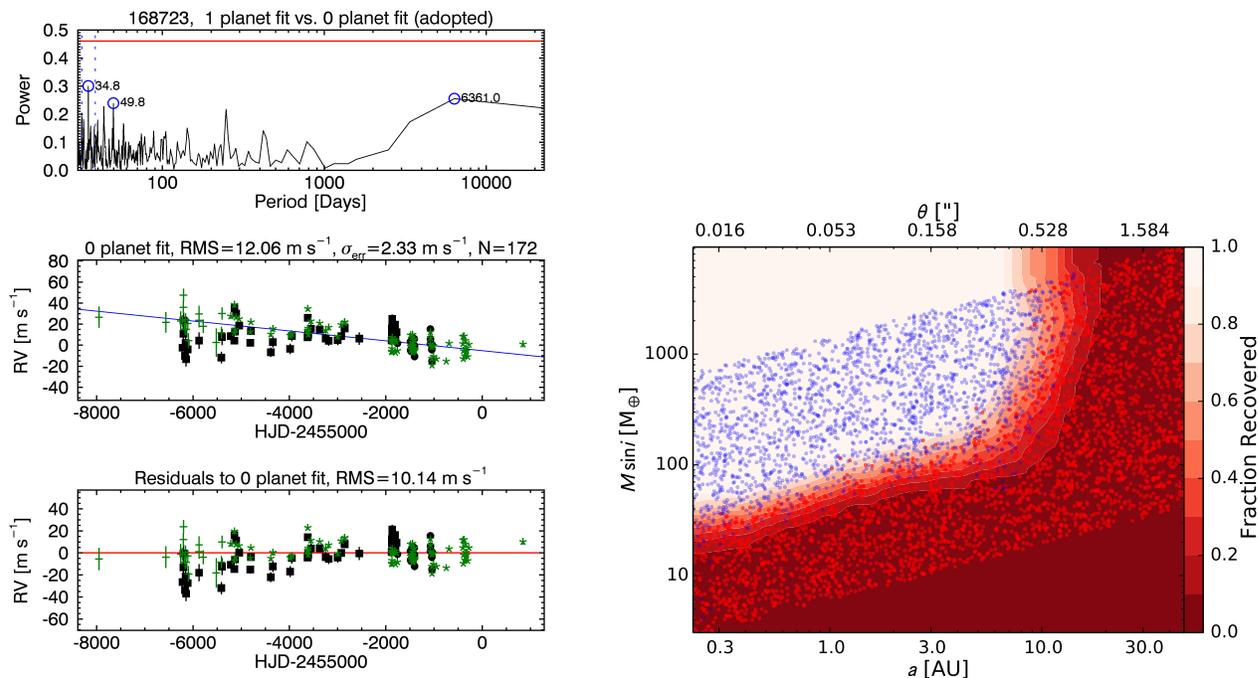
Fig. 74.— Results from an automated search for planets orbiting the star HD 168723 (HIP 89962; program(s) = C) based on RVs from Lick and/or Keck Observatory. The set of plots on the left (analogous to Figs. 3 and 4) show the planet search results and the plot on the right shows the completeness limits (analogous to Fig. 6). See the captions of those figures for detailed descriptions. The Lick data for this star show a marginal linear trend in the RV time series while the long-baseline pre-upgrade Keck data (code = k) does not show the trend.
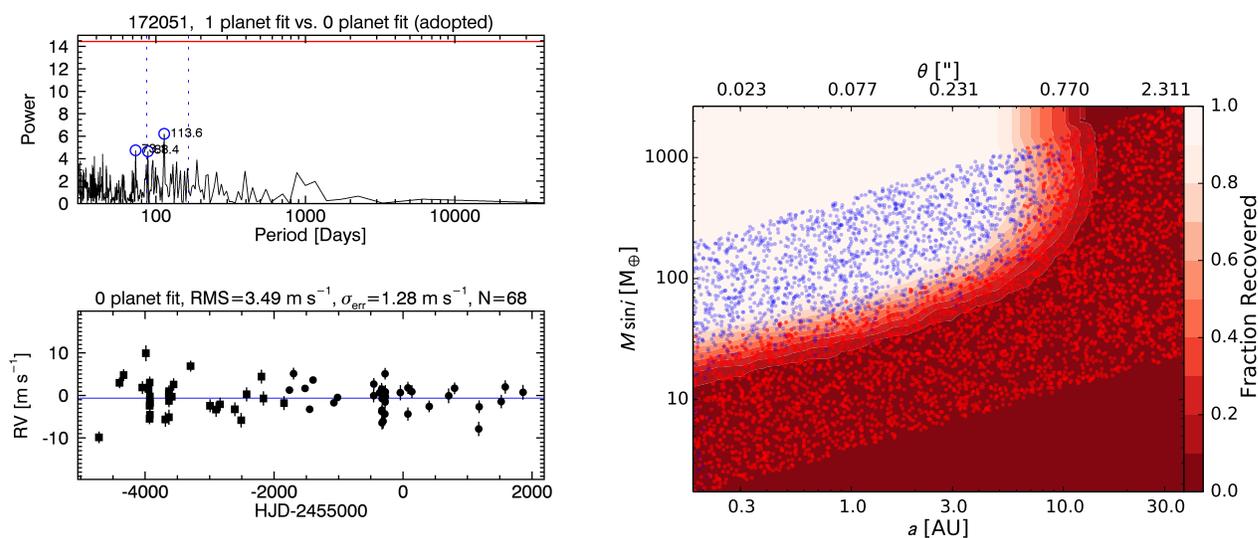
Fig. 75.— Results from an automated search for planets orbiting the star HD 172051 (HIP 91438; program(s) = S) based on RVs from Lick and/or Keck Observatory. The set of plots on the left (analogous to Figs. 3 and 4) show the planet search results and the plot on the right shows the completeness limits (analogous to Fig. 6). See the captions of those figures for detailed descriptions.
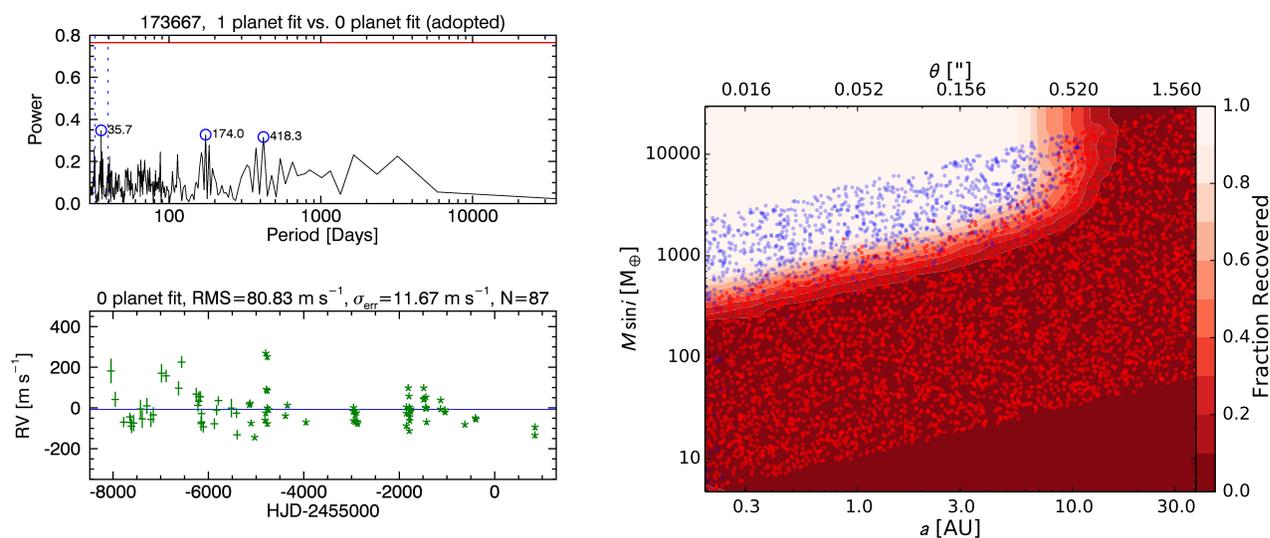
Fig. 76.— Results from an automated search for planets orbiting the star HD 173667 (HIP 92043; program(s) = C, A) based on RVs from Lick and/or Keck Observatory. The set of plots on the left (analogous to Figs. 3 and 4) show the planet search results and the plot on the right shows the completeness limits (analogous to Fig. 6). See the captions of those figures for detailed descriptions.
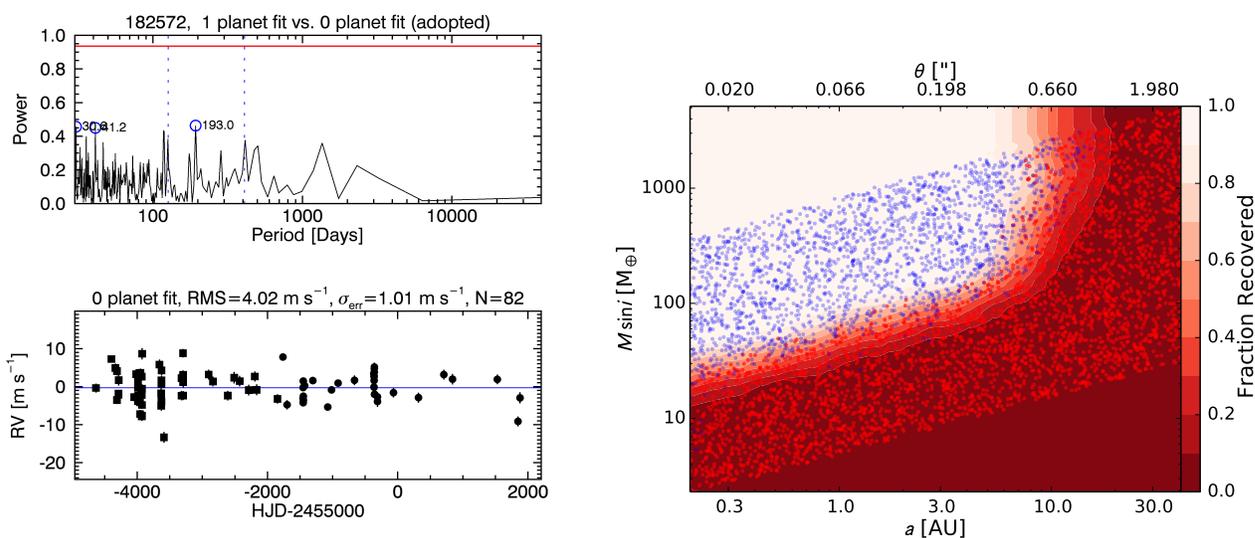
Fig. 77.— Results from an automated search for planets orbiting the star HD 182572 (HIP 95447; program(s) = S, A) based on RVs from Lick and/or Keck Observatory. The set of plots on the left (analogous to Figs. 3 and 4) show the planet search results and the plot on the right shows the completeness limits (analogous to Fig. 6). See the captions of those figures for detailed descriptions.
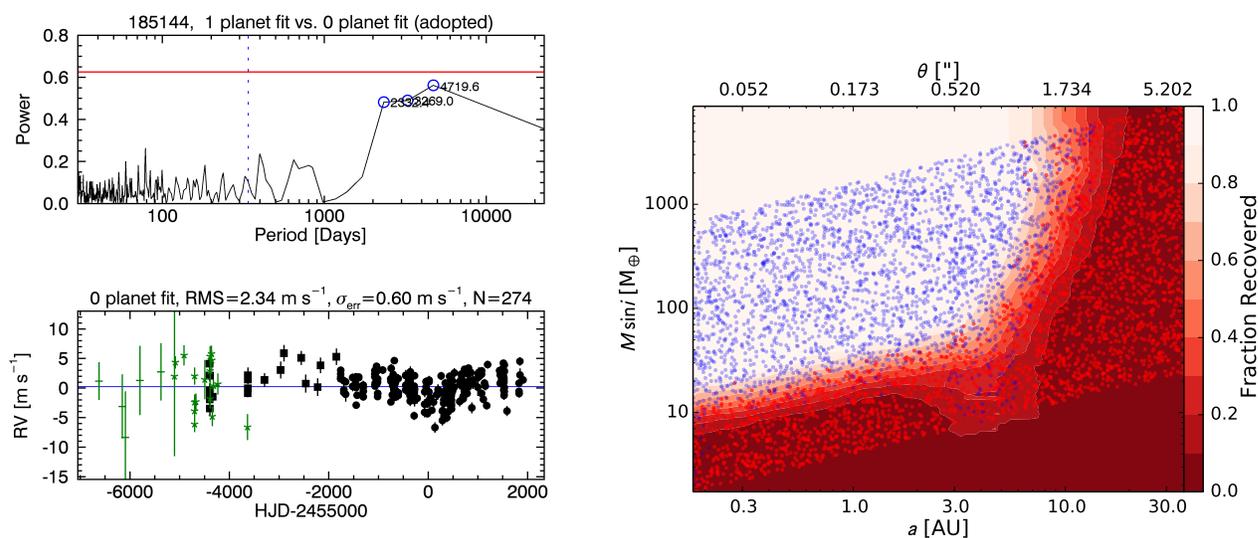
Fig. 78.— Results from an automated search for planets orbiting the star HD 185144 (HIP 96100; program(s) = S, C, A) based on RVs from Lick and/or Keck Observatory. The set of plots on the left (analogous to Figs. 3 and 4) show the planet search results and the plot on the right shows the completeness limits (analogous to Fig. 6). See the captions of those figures for detailed descriptions.
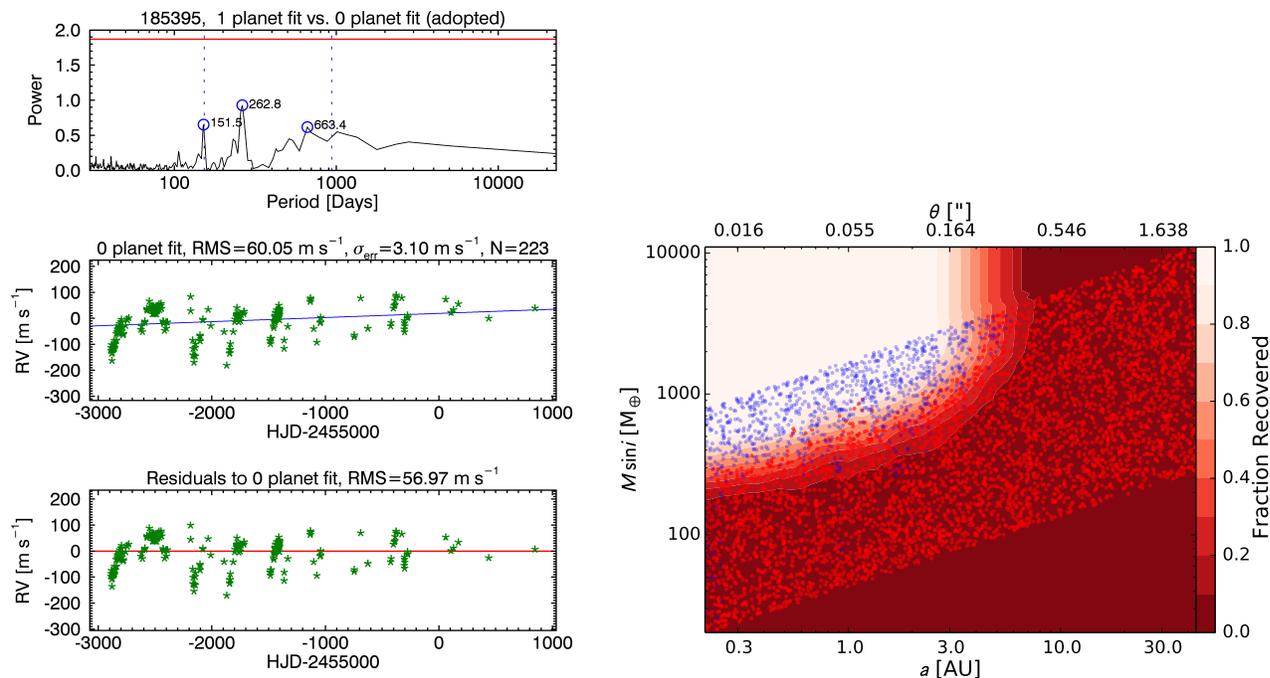
Fig. 79.— Results from an automated search for planets orbiting the star HD 185395 (HIP 96441; program(s) = C, A) based on RVs from Lick and/or Keck Observatory. The set of plots on the left (analogous to Figs. 3 and 4) show the planet search results and the plot on the right shows the completeness limits (analogous to Fig. 6). See the captions of those figures for detailed descriptions. This early-type star (F4 V) has high jitter and a claimed, controversial planet with $P \approx 150$ days. We see evidence in our Lick data for RV variation at this period and other periods related by the yearly alias. Our pipeline formally adopts a linear trend model for the RVs.
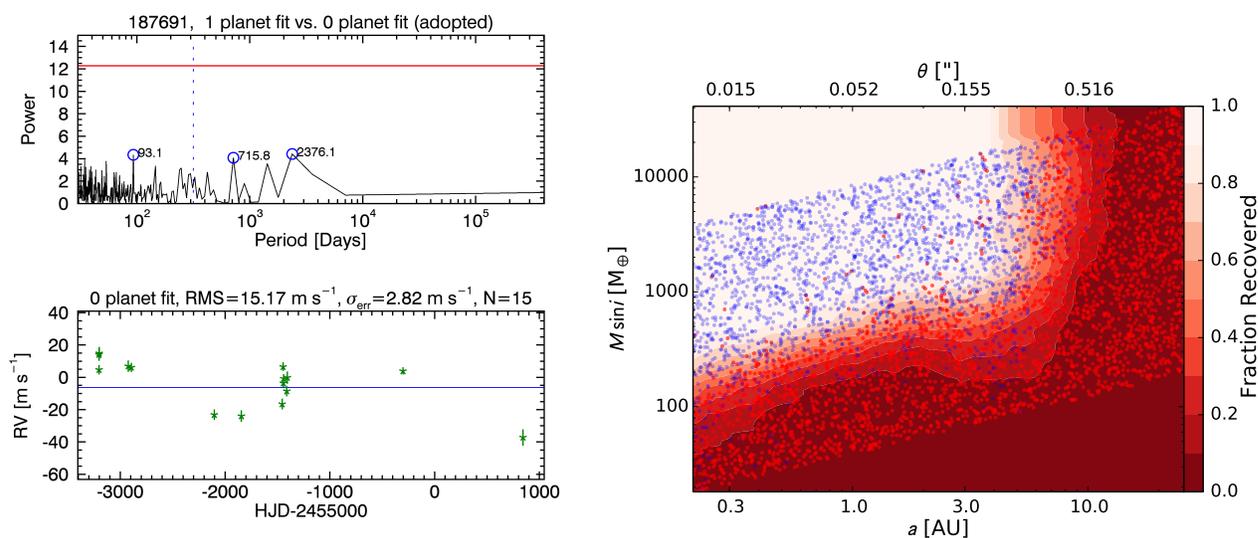
Fig. 80.— Results from an automated search for planets orbiting the star HD 187691 (HIP 97675; program(s) = A) based on RVs from Lick and/or Keck Observatory. The set of plots on the left (analogous to Figs. 3 and 4) show the planet search results and the plot on the right shows the completeness limits (analogous to Fig. 6). See the captions of those figures for detailed descriptions.
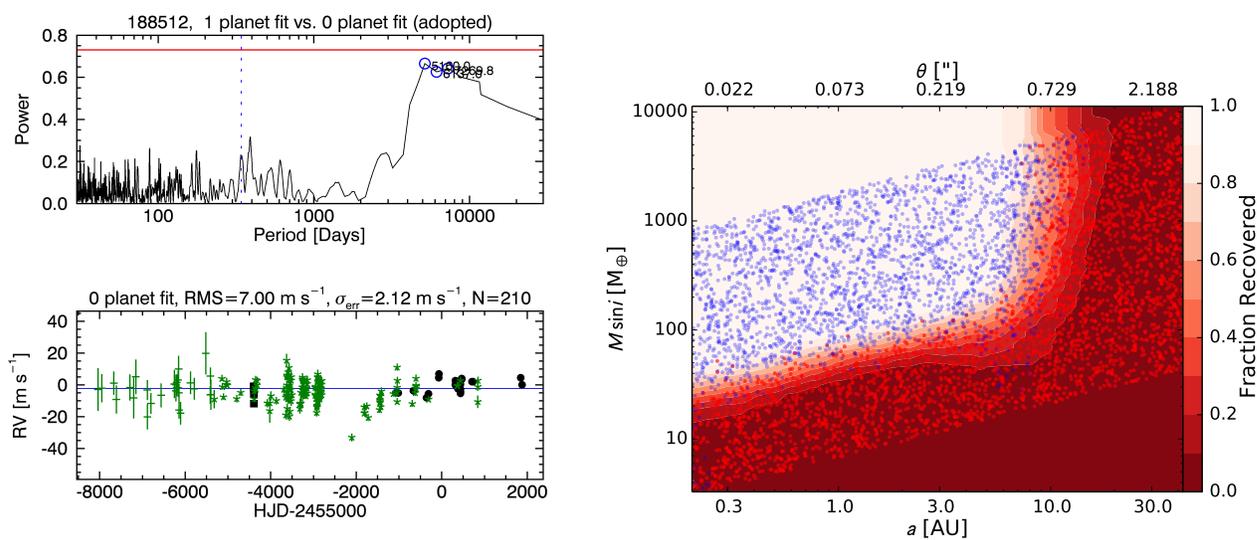
Fig. 81.— Results from an automated search for planets orbiting the star HD 188512 (HIP 98036; program(s) = S, C) based on RVs from Lick and/or Keck Observatory. The set of plots on the left (analogous to Figs. 3 and 4) show the planet search results and the plot on the right shows the completeness limits (analogous to Fig. 6). See the captions of those figures for detailed descriptions.
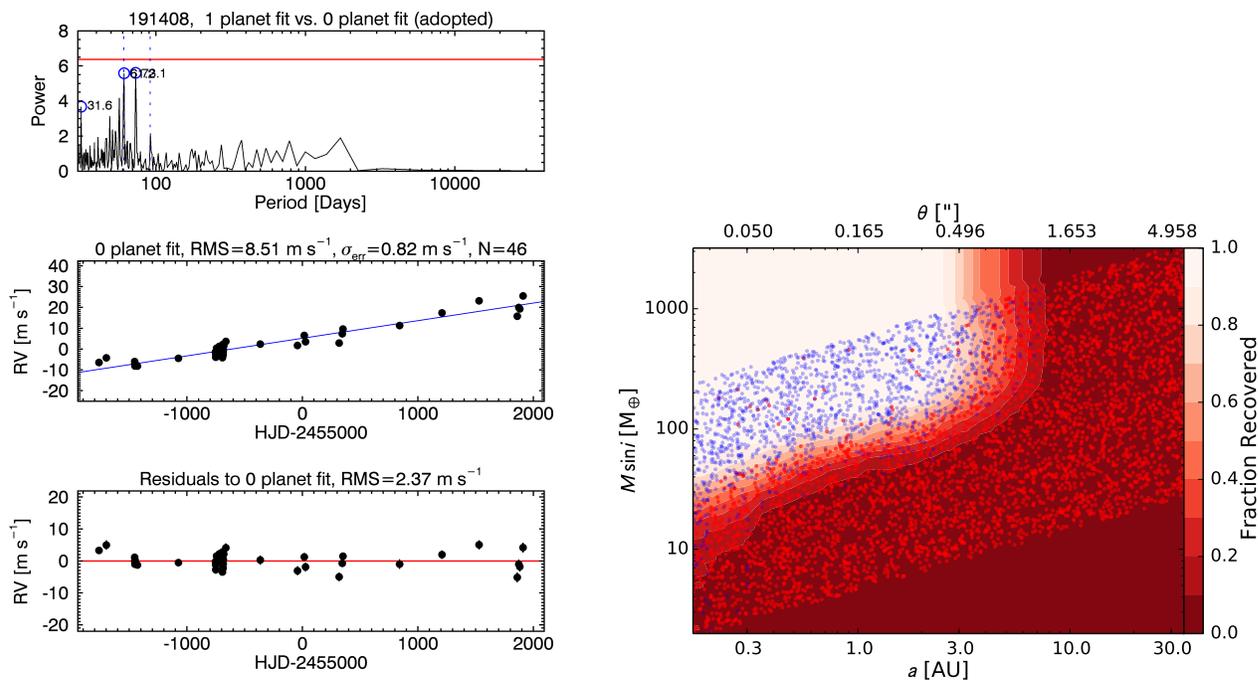
Fig. 82.— Results from an automated search for planets orbiting the star HD 191408 (HIP 99461; program(s) = S, C, A) based on RVs from Lick and/or Keck Observatory. The set of plots on the left (analogous to Figs. 3 and 4) show the planet search results and the plot on the right shows the completeness limits (analogous to Fig. 6). See the captions of those figures for detailed descriptions. This star shows a slight linear trend with no detectable curvature, presumably due to its common proper motion companion.
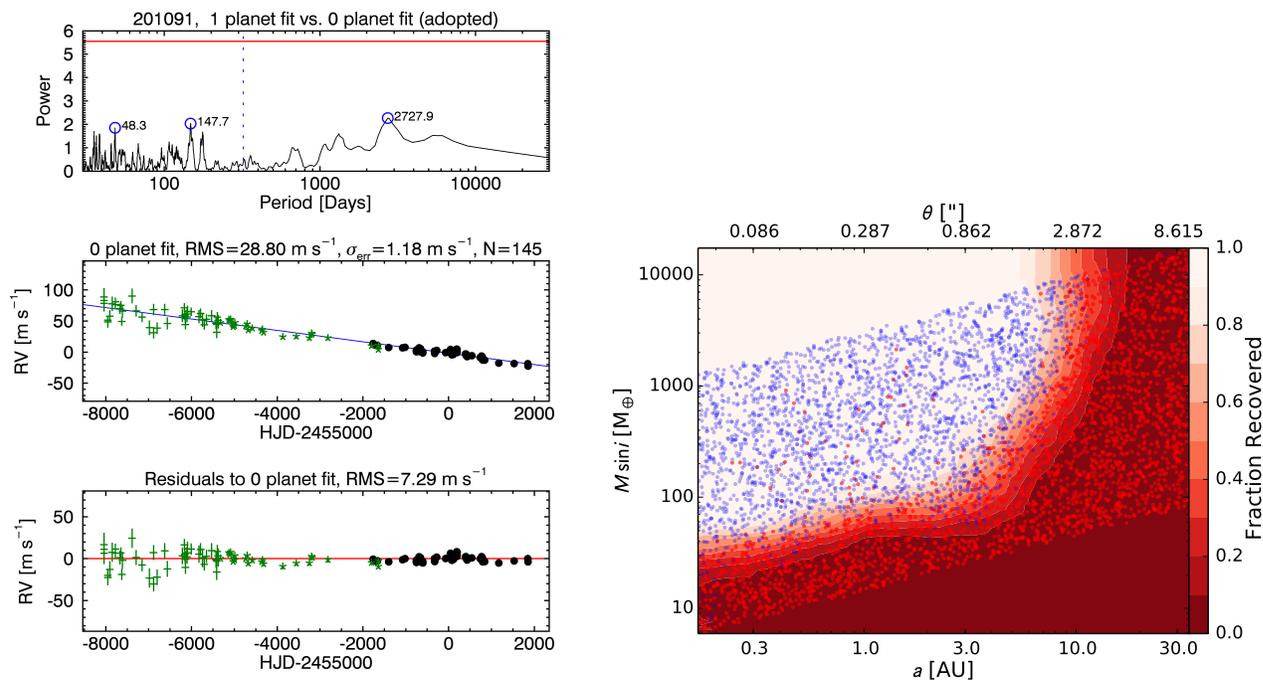
Fig. 83.— Results from an automated search for planets orbiting the star HD 201091 (HIP 104214; program(s) = S, C, A) based on RVs from Lick and/or Keck Observatory. The set of plots on the left (analogous to Figs. 3 and 4) show the planet search results and the plot on the right shows the completeness limits (analogous to Fig. 6). See the captions of those figures for detailed descriptions. This star shows a significant linear trend with no detectable curvature, presumably due to its known stellar companion.
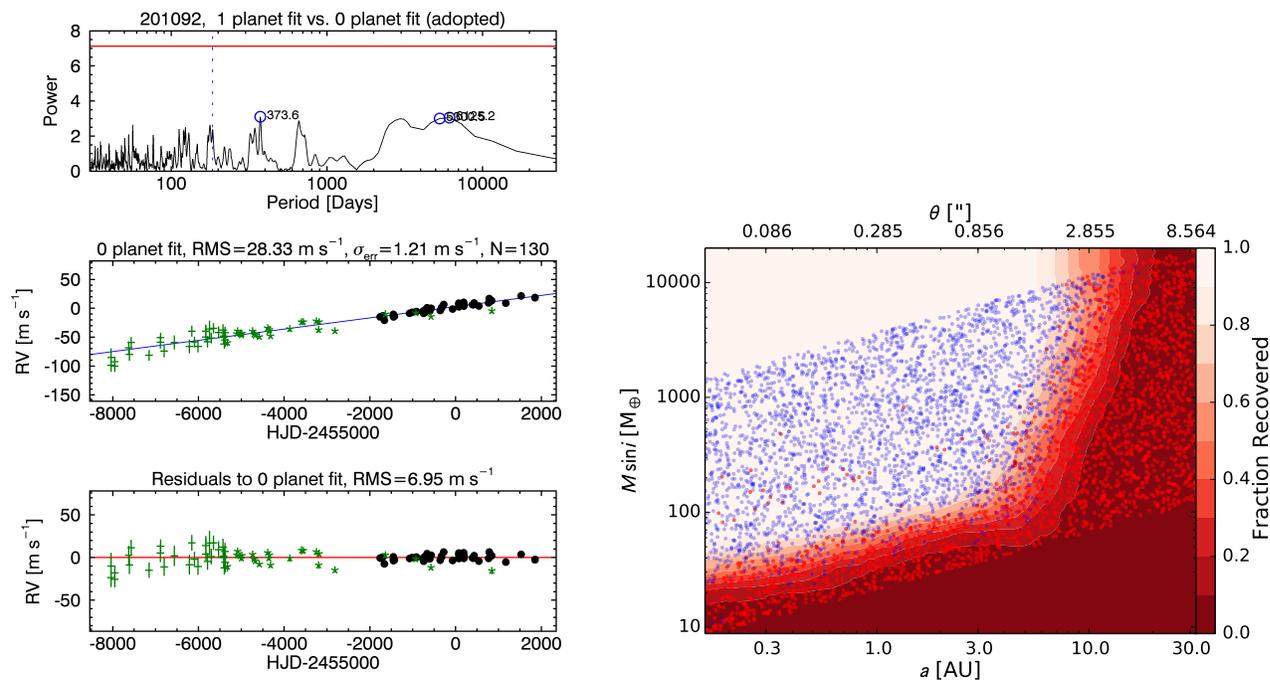
Fig. 84.— Results from an automated search for planets orbiting the star HD 201092 (HIP 104217; program(s) = S) based on RVs from Lick and/or Keck Observatory. The set of plots on the left (analogous to Figs. 3 and 4) show the planet search results and the plot on the right shows the completeness limits (analogous to Fig. 6). See the captions of those figures for detailed descriptions. This star shows a significant linear trend with no detectable curvature, presumably due to its known stellar companion.
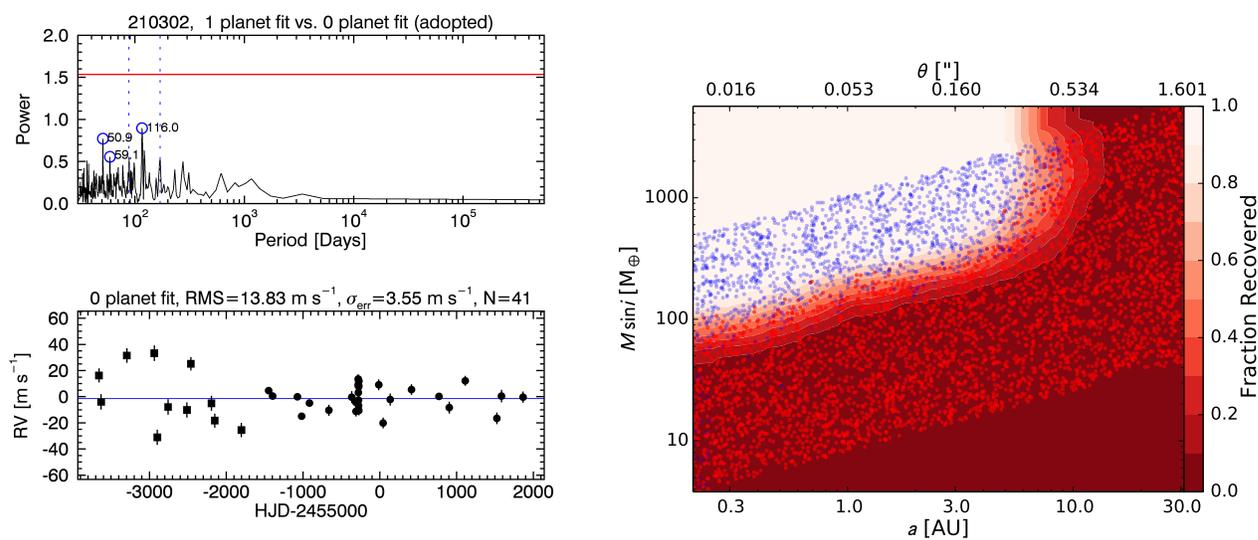
Fig. 85.— Results from an automated search for planets orbiting the star HD 210302 (HIP 109422; program(s) = A) based on RVs from Lick and/or Keck Observatory. The set of plots on the left (analogous to Figs. 3 and 4) show the planet search results and the plot on the right shows the completeness limits (analogous to Fig. 6). See the captions of those figures for detailed descriptions.
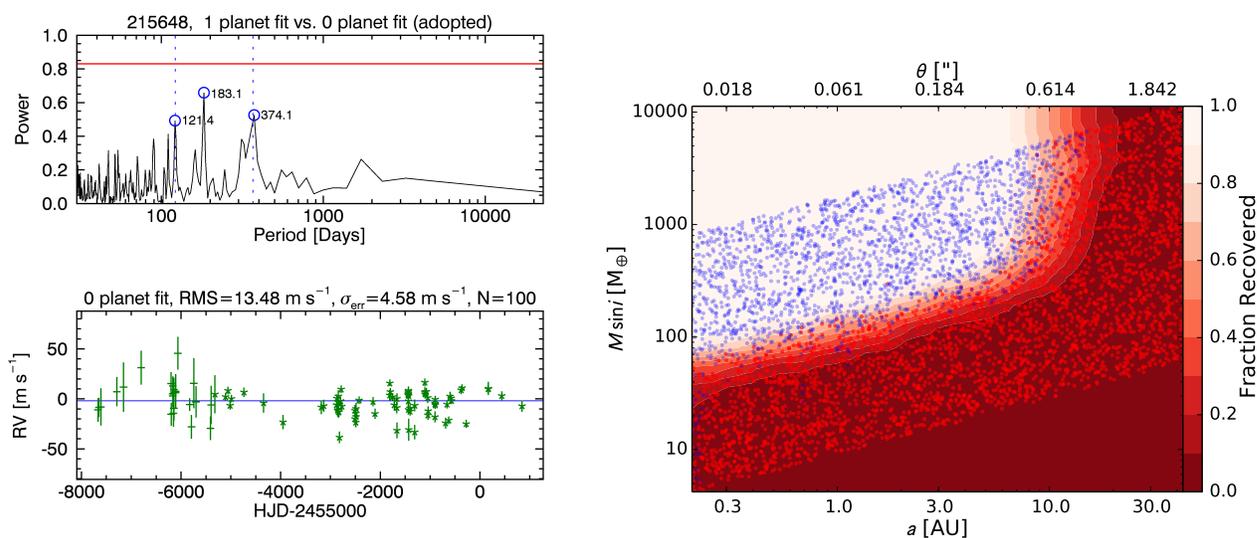
Fig. 86.— Results from an automated search for planets orbiting the star HD 215648 (HIP 112447; program(s) = S, C, A) based on RVs from Lick and/or Keck Observatory. The set of plots on the left (analogous to Figs. 3 and 4) show the planet search results and the plot on the right shows the completeness limits (analogous to Fig. 6). See the captions of those figures for detailed descriptions.
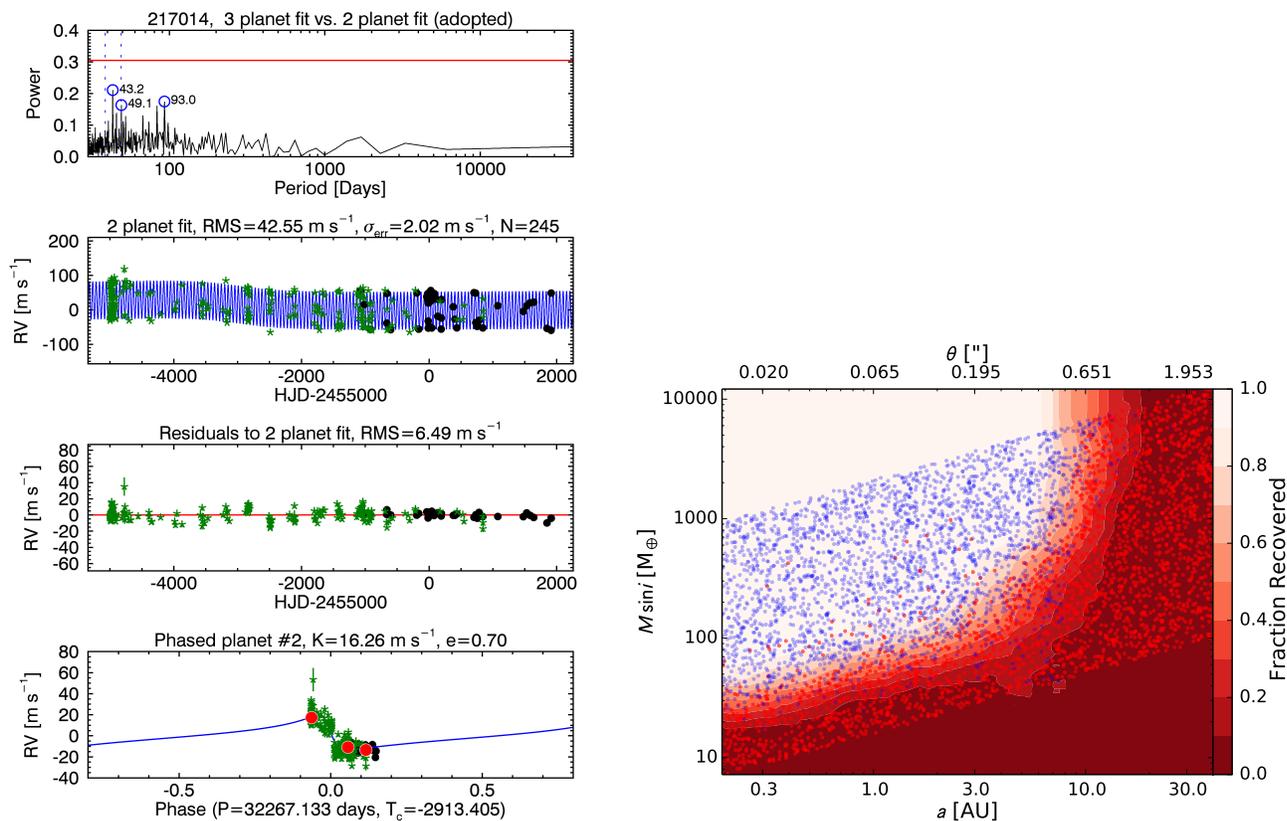
Fig. 87.— Results from an automated search for planets orbiting the star HD 217014 (HIP 113357; program(s) = S) based on RVs from Lick and/or Keck Observatory. The set of plots on the left (analogous to Figs. 3 and 4) show the planet search results and the plot on the right shows the completeness limits (analogous to Fig. 6). See the captions of those figures for detailed descriptions. This star host a hot Jupiter. We also detect a long-period signal but this is likely caused by instrumental offsets within the Lick dataset.
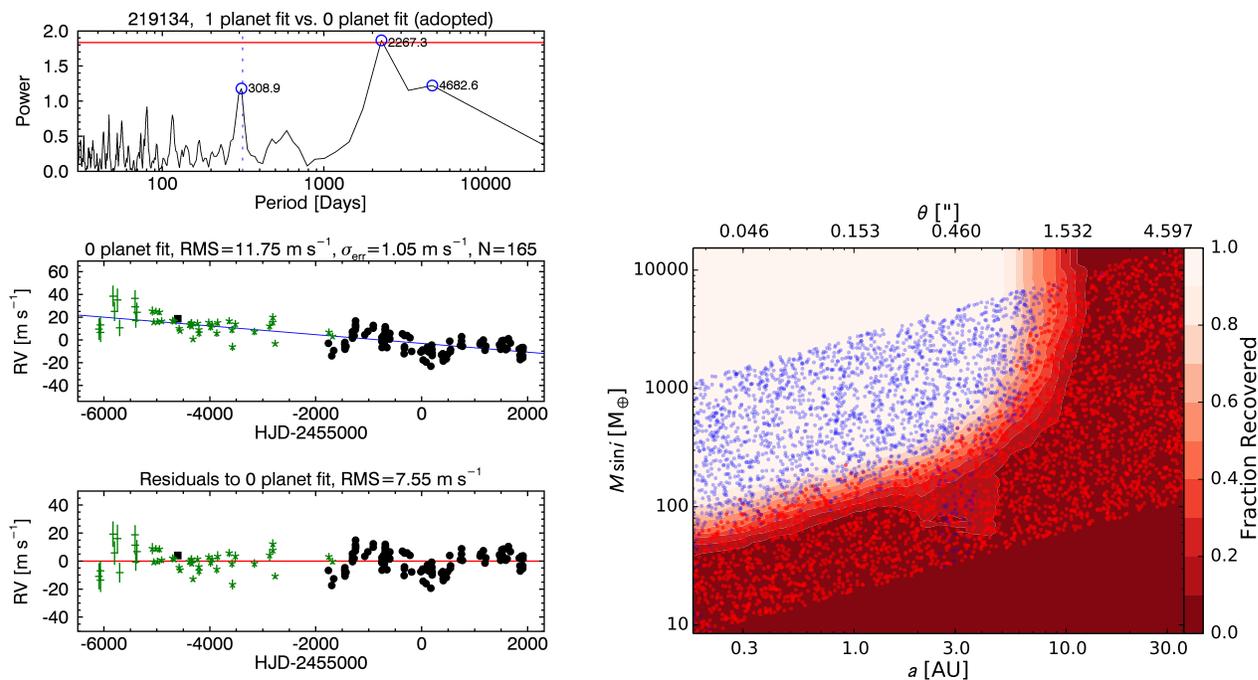
Fig. 88.— Results from an automated search for planets orbiting the star HD 219134 (HIP 114622; program(s) = S, C) based on RVs from Lick and/or Keck Observatory. The set of plots on the left (analogous to Figs. 3 and 4) show the planet search results and the plot on the right shows the completeness limits (analogous to Fig. 6). See the captions of those figures for detailed descriptions. This star has candidate planets including a giant planet in a 3 AU orbit that we will continue to examine as more RVs are gathered. Our automated pipeline formally prefers a model with a linear trend in the RV time series.
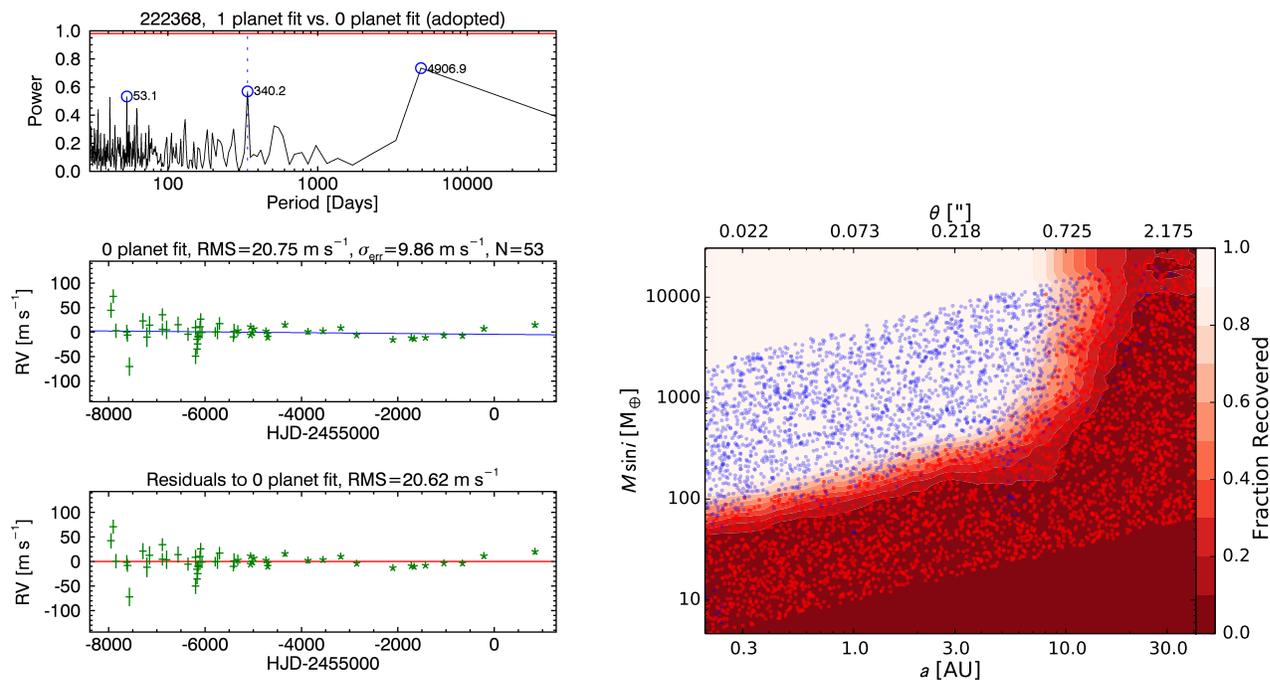
Fig. 89.— Results from an automated search for planets orbiting the star HD 222368 (HIP 116771; program(s) = S, C, A) based on RVs from Lick and/or Keck Observatory. The set of plots on the left (analogous to Figs. 3 and 4) show the planet search results and the plot on the right shows the completeness limits (analogous to Fig. 6). See the captions of those figures for detailed descriptions.